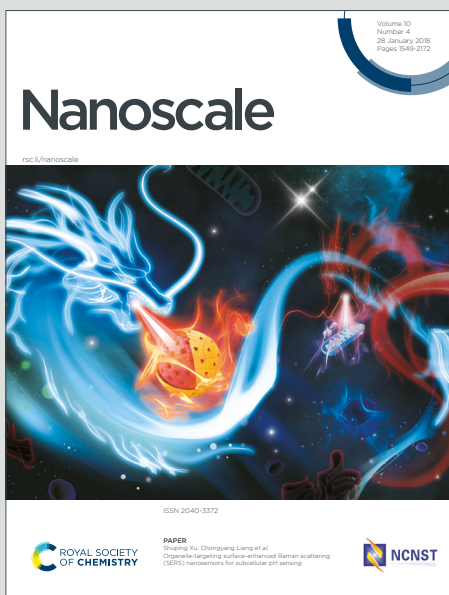


Nanoscale

Accepted Manuscript

This article can be cited before page numbers have been issued, to do this please use: M. S. Yesupatham, R. Murugesan, D. Richard, A. Radhakrishnan and A. Maruthapillai, *Nanoscale*, 2026, DOI: 10.1039/D5NR04327A.



This is an Accepted Manuscript, which has been through the Royal Society of Chemistry peer review process and has been accepted for publication.

Accepted Manuscripts are published online shortly after acceptance, before technical editing, formatting and proof reading. Using this free service, authors can make their results available to the community, in citable form, before we publish the edited article. We will replace this Accepted Manuscript with the edited and formatted Advance Article as soon as it is available.

You can find more information about Accepted Manuscripts in the [Information for Authors](#).

Please note that technical editing may introduce minor changes to the text and/or graphics, which may alter content. The journal's standard [Terms & Conditions](#) and the [Ethical guidelines](#) still apply. In no event shall the Royal Society of Chemistry be held responsible for any errors or omissions in this Accepted Manuscript or any consequences arising from the use of any information it contains.

Review

View Article Online

DOI: 10.1039/D5NR04327A

Synergistic Effects of Metallic and Non-Metallic Element-Doped Electrocatalysts for the Hydrogen Evolution Reaction: A Review

Received 00th January 20xx,
Accepted 00th January 20xx

DOI: 10.1039/x0xx00000x

Manova Santhosh Yesupatham^{a†}, Rajini Murugesan^{a†}, Donald Richard^a, Akshaya Radhakrishnan^a, Arthanareeswari Maruthapillai^{a*}

The hydrogen evolution reaction (HER) is a key electrochemical process for sustainable hydrogen production via water splitting. However, its practical implementation is hindered by sluggish reaction kinetics and reliance on noble metal catalysts like platinum, which are costly and scarce. To overcome these limitations, synergistic doping of metallic (e.g., Fe, Co, Ni, Mo, Mn, Cu, Pt) and non-metallic (e.g., P, N, B, O, S) elements has emerged as an effective strategy to enhance catalytic activity. This dual-doping approach enables fine-tuning of the catalyst's electronic environment, increases active site density, and improves hydrogen adsorption/desorption behaviour. Metallic dopants modulate conductivity and the electronic structure of active sites, while non-metallic heteroatoms introduce charge redistribution, surface defects, and chemical polarity—collectively accelerating HER kinetics. This review critically examines recent advances in the synthesis and performance of heteroatom doped HER electrocatalysts under acidic and alkaline conditions. Emphasis is placed on how compositional tuning, structural design, and interface engineering contribute to improved catalytic performance, including low overpotentials, favourable Tafel slopes, and long-term stability. These developments underscore the potential of heteroatom doping as a versatile platform for designing next generation HER catalysts for scalable and economically viable hydrogen energy systems.

1. Introduction

The global transition toward sustainable energy systems has intensified the search for alternative energy carriers capable of replacing fossil fuels, which are increasingly associated with environmental degradation, climate change, and geopolitical instability.¹ Among the various candidates, hydrogen (H₂) has emerged as a highly promising energy vector due to its high gravimetric energy density, carbon-free combustion, and broad applicability in transportation, chemical synthesis, fuel cells, and energy storage systems.^{2,3} Electrocatalytic hydrogen production via water splitting offers a clean and scalable route to H₂ generation, especially when driven by renewable electricity sources such as solar, wind, or tidal energy.^{4,5} Within this process, the HER is a critical half-reaction that governs the overall efficiency and viability of water electrolysis systems. Despite its simplicity in stoichiometry, the HER involves complex electron-proton transfer steps that are highly dependent on the energetics of the catalytic surface.^{6,7} Platinum-group metals (PGMs) are widely regarded as the benchmark HER catalysts due to their near-zero hydrogen adsorption free energy (ΔG_{H^*}) and exceptional exchange current densities.⁸ However, the

scarcity, high cost, and limited durability of these noble metals have posed significant barriers to their large-scale deployment in practical systems.⁹ As a result, extensive research efforts have been directed toward developing earth-abundant, cost-effective, and efficient non-precious metal-based HER catalysts.^{10,11} One of the most promising approaches in this domain is heteroatom doping, where foreign atoms either metallic or non-metallic are intentionally introduced into the host lattice of a catalytic material to modulate its physicochemical properties. Doping enables the tuning of electronic structures, creation of defect states, optimization of hydrogen adsorption sites, and enhancement of charge transfer kinetics.¹² Specifically, metallic dopants, such as 3d transition metals (e.g., Fe, Co, Ni, Mn, Cu), can significantly alter the d-band center of the host material, thereby adjusting the hydrogen binding energy and improving the intrinsic catalytic activity.¹³ On the other hand, non-metallic dopants such as nitrogen (N), phosphorus (P), sulfur (S), boron (B), and oxygen (O), play an essential role in inducing charge redistribution, defect engineering, and improving hydrophilicity and conductivity.¹⁴ Recent studies have demonstrated that synergistic co-doping of both metallic and non-metallic elements can yield even greater improvements in HER activity than single element doping strategies.¹⁵ This synergistic enhancement arises from the complementary effects of the two dopants: while metallic dopants optimize the electronic configuration of active sites, non-metallic elements further modulate the local charge environment, induce lattice strain, and stabilize catalytic intermediates.^{16,14} For example, in carbon-based materials,¹⁷

[†]These authors equally contributed this work.

^aDepartment of Chemistry, SRM Institute of Science and Technology, Kattankulathur, Tamil Nadu, 603203, India

*Correspondence should be addressed to: arthanam@srmist.edu.in

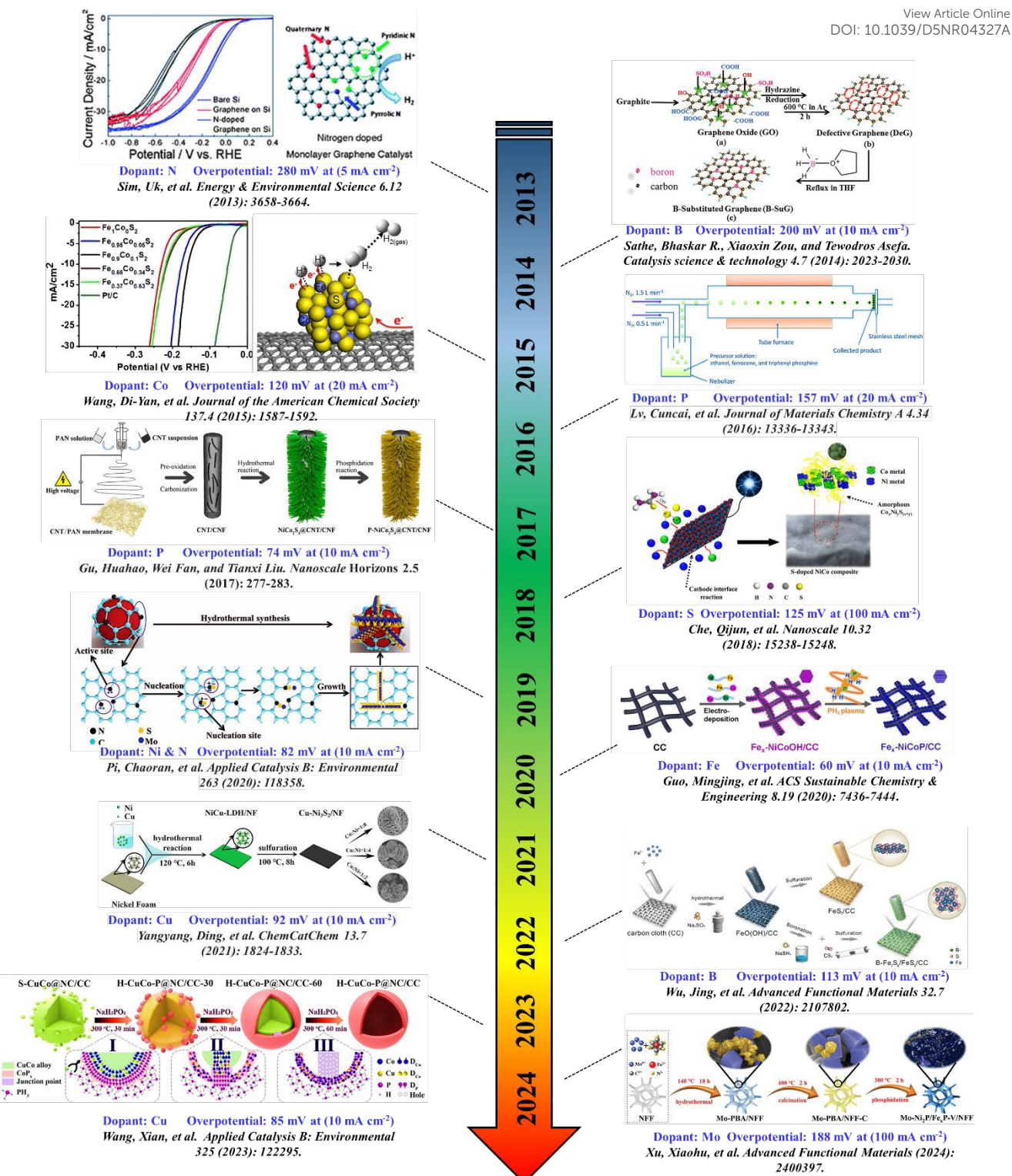


Fig. 1 Schematic representation of historical progress in Heteroatom doping for electrocatalytic HER. reproduced from Ref. [45,62,211,212,74,121,151,168,174,198,209,210] with permission. Copyright 2013 to 2024.

the dual incorporation of transition metals with N or P not only creates M-N_x or M-P_x moieties with high activity but also enhances the electron delocalization throughout the matrix, leading to improved conductivity and reaction kinetics.¹⁸ Moreover, synergistic doping can influence the **Figure 1** thermodynamics of hydrogen adsorption and desorption,

tuning the ΔG_H^* toward thermoneutrality (~ 0 eV), which is a key criterion based on the volcano plot relationship for optimal HER catalysts. In transition metal chalcogen transport, and phosphides, co-doping can promote phase transformation, enhance interfacial charge transport, and increase the electrochemically active surface area.¹⁹ Additionally, co-doped

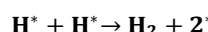
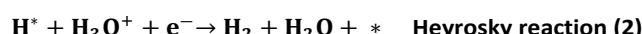
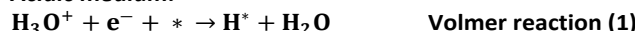
systems often exhibit superior durability under harsh electrochemical conditions, attributable to stabilized bonding configurations and suppressed leaching of active species. Despite significant progress, the rational design of synergistically doped HER catalysts remains a complex challenge. Critical aspects such as dopant selection, atomic configuration, dopant host interaction, and synthetic controllability need to be systematically investigated. Advanced characterization techniques such as X-ray absorption spectroscopy (XAS), transmission electron microscopy (TEM), and density functional theory (DFT) simulations are increasingly being employed to gain atomistic-level insights into the role of dopants and their interactions with the host material. This review aims to provide a comprehensive overview of recent advancements in the development of synergistically doped metallic and non-metallic HER electrocatalysts. We focus on the underlying mechanisms of activity enhancement, the interplay between dopant species, and the emerging design principles that govern catalyst performance. Special emphasis is placed on how electronic structure tuning via co-doping strategies can generate active sites with optimized hydrogen adsorption energies. While several comprehensive reviews have discussed HER electrocatalysts based on either metallic or non-metallic catalyst strategies, most existing works remain largely material-centric or focus on single-dopant effects, with limited emphasis on comparative or synergistic design principles. In contrast, the present review introduces a unified framework that systematically examines metallic and non-metallic strategies from a mechanism-driven perspective, highlighting how different dopant types modulate electronic structure, defect chemistry, and hydrogen adsorption energetics across diverse material platforms. By explicitly correlating dopant-induced electronic tuning with HER activity and stability, this review goes beyond descriptive classification and provides generalized structure-activity relationships and rational design guidelines for next-generation, earth-abundant HER electrocatalysts.²⁰

2. Hydrogen Evolution Reaction Mechanism

An imperative electrochemical mechanism called the HER converts protons (H^+) in an aqueous solution into hydrogen gas (H_2). It originates while on electrolysis, considered the process of cutting down water into its parts of hydrogen and oxygen by way of an electric current. The three fundamental components comprise a normal electrolyzer arrangement: the solution of an electrolyte and two electrodes (the cathode and anode) that have been coated with catalysts, and the electrolyte altogether.²¹ There are several phases to the HER occurring at the cathode, and the electrolyte's state of pH can have an impact on those phases.²² The hydrogen production mechanism within an acidic solution is usually explained by two main phases. At the beginning, H^+ ions near the electrode surface take in electrons for the reduction which forms hydrogen molecules that are adsorbed onto the electrode surface²³ (1). There are two ways in which these adsorbed hydrogen molecules might be eliminated from the electrode surface. One approach is the Volmer-Tafel mechanism-based mixing of two

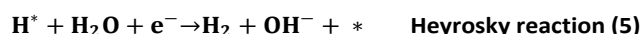
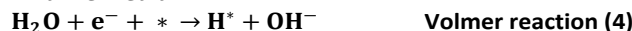
adsorbed hydrogen atoms (2), which proceeds by their desorption from the electrode surface. The alternative process involves the Volmer-Heyrovsky mechanism-driven response of the adsorbed hydrogen atom with an additional H^+ ion and electron (3). As a result, the latter path usually has an apparent activation energy greater than surface recombination.²⁴

Acidic medium:



The process of the hydrogen evolution mechanism pathway in alkaline environment is similar to acidic environment. However, it moves two or three orders of magnitude less quickly than it moves under acidic circumstances. Furthermore, in alkaline HER the water dissociation phase (4) is where Hads intermediates are formed.²⁵

Alkaline medium:



The development of exceptionally well electrocatalysts requires

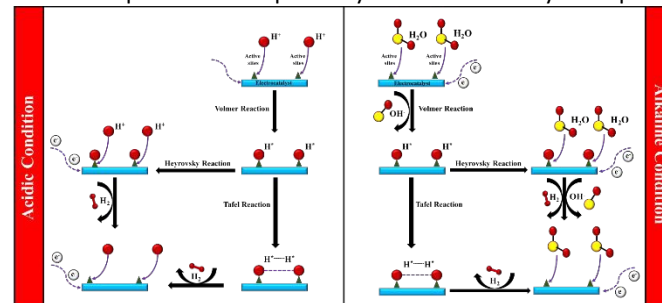


Figure 2. Acidic and alkaline conditions mechanism for HER.

a knowledge of the HER mechanism. The overall HER mechanism is shown in (Figure 2), whereas adsorbed hydrogen undergoes a Volmer reaction to generate the intermediate form of H^* . This is followed by a Tafel or Heyrovsky reaction to eliminate hydrogen and release H_2 gas. A standard measure for evaluating the catalyst's efficiency in starting the reaction is the Gibbs free energy of hydrogen adsorption ($\Delta G H^*$), which represents the amount of H^* binding to the electrocatalyst surface.¹⁹ When $\Delta G H^*$ is close to zero, it indicates that the adsorption and desorption processes are in equilibrium which promotes the evolution of hydrogen.²⁶

3. Doping: An Electronic Structure Tuning Strategy

Doping, specifically heteroatom doping, is a complex method in materials science that involves deliberately introducing atoms from different elements to fine-tune the electrical structure of materials.²⁷ Many fields depend on this method because it gives researchers unmatched control over the chemical and physical qualities of materials. Heteroatom doping utilizes the capacity of foreign atoms to modify the electronic band structure of host



ARTICLE

Journal Name

materials, therefore impacting their conductivity, catalytic activity, and optical properties shown in (Figure 3).¹⁴ Researchers may precisely modify the electrical characteristics of materials such as semiconductors, carbon-based materials, and transition metal oxides by deliberately introducing atoms like nitrogen, boron, phosphorus, sulphur, and others into their lattice structure.²⁸ Customization is essential for a wide range of applications, including semiconductor devices, where doping can control carrier quantities and types (n-type or p-type), and catalysis, where doping improves catalytic efficiency and selectivity.²⁹ Furthermore, heteroatom-doped materials in energy storage systems such as lithium-ion batteries and fuel cells demonstrate higher electrochemical performance due to improved charge transfer kinetics and stability during operation.³⁰ Heteroatom-doped materials are synthesized using sophisticated techniques such as chemical vapor deposition (CVD), sol-gel procedures, and plasma-enhanced processes. These techniques allow for accurate control of the concentration and distribution of the dopants.¹⁵ Characterization techniques such as X-ray photoelectron spectroscopy (XPS), transmission electron microscopy (TEM), and computational modeling methods like density functional theory (DFT) are

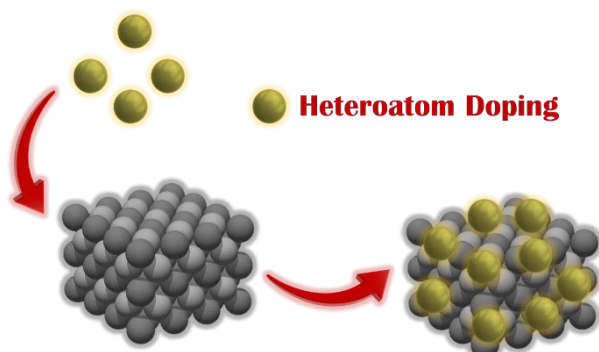


Figure 3. Schematic illustration of heteroatom doping: incorporation of foreign atoms (yellow spheres) into the host material (gray lattice) to modify its electronic structure and enhance electrocatalytic performance.

crucial for comprehending the structural and electrical modifications caused by doping. These methods offer valuable information on the incorporation of heteroatoms into the host lattice, the modification of local bonding arrangements, and the generation of novel electronic states inside the band gap.³¹ A comprehensive comprehension of these fundamental principles is crucial for maximizing the efficiency of material performance and propelling advancements in technological applications. In addition to fundamental research, the technique of heteroatom doping shows potential for tackling urgent global issues such as environmental cleanup and the development of sustainable energy alternatives.³² Materials that have been infused with heteroatoms demonstrate improved capacities in breaking down pollutants, purifying water, and converting renewable energy. This emphasizes their potential to significantly contribute to environmental sustainability.³³ Challenges in this subject involve the consistent distribution of doping agents in large-scale manufacturing, guaranteeing the durability of doped materials over time, and refining doping techniques for uses.³²

Future research endeavours seek to investigate innovative doping techniques, elucidate the underlying principles³² of doping at the atomic level, and incorporate materials doped with heteroatoms into usable devices and systems. In the field of materials science, heteroatom doping is considered a fundamental aspect that provides numerous possibilities for innovation and the advancement of cutting-edge technologies that will have a significant impact on our future.³⁴

Doping is a widely employed strategy in materials science to tailor the electronic properties of materials. In the context of heteroatom doping, doping involves the intentional introduction of foreign atoms into a material's lattice to modulate its electronic structure.²⁸ This approach enables the tuning of the material's bandgap, Fermi level, and charge carrier density, thereby enhancing its performance in various applications. Heteroatom doping has emerged as a powerful tool for designing materials with tailored electronic properties.^{28,35} By strategically selecting the dopant atoms and their concentrations, researchers can engineer the material's electronic structure to suit specific requirements. For instance, doping can enhance the catalytic activity, optical absorption, or electrical conductivity of materials, making them more suitable for applications in energy storage, optoelectronics, and sensing.³⁶ Theoretical modeling and simulations play a crucial role in understanding the effects of doping on the electronic structure of materials.³⁷ By employing density functional theory (DFT) and other computational methods, researchers can predict the dopant-induced changes in the material's band structure, density of states, and charge distribution. These insights enable the rational design of doped materials with optimized electronic properties, accelerating the discovery of novel materials for various technological applications.³⁸

3.1 Tuning the Electronic Structure for Enhanced Electrocatalytic Activity

The intrinsic activity of electrocatalysts is heavily influenced by their electronic structure, making it a central focus in catalyst design.³⁹ One effective strategy to boost the water-splitting efficiency of transition metal nanomaterials is heteroatom doping, which modifies their electronic configuration, energy bands, and interaction with reactive species.¹⁴ Incorporating foreign elements has been shown to enhance surface wettability, reduce kinetic barriers, and introduce additional active sites by altering the host material's surface electronic features. These modifications directly impact the catalyst's ability to bind oxygen-containing intermediates, thereby improving its electrocatalytic behaviour.¹⁶ Such engineering methods can lead to rearrangements in spin and charge distributions, which further amplify catalytic performance.⁴⁰ Additionally, doping can disrupt the original atomic ratios, create localized electric field distortions and shift the electronic density. Overall, tailoring the electronic structure through doping serves as a powerful approach to optimize Fermi level positioning and surface reaction dynamics both of which are crucial for efficient overall water splitting.⁴¹

3.2 Modulation of Active Sites for Optimal Electrocatalysis



Identifying and understanding the nature of active sites in electrocatalysts is essential for unravelling reaction mechanisms and developing more effective catalytic materials. These active sites are the specific locations on the catalyst surface where electrochemical reactions take place, and their intrinsic reactivity depends on how they interact with key intermediates, such as oxygen- and hydrogen-containing species.⁴² Doping plays a critical role in modifying these sites in two primary ways: (a) by increasing the quantity of accessible active sites, thus raising their overall density and enhancing catalytic output, and (b) by altering the chemical nature of the sites, thereby tuning their affinity and reactivity toward specific intermediates.⁴³ As discussed, the introduction of cations or ionic dopants can fine-tune the properties of active sites, leading to improved reaction kinetics and potentially faster catalytic processes.⁴⁴

3.3 Harnessing Synergistic Effects through Heteroatom Doping for Enhanced HER

Heteroatom doping has emerged as a highly effective strategy for enhancing HER activity, primarily by modulating the electronic environment and accelerating charge transfer processes.⁴⁵ By introducing dopants with varying electronegativity or valence states, strong synergistic effects can be achieved, leading to optimized electronic structures that enhance intrinsic catalytic activity.⁴⁶ These effects can improve the interaction between the catalyst surface and hydrogen-containing intermediates, reduce energy barriers, and facilitate more efficient electron conduction and interfacial charge transport.⁴⁷ Synergistic modifications also influence surface morphology and increase the density of accessible active sites, which are crucial for improving catalytic kinetics.⁴⁸ Additionally, heteroatom doping can fine-tune the adsorption energies of intermediates involved in HER, especially the hydrogen adsorption–desorption step, often the rate-determining step in the process. This results in faster reaction rates and lower overpotentials, thus significantly boosting HER efficiency.⁴⁹ However, the benefits of doping depend heavily on maintaining an optimal dopant concentration. Excessive doping may lead to dopant clustering, structural instability, or the formation of secondary phases, which can negatively affect catalytic performance.¹⁶ Therefore, achieving uniform and controlled doping within the solubility limit is vital to preserve the desired properties. Co-doping strategies involving both cationic and anionic elements can further enhance HER performance through complementary effects on the electronic structure and surface chemistry.⁵⁰ While challenges remain such as understanding dopant distribution, real-time behaviour during catalysis, and correlating dopant levels with catalytic performance ongoing research continues to refine these approaches. Overall, the rational design of synergistically doped materials offers a promising pathway toward the development of highly efficient and durable HER electrocatalysts.⁴⁸

4. Heteroatom Doping Strategies for Enhanced Electrocatalytic HER

Heteroatom doping has emerged as a powerful strategy to enhance the electrocatalytic performance of materials for HER.⁵¹ Depending on the nature of the dopant, heteroatom doping is broadly categorized into metallic and non-metallic types shown in (Figure 4).¹⁴ Metallic dopants such as iron (Fe), cobalt (Co), nickel (Ni), molybdenum (Mo), manganese (Mn), copper (Cu), and platinum (Pt) are commonly introduced to improve electrical conductivity, lower the energy barrier for hydrogen adsorption, and facilitate faster charge transfer

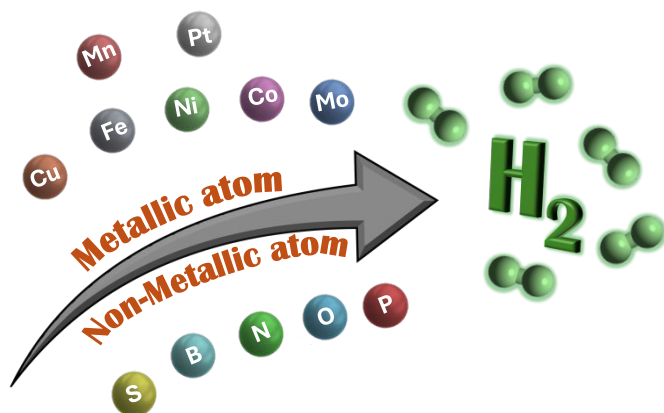


Figure 4. Doping of metallic and non-metallic atoms to enhance catalytic activity for HER.

kinetics.¹⁶ These transition and noble metals serve as active catalytic centers, significantly boosting HER efficiency.⁵² On the other hand, non-metallic dopants like phosphorus (P), nitrogen (N), boron (B), oxygen (O), and sulfur (S) modulate the electronic structure of the catalyst, introduce defect sites, and adjust the binding energy of reaction intermediates. Such modifications enhance intrinsic activity and provide abundant accessible active sites.⁵³ Overall, the deliberate choice of heteroatom dopants—metallic or non-metallic enables the fine-tuning of catalytic behavior, offering a versatile platform for the design of cost-effective and high-performance electrocatalysts for sustainable hydrogen production. In the following sections, we will systematically explore how each class of dopants—metallic and non-metallic—contributes to HER performance, supported by recent advancements and material-specific examples.

4.1 Metallic Heteroatom Doping

The incorporation of metallic atoms into a host matrix is a powerful strategy for engineering advanced catalysts, primarily due to their strong chemical compatibility with the base metal lattice.⁵⁴ This often leads to the formation of highly uniform solid solutions or alloy phases, which can be exploited to finely tune the material's intrinsic properties.⁵⁵ Among various dopants, 3d transition metals owing to their partially filled or vacant d-orbitals are particularly effective in boosting catalytic performance. Their influence on catalytic behaviour is often



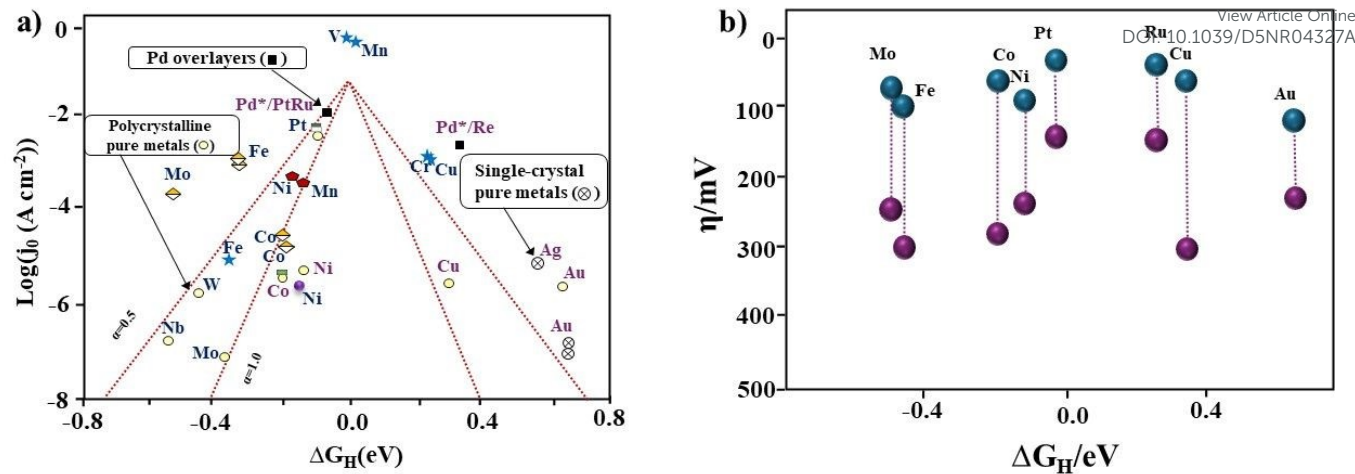


Figure 5. (a) Correlation between HER activity and hydrogen ΔG_H^* for various metallic systems, including heteroatom-doped non-noble metal catalysts are represented. (b) The overpotential of non-noble metal catalysts doped with metallic heteroatoms is directly influenced by the ΔG_H of the catalytic sites, which governs their hydrogen evolution efficiency.

interpreted through the lens of the "volcano plot" a conceptual framework that correlates catalytic activity with hydrogen adsorption energy (ΔG_H^*), especially relevant for HER shown in (Figure 5a).⁵⁶ The peak of this curve signifies an optimal balance: where hydrogen binds neither too strongly nor too weakly, enabling the most efficient catalysis. Dopants that shift the catalyst's ΔG_H^* value closer to this thermoneutral point can significantly enhance HER efficiency.⁵⁷ However, this enhancement isn't solely dictated by adsorption energy. As evidenced in comparative studies shown in (Figure 5b), introducing a range of both noble and non-noble metallic elements can reduce overpotentials markedly from high (blue zone) to low (pink zone) indicating improved catalytic performance.^{56,57} Yet, some dopants achieve remarkable activity even when their ΔG_H^* values deviate from the volcano peak, suggesting additional contributing factors. This implies

that the catalytic output is also shaped by the local atomic environment and the electronic structure of the host material. As shown in Table 1, metal dopants mainly improve how hydrogen binds to the catalyst, while non-metal dopants help by changing the surface environment and active sites. Dopant-induced changes in coordination geometry and electron distribution can alter active site behaviour beyond simple thermodynamic predictions. Thus, in understanding the role of heterometallic dopants in non-noble metal catalysts for HER, it's essential to consider not only adsorption energetics but also the complex interplay of structural and electronic modifications introduced by doping. Selected examples highlighting these effects will be explored in the following sections.

Key aspect	Metallic dopants	Non-metallic dopants
Electronic modulation	Modify the electronic structure of metal centers, often through d-band tuning and metal-metal interactions, which influences catalytic behaviour.	Redistribute charge density around host atoms, producing polarized sites and altering surface electronic environments.
Effect on ΔG_H^*	Regulate hydrogen adsorption free energy more directly via metal-hydrogen interactions.	Influence ΔG_H^* indirectly by altering the local electronic structure of neighbouring atoms.
Nature of active sites	Generate metal-centered or bimetallic active sites responsible for HER.	Produce heteroatom-based or metal-heteroatom (M-X) sites that participate in hydrogen adsorption.
Structural influence	Induce lattice distortion, defect formation or phase evolution within the catalyst structure.	Promote defect generation, edge exposure and surface functionalization.
Role in HER performance	Primarily enhance intrinsic catalytic activity and charge transfer kinetics.	Improve surface reactivity and contribute to stabilization of reaction intermediates.

Table 1: Key Differences between Metallic and Non-Metallic Dopants in Hydrogen Evolution Reaction Catalysts.

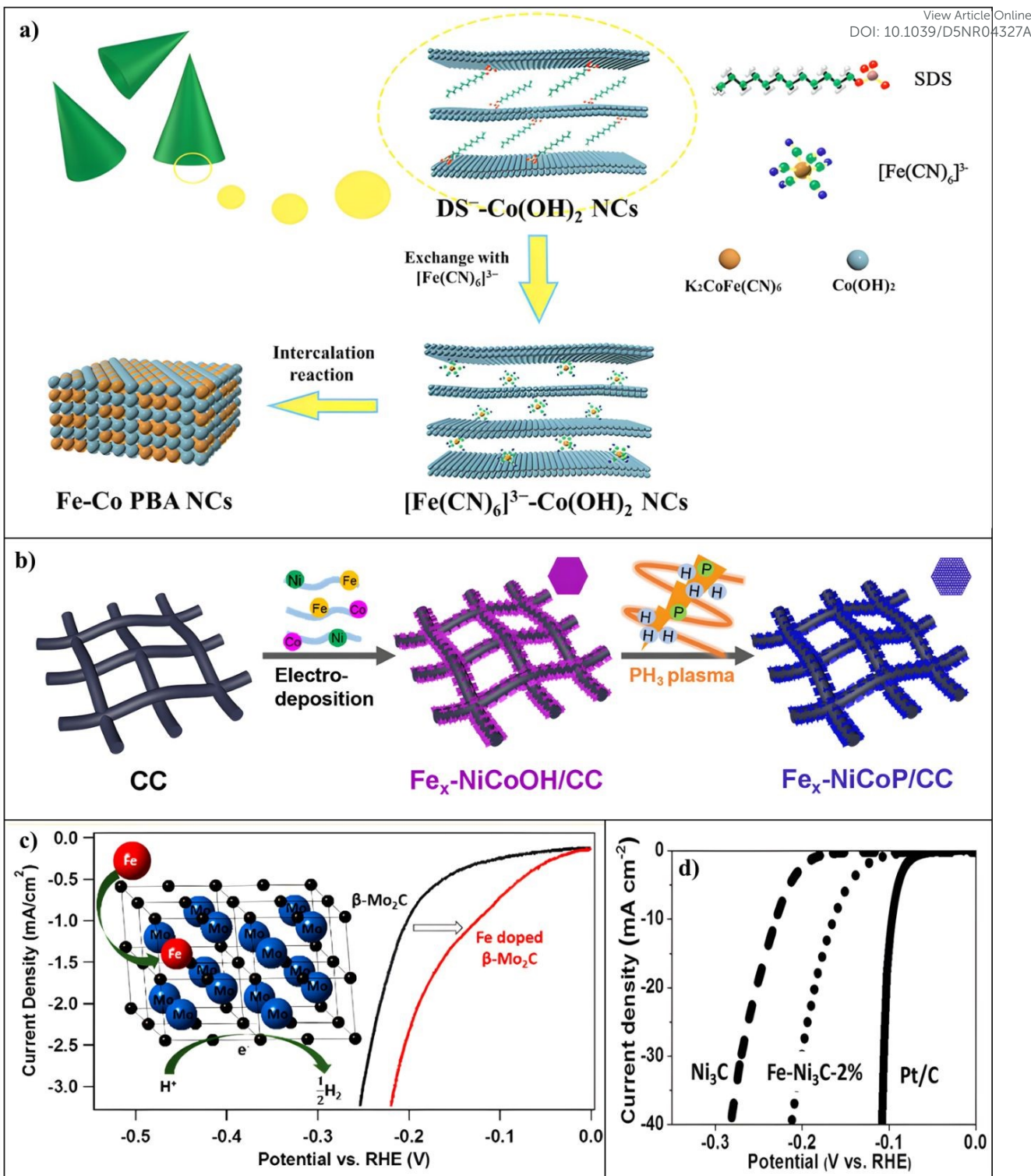


Figure 6. (a) Schematic illustrating the mechanism by which Fe-Co PBA NCs emerges from Co (OH)₂ NCs. reproduced from Ref.[⁶¹] with permission. Copyright 2018, ACS. **(b)** A diagrammatic illustration of the Fe_x-NiCoP/CC synthesis method. reproduced from Ref.[⁶²] with permission. Copyright 2020, ACS. **(c)** Polarisation curves for Fe-doped β-Mo₂C and pure β-Mo₂C. reproduced from Ref.[⁶⁶] with permission. Copyright 2015, ACS. **(d)** Sample polarisation curves for Ni₃C, Fe-Ni₃C-2%, and Pt/C in 0.5 M H₂SO₄. reproduced from Ref.[⁷⁰] with permission. Copyright 2017, Wiley.

4.1.1 Fe-Doped Electrocatalysts for HER

Fe atom's versatility and abundance of d-band electrons enable them to successfully control the electronic structure of host catalysts.¹⁶ Due to their comparable atomic radii and electrical structures, Co and Ni are examples of substrate metal atoms

that have been the focus of most research on Fe-doped catalysts until now. An appropriate amount of iron salt is usually added as an intermediate during synthesis to accomplish Fe doping. One of the main processes are that come from Fe doping, that's Fe alters electronic structure and lowers

ARTICLE

Journal Name

ΔG° .⁵⁸⁻⁶⁰ As reported by Xiaosong Guo and co-workers have alternate route for the manufacture of Fe-Co Prussian Blue Analogue (PBA) nanoclusters is developed responsible for the overall increased catalytic performances, employing room-temperature layer-structured $\text{Co}(\text{OH})_2$ nanoparticles as sacrificial templates shown in (Figure 6a). To achieve extremely uniform Fe doping on the atomic level, the multilayered $\text{Co}(\text{OH})_2$ nanocrystal matrix first intercalates and evenly anchors $[\text{Fe}(\text{CN})_6]^{3-}$ anions. Stable Fe-Co PBA catalysts are then formed when the embedded $[\text{Fe}(\text{CN})_6]^{3-}$ anions interact with neighbouring $\text{Co}(\text{OH})_2$ host layers. Crucially, these Fe-Co PBA catalysts embed themselves in the $\text{Co}(\text{OH})_2$ substrate layers, hence inhibiting Fe-Co PBA nanoparticle aggregation and hyperproliferation. XPS shows that Fe inclusion causes negative shifts in the Co 2p and P 2p peaks, indicating altered electronic states. These modifications strengthen Fe-Co interactions and boost HER activity. The Fe-Co_xP catalyst exhibited a significant increase in HER catalytic activity. This offers a straightforward and efficient way to achieve heteroatom doping.⁶¹ *Mingjing Guo and co-workers* developed an electrode placement and PH_3 plasma treatment was used to effectively construct Fe-doped Ni-Co phosphide nanoplates that incorporate a hierarchical

nanostructure on a carbon cloth (Fe_x-NiCoP) shown in (Figure 6b). The electrocatalytic activity is further enhanced by the planar flaws in the nanocrystals caused by Fe doping, which encourages the ingestion of active sites. Ultimately, the electrocatalytic efficacy of the catalyst may also be influenced by potential electronic interactions between metal cations following Fe doping with the right amount of content. After phosphorization, XPS results show the creation of partly charged $\text{Ni}^{\delta+}$, $\text{Co}^{\delta+}$, $\text{Fe}^{\delta+}$, and $\text{P}^{\delta-}$ species, indicating strong electronic interactions. These characteristics allow proton adsorption and improve electrocatalytic performance. DFT calculations show that slight Fe doping improves HER activity by promoting H_2O adsorption on active sites. Fe_x-NiCoP with Fe doping has the highest HER performance, with stability lasting 25 hrs and an η_{10} of just 60 mV.⁶² *Chun Tang and co-workers* reported a Fe-doped CoP nanoarray on Ti foil (Fe-CoP/Ti) is a strong monolithic HER catalyst with higher activity than a CoP nanoarray. Because of their distinct valence, ionic radius, and ion mass, Co^{2+} adsorbs on Ti foil at a higher pace than Fe^{3+} , which may explain why the Fe/Co atomic proportions in the solutions and final products differ. In a two-electrode electrolyzer, an HER overpotential with 78 mV for 10 mA cm^{-2}

S. No	Catalyst	Electrolyte	Overpotential (η) At 10 mA cm^{-2}	Tafel slope (mV dec ⁻¹)	C_{dl} (mF cm ⁻²)	Stability (hours)	Reference
1	Fe-Co _x P	0.5 M H_2SO_4	127	55	-	4h	61
2	Fe _x -NiCoP	0.1 M KOH	60	51	71.40	25h	62
3	Fe-CoP/Ti	0.1 M KOH	78	75	-	20h	63
4	Fe-WO _x P/rGO	0.5 M H_2SO_4	54	41	34.60	24h	64
5	Fe-NiS ₂	0.5 M H_2SO_4	121	37	-	15h	65
6	Fe-doped β -Mo ₂ C	0.1 M HClO_4	240	-	-	9h	66
7	Co _{0.68} Fe _{0.32} P	0.1 M KOH	116	64	-	1h	67
8	Ni _{1.85} Fe _{0.15} P	1.0 M KOH	106	47	6.04	20h	68
9	Fe _{0.27} Co _{0.73} P	1.0 M KOH	186	59	1.02	40h	69
10	Fe-Ni ₃ C-2%	1.0 M KOH	292	41	-	10h	70

Table 2. Fe-Doped Electrocatalysts for HER



necessitates a voltage in the cell of 1.60 V for water-splitting current. With an activating energy as low as 39.6 J mol^{-1} , it yields a hydrogen production rate of $6.06 \text{ L min}^{-1} \text{ g}^{-1}$ for 1wt% NaBH_4 beneath ambient conditions.⁶³ *Tadele Hunde Wondimu and co-workers* reported the Fe-doped WO_3 deposited directly over reduced graphene oxide in the form of a nanoplate-like structure, and reduction is then accomplished using PH_3 produced *in situ* using sodium hypophosphite. Fe-doped tungsten trioxide nanoplates (Fe- WO_3) are converted into Fe-doped tungsten oxide phosphate (Fe- WOxP) by PH_3 , which functions as a phosphorus precursor and reducing agent. Fe- WOxP on reduced graphene oxide (Fe- WOxP/rGO) is the product of this. The numerous oxygen vacancies within the nanoplate-like framework of Fe- WOxP and the rGO nanosheets that operate work in concert to increase the catalytic ability and conducting capacity of the synthesized material. In 0.5 M H_2SO_4 , Fe- WOxP/rGO demonstrated remarkable electrocatalytic activity despite a low overpotential of 54 mV, which is adequate to attain a current density of 10 mA cm^{-2} and stable for more than 24 hrs.⁶⁴ *Junqing Yan and co-workers* developed Fe-doped NiS_2 (Fe- NiS_2) nanosheets that exhibit strong activity and repeatability in the electrochemical process. Fe^{3+} is added to the lattice to increase the NiS_2 semiconductor's conductivity. Fe-doped NiS_2 nanosheets (Fe- NiS_2) are produced by sulfidating $\text{NiFeO}_x/\alpha\text{-Ni(OH)}_2$ nanosheets during the production process. Interestingly, on the surface of the Ni(OH)_2 nanosheet, the previously dispersed NiFe_2O_4 nanoparticles change into sulfide and integrate into the crystal structure of the ensuing NiS_2 sample. DFT calculations reveal that the electrocatalytic HER transition state can lower the activation energy of H_2 production. After sulfuration, XPS retains its original composition, whereas FeNiS/CdS provides much improved and stable HER performance. Enhanced HER capabilities in the resulting Fe- NiS_2 nanosheet sample result from adding surface Fe sites, which boost electrocatalytic performance. These attributes include a tiny overpotential of 121 mV at 10 mA cm^{-2} and a low Tafel slope of 37 mV/dec.⁶⁵ *Cheng Wan and co-workers* first time reported a unique amine-metal oxide synthesis technique, molybdenum carbide nanoparticles with the Fe_2N composition may be doped with varying concentrations of iron (0-8 wt%). A graphitic carbon framework is formed by the Fe-doped catalyst during the $\beta\text{-Mo}_2\text{C}$ synthesis process. The frequent catalyst that encourages the formation of graphitic carbon. There is no discernible difference in the Fe oxidation states between 0 and 2+ in Fe-doped $\beta\text{-Mo}_2\text{C}$. The valence bands (VB) are altered by the partly oxidized Fe, leading to wider VB. Tests using the HER indicate that Fe-doped $\beta\text{-Mo}_2\text{C}$ is a more active electrocatalyst than pure $\beta\text{-Mo}_2\text{C}$ made from different sources of molybdenum. The wider valence bands of $\beta\text{-Mo}_2\text{C}$, more carbon-based graphitic supports, and the highly active $\text{Fe}_2(\text{MoO}_4)_3$ product on the outermost layer following Fe doping are all thought to be responsible for this increased activity shown in (Figure 6c).⁶⁶ *Feng Li and co-workers* have reported the different Fe doping levels for the optimized porous cobalt phosphide polyhedron indicate substantially better HER performance. It has lower onset overpotentials, higher current densities, less tafel slopes, and superior electrochemical

stability throughout HER. By using Co and Fe-containing MOFs in a one-step phosphorization procedure at a low temperature, porous polyhedrons containing CoP doped with Fe were developed. The $\text{Co}_{0.68}\text{Fe}_{0.32}\text{P}$ precursor sample, according to morphological examination, has a structure made up of uniformly dispersed MIL-88B related to ZIF-67 polyhedrons each with an average size of 2 μm . The energy-dispersive spectroscopic spectra of Co and Fe were used to validate their elemental makeup. $\text{Co}_{0.68}\text{Fe}_{0.32}\text{P}$ outperformed previous non-noble-based electrocatalysts described in the literature in terms of long-term stability and significantly enhanced electrocatalytic activity for the HER with overpotentials as low as 116 mV in 10 mA cm^{-2} .⁶⁷ *Pengyan Wang and co-works* have reported that $\text{Ni}_{1.85}\text{Fe}_{0.15}\text{P}$ nanosheet arrays over nickel foam electrodes (NSAs/NF) demonstrate exceptional and very stable electrocatalytic activity for HER. Fe-doping causes a little shift in the diffraction peaks to greater angles, indicating that Fe ions have been substituted within the Ni_2P lattices. Because the atomic sizes of Ni and Fe are comparable the crystalline structure of Ni_2P does not change when Ni is replaced with Fe. The resulting $\text{Ni}_{1.85}\text{Fe}_{0.15}\text{P}$ nanosheet arrays over a (NSAs/NF) electrode show extraordinary electrocatalytic activity in the HER and they require just 106 mV overpotentials to reach a current density of 10 mA cm^{-2} and to remain stable for 20h.⁶⁸ *Can Lin and co-workers* have reported that the Fe-Co_xP NPs were grown in a single step by adding iron while a metal-organic framework (ZIF-67) was synthesized *in situ* method and then treated with phosphate. An insignificant amount of iron phosphide was formed which helped with charge redistribution and improved the electrocatalyst's catalytic activity in concert. The performance of CoP's HER was enhanced by the addition of Fe. This enhancement can be ascribed to the difference in the electronegativities between the Fe and Co which promotes the faster rate of H_2O breakdown and increases the adsorption and bonding capacity to the intermediate H produced during HER. XPS reveals successful Fe doping in CoP, with dominating Co-P bonding and minor Fe-P species, whereas surface oxidation introduces M-O bonds. The small amount of iron phosphide causes charge redistribution, which improves electrocatalytic performance. The optimized $\text{Fe}_{0.27}\text{Co}_{0.73}\text{P}$ exhibits a very low overpotential of 186 mV at a current density of 10 mA cm^{-2} , and it remains stable for an amazing 40h.⁶⁹ *Hasosen Fan and co-workers* have developed the HER performance of Ni_3C nanosheets that operate doped with 2.0 at% Fe nanodots is remarkable. The electrical characteristics and surface properties of Ni_3C are optimized by the addition of Fe which results in increased catalytic efficiency during the generation of hydrogen. In particular, in a KOH solution, the Fe-doped Ni_3C nanosheets demonstrate exceptional electrocatalytic characteristics for HER including a modest tafel slope of 41.3 mV dec⁻¹ and a low overpotential of 292 mV shown in (Figure 6d).⁷⁰ The Fe-doped HER electrocatalysts are summarised in Table 2.

4.1.2 Co-Doped Electrocatalysts for HER



ARTICLE

Journal Name

Cobalt doping is a tactical technique used in electrocatalysis particularly to improve catalyst performance in the HER. Small quantities of cobalt are added to the catalyst lattices which can effectively change the electronic structure. When cobalt is doped into catalyst materials it encourages the adhesion and breakdown of water molecules which increases the overall reaction efficiency. And because of its modest H-bonding energy cobalt is thought to be a possible catalyst for the HER. Cobalt doping has several benefits including as low cost, stability in electrochemical settings, and advantageous electrical characteristics.^{71–73} As reported by *Di Yan Wang and co-workers* co-doped nanosheets of iron pyrite FeS_2 were synthesized and closely bonded with nanotubes of carbon ($\text{Fe}_{1-x}\text{Co}_x\text{S}_2/\text{CNT}$ hybrid catalysts). To crystallize the $\text{Fe}_{1-x}\text{Co}_x\text{S}_2$ catalysts and decrease the CNT a high-temperature solvothermal technique was employed in conjunction with the low-temperature fluid phase reaction during the synthesis. Comparing the FeS_2 -CNT and $\text{Fe}_{0.9}\text{Co}_{0.1}\text{S}_2$ -CNT surfaces to the Pt (111) surface the former showed similar molecules of hydrogen adsorption energy (EH_2) and just slightly greater hydrogen adsorption energy (EH). The findings demonstrate a low overpotential of about 120 mV at 20 mA cm⁻² and long-term durability that exceeds 40h of continuous HER function. DFT

results show that addition of Co to FeS_2 catalysts lowers the energy barrier for hydrogen atom adsorption in transition state 1 (TS_1).⁷⁴ *Guoyuan and co-workers* first time reported a unique catalyst $\text{Co-WSe}_2/\text{MWNTs}$ was effectively synthesized as a heterostructure for the electrocatalytic HER process shown in (Figure 7a). By using the MWNTs for a very effective topological template curved Co-WSe_2 nanosheets were easier to nucleate and develop resulting in an abundance of readily available active sites. Cobalt atoms increased the inherent activity of these active sites in TMDs by bringing the ΔGH closer to 0 eV. Because of MWNT's remarkable conductivity and the close contact between Co-WSe_2 nanosheets along with MWNT electrons may move quickly across the catalyst. The resultant $\text{Co-WSe}_2/\text{MWNTs}$ show an overpotential of 174 mV at 10 mA cm⁻² promising electrocatalytic capability.⁷⁵ *Bora Seo and co-workers* have reported that the successful addition of cobalt to MoS_2 by covalent doping is demonstrated by the notable enhancement in HER activity. This alteration successfully affects the electronic configuration of MoS_2 in addition to causing dynamic alterations in the atomic structures of the catalyst under operando circumstances. XPS shows mixed $\text{Mo}^{4+}/\text{Mo}^{5+}/\text{Mo}^{6+}$ states and increasing surface oxidation with decreasing MoS_2 layer number, indicating the development of

S. No	Catalyst	Electrolyte	Overpotential (η) At 10 mA cm ⁻²	Tafel slope (mV dec ⁻¹)	C_{dl} (mF cm ⁻²)	Stability (hours)	Reference
1	$\text{Fe}_{0.9}\text{Co}_{0.1}\text{S}_2$ -CNT	0.5 M H_2SO_4	120 at (20 mA cm ⁻²)	46	-	40h	⁷⁴
2	$\text{Co-WSe}_2/\text{MWNT}$	1.0 M KOH	174	37	1.9	3h	⁷⁵
3	$\text{Co-MoS}_2/\text{BCCF2}$	1.0 M KOH	48	52	-	12h	⁷⁶
4	Co- Mo_2C nanowires	0.5 M H_2SO_4	140	39	7.51	24h	⁷⁷
5	$\text{Co}_2\text{Mo}_9\text{S}_{26}$	0.5 M H_2SO_4	260	64	-	4h	⁷⁸
6	$\text{Co-Ni}_3\text{S}_2$ @CNT/GNF	6.0 M KOH	115	138	-	20h	⁷⁹
7	CoMoS-2-C	0.5 M H_2SO_4	135	50	-	3h	⁸⁰
8	$\text{Co}_{0.1}\text{Ni}_{0.75}\text{Se}/\text{rGO}$	0.5 M H_2SO_4	103	43	1.71	30h	⁸¹
9	$(\text{Cu}_{0.83}\text{Co}_{0.17})_3$	0.5 M H_2SO_4	46	32	-	24h	⁸²
10	$\text{Co-MoS}_2/\text{NiS}_2/\text{CC}$	0.5 M H_2SO_4	92	47	-	40h	⁸³

Table 3. Co-Doped Electrocatalysts for HER



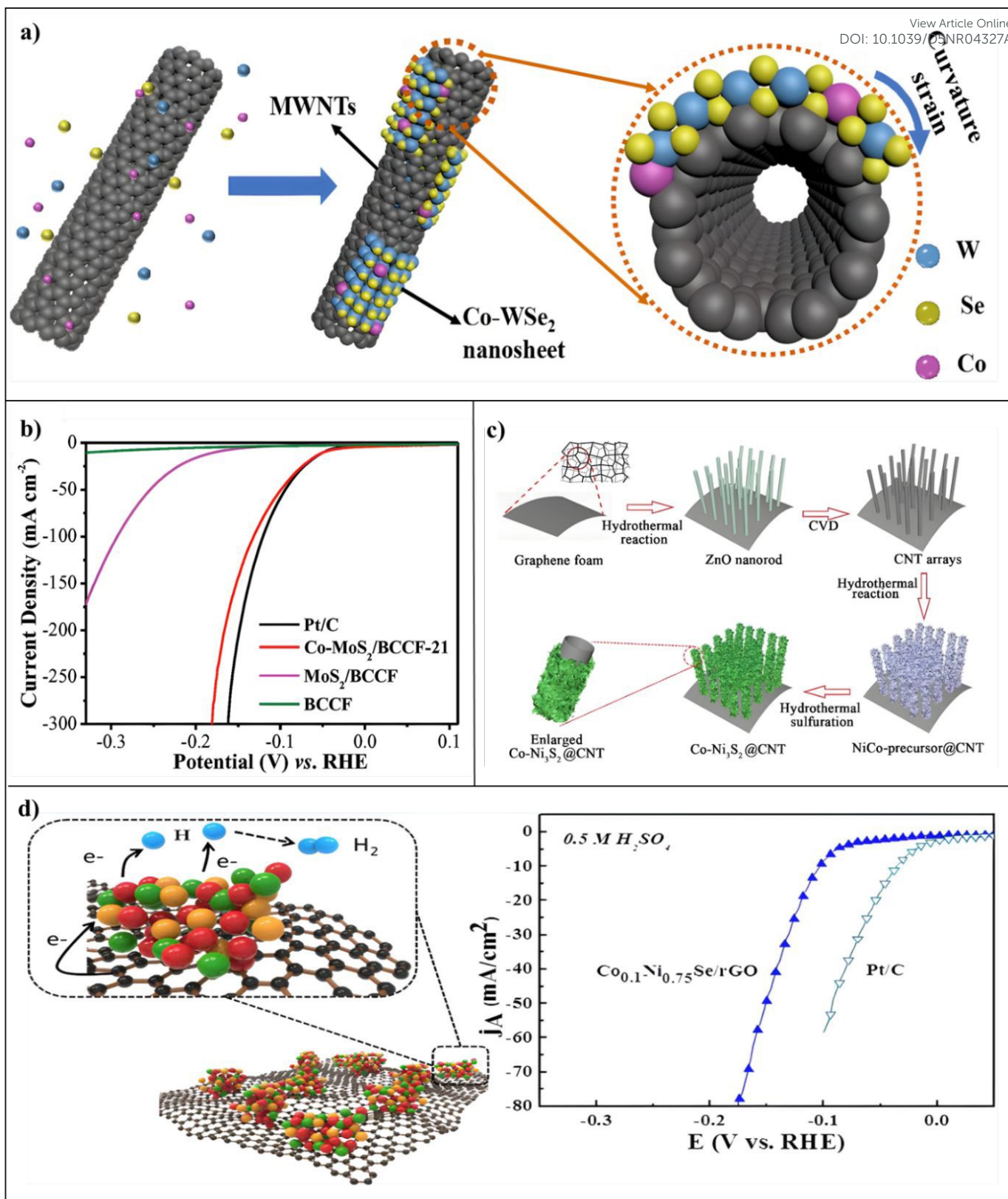


Figure 7. (a) A schematic representation of the heterostructure formed by Co-doped WSe_2 /MWNT synthesis. reproduced from Ref.[⁷⁵] with permission. Copyright 2018, RSC. (b) The HER polarisation curves for Co-MoS₂/BCCF-21. reproduced from Ref.[⁷⁶] with permission. Copyright 2018, Wiley. (c) A demonstration of the Co-Ni₃S₂@CNTs/GNF synthesis process. reproduced from Ref.[⁷⁹] with permission. Copyright 2013, RSC. (d) LSV curves for $\text{Co}_{0.1}\text{Ni}_{0.75}\text{Se}/\text{rGO}$. reproduced from Ref.[⁸¹] with permission. Copyright 2018, ACS.

distorted 1T-MoS₂ with more exposed edge sites. The transition from S^{2-} to unsaturated S_2^{2-} ligands, along with increased

oxidation, leads to more active sites and better HER activity. In DFT study shows the Mo-adjusted electron density lowers the

ARTICLE

Journal Name

free energy of hydrogen adsorption which eventually improves HER performance. Interestingly, MoS_2 doped with covalent coupling cobalt has a low overpotential of around 48 mV at 10 mA cm⁻² shown in (Figure 7b).⁷⁶ *Huanlei Lin and co-workers* developed the simple cobalt doping approach used to improve the electrocatalytic HER on Mo_2C nanowires using Co-modified MoO_x -amine precursors. When co-doping is effective inside the Mo_2C crystal structure the electron density increases near the fermi level weakening the Mo-H bond and promoting HER kinetics. Co is already well-known for maximizing the catalytic activity of active components in electrocatalysis. Its effectiveness is attributed to surface composition and customized electrical characteristics which are essential for catalytic turnover. The Co- Mo_2C nanowires show a modest overpotential of 140 mV at 10 mA cm⁻² as anticipated.⁷⁷ *Isolda Roger and co-workers* have reported the direct synthesis of a ternary chalcogenide with its constituents $\text{Co}_2\text{Mo}_9\text{S}_{26}$ using fluorine-doped tin oxide (FTO) electrode produced a compound with good HER activity. The direct hydrothermal depositing of metal chalcogenides onto thin oxide electrodes has not yet been reported despite the simplicity and scalability of these procedures. This development might simplify the field by removing the requirement for distinct stages for catalyst deposition and hydrothermal synthesis. XPS reveals the presence of Mo, Co, and S on the film surface, with Mo primarily in the Mo^{4+} state and minor $\text{Mo}^{5+}/\text{Mo}^{6+}$ species from surface oxides. Co has mixed $\text{Co}^{2+}/\text{Co}^{3+}$ valence states, while sulfur mostly occurs as S^{2-} , which is compatible with MoS_2 -based materials. A high-resolution spectrum in the Co 2p region confirmed the presence of cobalt on the film surface exhibiting two a dual state of Co^{2+} and Co^{3+} that support increased HER activity. In acidic conditions, these films demonstrate impressive HER activity attaining current densities of 10 mA cm⁻² at a moderate overpotential of 260 mV.⁷⁸ *Feifei Wang and co-workers* have developed the robust electrical conductivity is demonstrated by a CNT/GNF hybrid with a three-dimensional in nature conductive network that includes Co-doped Ni_3S_2 nanoparticles that are produced using a simple hydrothermal technique shown in (Figure 7c). During the redox process, the tectorum-like Co- Ni_3S_2 nanosheet geometry improves both ion and electron transport. When cobalt doping is added the electrochemical characteristics are greatly enhanced and, in comparison to other materials, the theoretical specific capacity is exceptional. In alkaline solution, the Co- Ni_3S_2 @CNT/GNF electrode has excellent HER activity attaining the lowest overpotential of 155 mV at 10 mA cm⁻².⁷⁹ *Xiaoping Dai and co-workers* have reported the cobalt doping of molybdenum disulfide was carried out using a deposition and precipitation technique to guarantee that it would not interfere with industrial operations. A thorough investigation was conducted into the effect of Co doping on molybdenum disulfides for HER performance. CoMoS-2 resembles MoS_3 with many bridging disulfides (S_2^{2-}), while CoMoS-2-C and MoS-C are closer to MoS_2 due to Co substitution at MoS_2 edges and enhanced crystallinity. The XPS spectra confirm dominant, well-dispersed CoMoS phases on carbon, with mixed Mo oxidation states, $\text{S}_2^{2-}/\text{S}^{2-}$ ligands, and little Co_9S_8 production. DFT

calculations reveal a trend in HER activity in doped catalysts. The optimized Co-doped MoS_2 catalyst exhibits a low onset potential, favorable tafel slope, and a high exchange current density all of which significantly improve HER performance. The generation of a Co-Mo-S phase is responsible for this enhancement as is the efficient reduction of charge-transfer impedance the promotion of structural and electrical modulations among MoS_2 and Co and the optimization of active surface area. With its low starting potential of 90 mV modest tafel slope of 50 mV dec⁻¹ and high exchange current density of 0.03 mA cm⁻² the optimised CoMoS-2-C catalyst exhibits remarkable HER performance.⁸⁰ Unique Cobalt-Doped $\text{Ni}_{0.85}\text{Se}$ Chalcogenides ($\text{CoxNi}_{0.85-x}\text{Se}$) have been reported by *Wenjun Zhao and co-workers* as stable and extremely effective catalysts for the hydrogen evolution process during the electrolysis of water. The $\text{CoxNi}_{0.85-x}\text{Se}$ catalysts have unique physical characteristics when compared with pure $\text{Ni}_{0.85}\text{Se}$, leading to diverse catalytic outcomes for HER. In comparison to unsupported $\text{Co}_{0.1}\text{Ni}_{0.75}\text{Se}$ catalysts, experimental data show that $\text{Co}_{0.1}\text{Ni}_{0.75}\text{Se}/\text{rGO}$ displays a smaller Tafel slope and a lower overpotential. The incorporation of rGO is associated with this improvement because it effectively stops $\text{Co}_{0.1}\text{Ni}_{0.75}\text{Se}$ from combining, exposing more active sites and enhancing conductivity and ECSA. By reducing the HER overpotential by 103 mV at a current density of 10 mA cm⁻², the $\text{Co}_{0.1}\text{Ni}_{0.75}\text{Se}/\text{rGO}$ catalyst produces a lower Tafel slope of 43 mV/dec shown in (Figure 7d).⁸¹ The electrochemical activity of the ($\text{Cu}_{0.83}\text{Co}_{0.17}\text{)}_3\text{P}:3\text{S}$:30S catalyst for the HER process has been reported by *Prasad Prakash Patel and co-workers*. Like noble metal catalyst systems, the simultaneous incorporation of S and Co into the Cu_3P lattice offers a unique chance to modify its electronic configuration and physical, electrical, and electrocatalytic capabilities. When Compared to Pt/C the ($\text{Cu}_{0.83}\text{Co}_{0.17}\text{)}_3\text{P}:3\text{S}$ system showed equivalent or better-applied bias photon-to-current efficiency during evaluation as a HER catalyst. Theoretical and experimental results demonstrate that ($\text{Cu}_{0.83}\text{Co}_{0.17}\text{)}_3\text{P}:3\text{S}$ nanoparticles display Pt-like electrochemical performance across all pH conditions. DFT and XPS confirm that the insertion of Co and S into the Cu_3P lattice affects the electrical structure. The development of a single-phase hexagonal structure resembling Cu_3P was confirmed by structural study. Importantly, at 10 mA cm⁻², the produced catalyst showed a low overpotential of 46 mV.⁸² Cobalt doping in $\text{MoS}_2/\text{Ni}_3\text{S}_2$ nanosheet array catalysts has been reported by *Yunhua Zheng and co-workers* to improve the hydrogen evolution process. By combining Co-MoS₂ nanosheets in order with Ni_3S_2 nanosheets, a simple three-step hydrothermal technique was used to produce the Co-doped $\text{MoS}_2/\text{Ni}_3\text{S}_2$ nanosheet arrangement in situ on a carbon cloth substrate (Co-MoS₂/Ni₃S₂/CC). The Co-MoS₂/Ni₃S₂/CC structure that results from the addition of Co atoms and multiple heterostructures provides high conductivity and a large number of accessible active sites, which promotes a synergistic effect that improves the electrocatalytic capabilities for HER. Additionally, efforts have been directed at enhancing MoS_2 electrocatalysis using morphological management, heterostructure development, heteroatomic doping, and the use of conductive substrates to



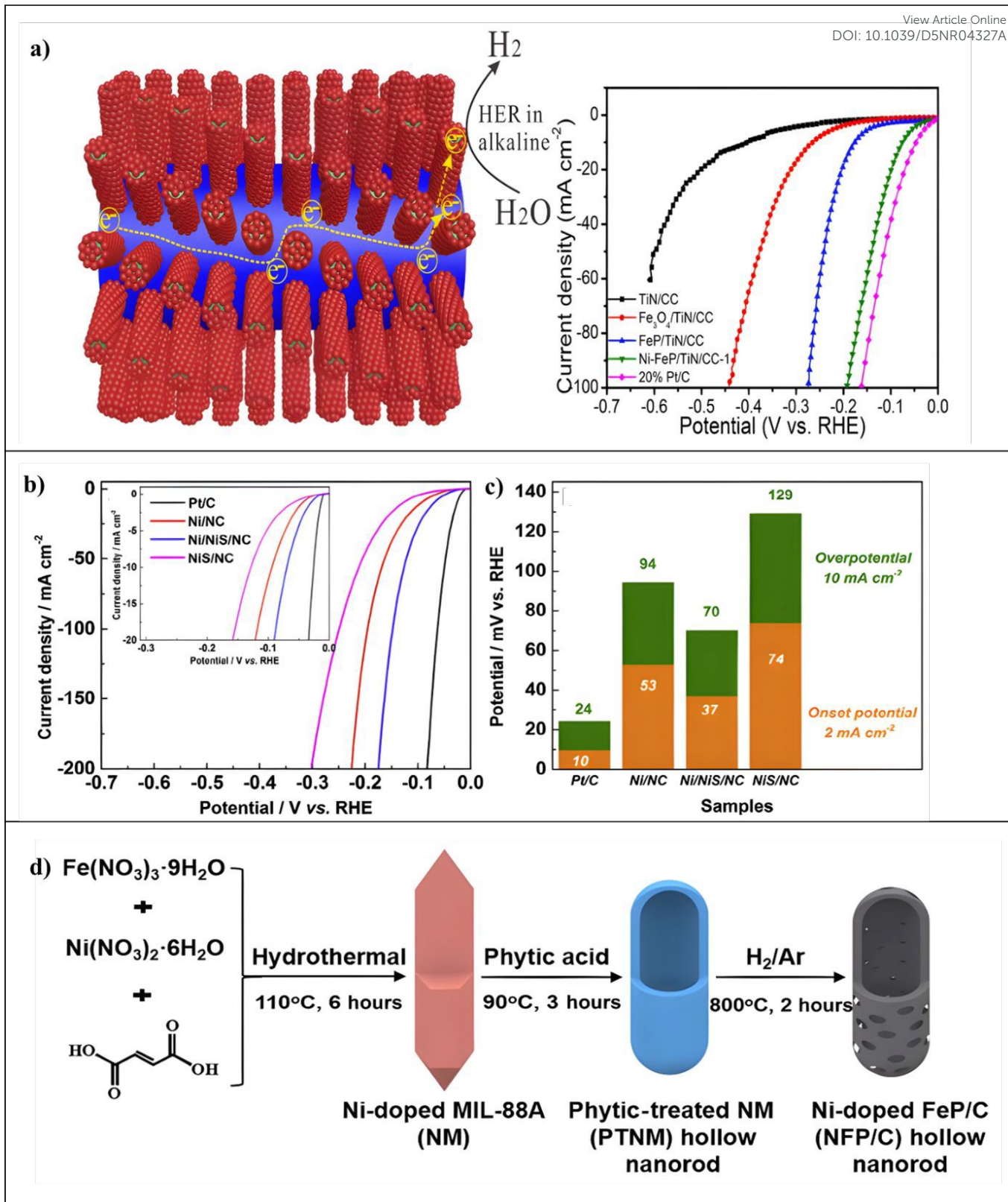


Figure 8. (a) A diagrammatic illustration of the hierarchical Ni-FeP/TiN/CC electrocatalyst preparation process and curves of polarisation. reproduced from Ref.[⁸⁵] with permission. Copyright 2018, Elsevier. (b) Ni/NC, Ni/NiS/NC, NiS/NC, and commercial Pt/C catalysts LSV curves in 1 M KOH at a scan rate of 5 mV s⁻¹; (c) The catalysts spectrum of onset and overpotential reproduced from Ref.[⁸⁹] with permission. Copyright 2018, Elsevier. (d) Diagrammatic representation of the Ni-doped FeP/C hollow nanorod production. reproduced from Ref.[⁹³] with permission. Copyright 2019, Science.

raise conductive properties and active site accessibility. Interestingly, the optimized Co-MoS₂/NiS₂/CC electrocatalyst shows outstanding electrocatalytic activity simultaneously in

0.1 M KOH, with a low overpotential of 92 mV and 122 mV to generate current densities of 10 and 50 mA cm⁻² in 0.5 M H₂SO₄. In addition, the catalyst exhibits remarkable long-term stability

ARTICLE

Journal Name

with a Tafel slope of just 47 mV dec^{-1} .⁸³ The Co-doped HER electrocatalysts are summarised in **Table 3**.

4.1.3 Ni-Doped Electrocatalysts for HER

Referring to the widely known volcano-type curve for the HER, Nickel (Ni) metal is located close to the peak, indicating that it can successfully modify the ΔG_{H^*} for the benefit of HER catalysis. Observations have shown that Ni^{2+} ions could break the H-OH connection which accelerates the breakdown of water molecules into protons. As in the cases of iron (Fe) and cobalt (Co) doping the primary mechanism underlying the increased activity of Ni-doped electrocatalysts is the modification of the electronic configuration that occurs following the addition of Ni atoms. Since strong metal-support contacts arrive Ni-doped catalysts exhibit increased stability and reduce catalytic degradation over prolonged electrochemical cycling. By altering surface charge distribution and promoting proton transfer activities at the catalyst-electrolyte interface nickel doping also affects electrolyte relationships. Moreover, nickel addition modifies TMDs' electrical structure promoting effective electron transport during the HER.^{91,94,95} *Xin-Yao Yu and co-workers* have reported Ni-Co-MoS₂ nanoboxes showing increased electrocatalytic activity for hydrogen evolution. Uniform Ni-Co Prussian blue

doped into MoS₂ nanosheets. Specified Ni-Co-MoS₂ nanoboxes made from very thin nanosheets were the final product of these methods. The hollow structure and large surface area of ultrathin MoS₂ nanosheets promote electrochemical responses; edge-terminated structures boost electroactive sites; defect-rich MoS₂ nanosheets reveal more active edges; and doping transition metals optimise electrical structures and expand interlayers are some of the reasons for the enhanced HER activity of Ni-Co-MoS₂ nanoboxes.⁸⁴ Ni-incorporated amorphous FeP nanoparticles porous TiN nanowires, and graphitic carbon fibers (Ni-FeP/TiN/CC) were synthesized in a hierarchical structure by *Xiang Peng and co-workers* using a step-by-step method. To modify the electrical structure of the FeP/TiN/CC composite to produce an amorphous surface, they used plasma implantation of Ni ions. The HER efficiency was greatly increased by this simultaneous doping and amorphization technique. An active amorphous surface a conducting nanowire scaffold, and the complementary actions of Ni and Fe atoms in the nanoparticles are responsible for the catalyst's remarkable efficiency. High densities of active sites are exposed by these characteristics, which also enhance charge transfer effectiveness and inhibit catalyst movement

S. No	Catalyst	Electrolyte	Overpotential (η) At 10 mA cm ⁻²	Tafel slope (mV dec^{-1})	C_{dl} (mF cm ⁻²)	Stability (hours & Cycles)	Reference
1	Ni-Co-MoS ₂	0.5M H ₂ SO ₄	155	51	11.7	1000 CV cycles	84
2	Ni-FeP/TiN/CC	1M KOH	71	73	-	10h	85
3	NiMo ₂ C/NF	-	150 at (100 mA cm ⁻²)	36.8	-	10000 CV cycles	86
4	Ni ₃ FeN/CC	1M KOH	105	61	52.55	20h	87
5	Ni _{2.3%} -CoS ₂ /CC	1M KOH	231 at (100 mA cm ⁻²)	106	-	12h	88
6	Ni/NiS/NC	1M KOH	70	45	22.19	3000 CV cycles	89
7	CoNi-HNP	1.0M PBS	41	35	130	20h	90
8	Ni-MoSe ₂	1M KOH	181	83	21	12h	91
9	Ni-CoP/Co ₂ P	1M KOH	125	73	4.4	12h	92
10	Ni-FeP/C	1M KOH	70	54	80.2	12h	93

Table 4. Ni-Doped Electrocatalysts for HER

analogue nanocubes were produced using a modified precipitation technique. Following that, nickel and cobalt were

and formation. For an overpotential of 75 mV and a cathodic current density of 10 mA cm⁻² the Ni-FeP/TiN/CC catalyst



exhibits outstanding HER performance shown in (Figure 8a).⁸⁵ Direct fabrication of Ni-doped Mo₂C nanowires on Ni Foam was reported by *Kun Xiong and co-workers* using a hydrothermal reaction together with a carburization procedure. The rationale for the increased catalytic activity of NiMo₂C/NF is the higher intrinsic activity that results from the synergistic interactions between Ni and Mo₂C. This is made possible by the 1D structure's high aspect ratio and large surface area which expose multiple Ni-doped Mo₂C sites. The computations using DFT show that adding Ni to Mo₂C modifies the charge distribution of the catalyst resulting in a synergistic effect that lowers the hydrogen binding energy. In addition to a low starting overpotential of 21 mV electrochemical studies show that the NiMo₂C/NF catalyst that was developed has good catalytic effectiveness for producing hydrogen. XPS confirms Mo₂C development with negligible surface oxides and no metallic Mo, which aligns with XRD data. Ni presence causes Mo 3d peak shifts and partial phase separation. Ni exists as both metallic and substituted species inside the Mo₂C lattice. Moreover, only 150 mV overpotential is needed to attain a 100 mA cm⁻² cathodic current density.⁸⁶ A 3D hierarchical catalyst made from Ni₃FeN for water splitting has been reported by *Zhihe Liu and co-workers*. To improve electronic conductivity and produce 3D conductive networks, carbon cloth was used as the scaffold. Ni₃FeN in the composite was produced using electrodeposition, which provides an effective process appropriate for large-scale manufacturing. A study into the bimetallic Ni₃FeN's development mechanism showed that Ni₃Fe functioned as an intermediary throughout the nitridation process affecting the final Ni₃FeN nano framework shape. A suggested mechanism highlights how both cationic atoms Ni and Fe work together to improve electrocatalytic activity. The composite not only shows excellent stability but also increased electrocatalytic activity, as shown by electrochemical experiments. In addition to an overpotential of 105 mV at 10 mA cm⁻² for the hydrogen evolution process, the Ni₃FeN/CC hierarchical electrocatalyst exhibits noticeably improved electrochemical characteristics for water splitting.⁸⁷ *Weizhen Fang and co-workers* reported an improved electrocatalyst that shows remarkable durability and efficiency for water splitting. It is composed of an array of Ni-doped cobalt di-sulfide nanowires supported on carbon cloth (Ni_{2.3%}-CoS₂/CC). The CoS₂ is well-known for its great efficiency in the HER and has a crystal structure that catalyzes reactions by using Ni ions. The CoS₂ electrocatalyst enhanced by Ni not only increases HER but also speeds up the OER process. This study shows that Ni-promoted CoS₂ may act as a bi-functional catalyst in the alkaline medium for both OER and HER. The Ni_{2.3%}-CoS₂/CC electrode, in the end, reaches a current density of 100 mA cm⁻² at a 231 mV overpotential for HER.⁸⁸ *Jieting Ding and co-workers* developed a mesoporous carbon composite doped with Ni, S, and N that serves as a bi-functional electrocatalyst for the OER and HER in water electrolysis. The porous structure of this composite is formed by synthesizing an N-doped porous carbon framework using NaCl as a template and integrating nickel-sulfide/nickel nanoparticles inside; the matrix is 3d and its pore size distribution is calculated using DFT. The improved HER and OER

performance of Ni/NiS/NC over Ni/NC and NiS/NC is due to changed surface characteristics and chemical states, as shown by XPS analysis. Effective mass diffusion and the elimination of hydrogen and oxygen gasses produced during electrolysis are made possible by the mesoporous structure and large surface area of the carbon matrix. Enhancing electrocatalytic efficiency and preventing particle aggregation are two benefits of adding transition metal compounds into the carbon matrix. The most active catalyst produced in this study is very efficient for water electrolysis as evidenced by its low HER overpotential of 70 mV at 10 mA cm⁻² and Tafel slope of 45 mV dec⁻¹ shown in (Figure 8b,c).⁸⁹ *Muhammad Imran Abdullah and co-workers* developed a simple method for producing Ni-doped Co hollow nanoparticles (CoNi-HNP) by combining non-3d high-valance metal tungsten with non-metallic additives (B and P) in an ultrasonic-assisted chemical reduction process. Using this method, the HER adsorption energy is maximized. As the most effective non-noble metal electrocatalyst for hydrogen production in neutral solutions, CoNi-HNP outperforms Pt/C in terms of stability and activity during prolonged electrolysis durations. In neutral pH electrolytes, CoNi-HNP notably reaches a current density of 10 mA cm⁻² at a low overpotential of 41 mV. The amounts of P and B additions have a major impact on the catalytic activity of CoNi-HNP. Low overpotential allow for high current densities and consistent performance with heavy mass loading over extended electrolysis periods.⁹⁰ *Yaqian Yang and co-workers* reported that Ni-doped MoSe₂ nanosheets with Ni-Se bonds to improve alkaline electrocatalytic hydrogen evolution. Using an ethanol solution, NiO₂ was evenly distributed over MoSe₂. After annealing, the NiO₂ nanoclusters became approximately 4 nm in size and were attached to the MoSe₂ nanosheets with the help of Ni-Se bonds. DFT calculations revealed that additional catalytic sites were formed at dopant atoms or adjacent Mo- or Se atoms. XPS reveals the formation of Ni-Se bonding and lower valence. Ni species indicates electronic modulation, which leads to proton reduction and increases HER activity. MoSe₂ has potential as a catalyst for hydrogen evolution, but its large overpotential due to its low active site density limits its practicality. While Ni is deposited at a rate of 4.5 at. % in 1 M KOH, MoSe₂ nanosheets' active sites are increased and the overpotential is reduced to 181 mV at 10 mA cm⁻². Due to the Ni-Se bond's development, Ni-doped MoSe₂ also shows outstanding stability over 12hrs.⁹¹ In both acidic and alkaline conditions, Ni-doped CoP/Co₂P nanospheres have been reported by *Tianyun Chen and co-workers* to be highly effective and stable catalysts for hydrogen evolution. Ni-induced modifications to electron valence states, which work in concert with Co atoms to improve catalyst efficiency, are responsible for the enhanced catalytic activity and long-term stability of Ni-doped CoP/Co₂P nanospheres. Ni-doped CoP/Co₂P nanospheres preserve their shape during electrolysis which helps speed up mass and electron transport and increases overall stability. A multitude of active catalytic



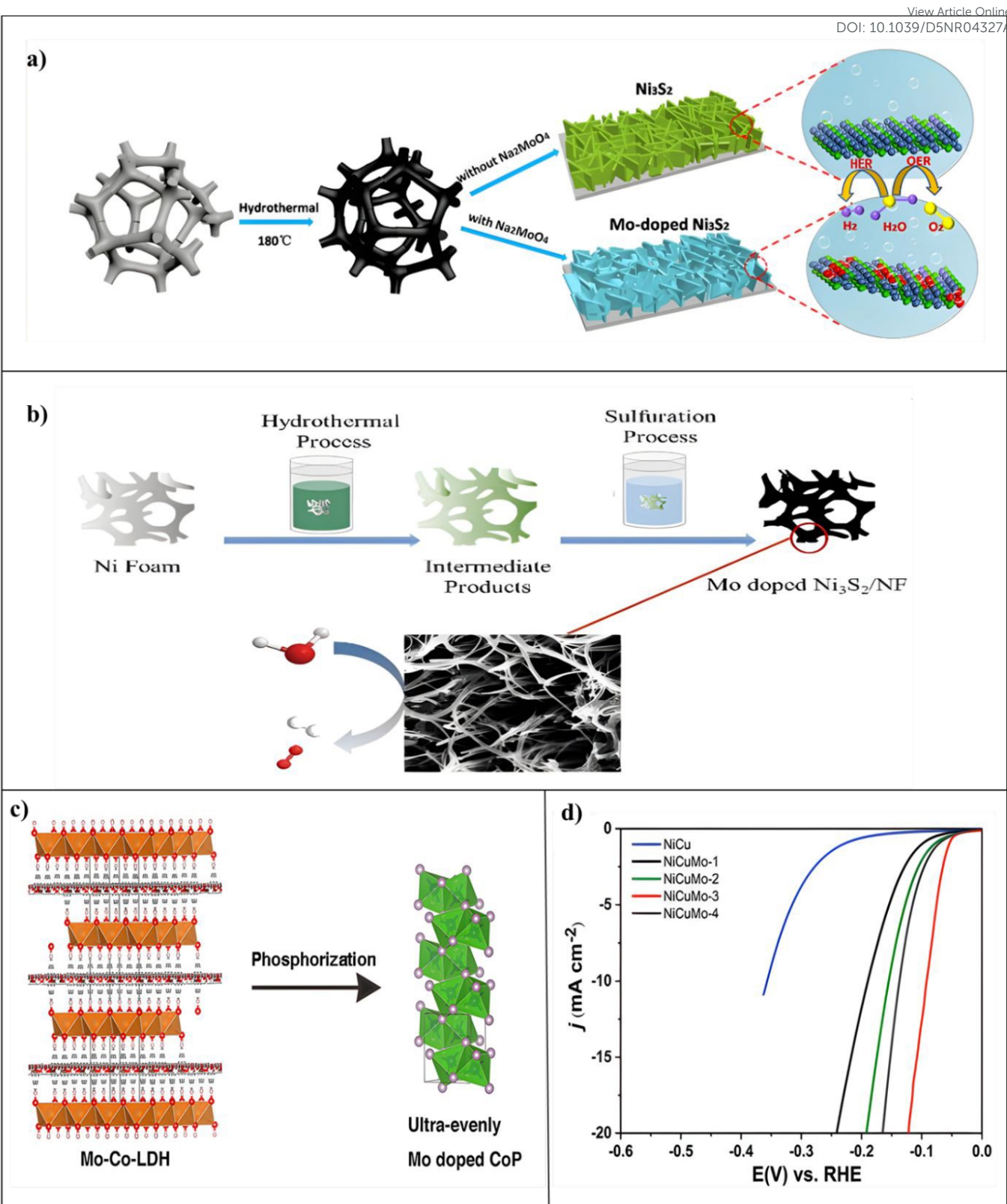


Figure 9. (a) A demonstration of the Mo-doped Ni_3S_2 nanosheet design. reproduced from Ref.[⁹⁶] with permission. Copyright 2018, Elsevier. **(b)** On nickel foam (NF), a 3D Mo-doped Ni_3S_2 nanowire network was successfully produced using a hydrothermal and sulfidation process. reproduced from Ref.[¹⁰³] with permission. Copyright 2018, Wiley. **(c)** Diagrammatic Representation of Ultra-Evenly Mo-Doped CoP Composite Formation. reproduced from Ref.[¹⁰¹] Copyright 2021, ACS. **(d)** NiCu and NiCuMo catalysts electrocatalytic HER performance in 0.5 M H_2SO_4 . reproduced from Ref.[⁹⁸] Copyright 2019, RSC.

sites are exposed, and a fast evolution of hydrogen gas is encouraged by the synergistic impact of Ni and CoP/Co₂P, which the energy needed for hydrogen absorption. A current density of 10 mA cm^{-2} is attained by this catalyst at an overpotential of

100 mV.⁹² In both acidic and alkaline conditions, Ni-doped FeP/C hollow nanorods have been reported by *Yan Zhou Lu and co-workers* to be highly effective and stable catalysts for hydrogen evolution shown in (Figure 8d). Ni-induced modifications to electron valence states, which work in concert with Co atoms to improve catalyst efficiency, are responsible for the enhanced catalytic activity and long-term stability of Ni-doped FeP/C hollow nanorods. These Ni-doped FeP/C hollow nanorods preserve their shape during electrolysis which helps speed up mass and electron transport and increases overall stability. DFT calculations provide insight into the catalytic role of nickel doping at the atomic level. XPS study shows that the catalyst's surface is oxidized to phosphates, that electrons are transferred from P to Fe as demonstrated by a negative shift for Fe 2p and a positive shift for P 2p shifts, and that Ni doping increases phosphide content. A multitude of active catalytic sites are exposed, and a fast evolution of hydrogen gas is encouraged by the synergistic impact of Ni and FeP/C, which lowers the energy needed for hydrogen absorption. A current density of 10 mA cm⁻² is attained by this catalyst at an

overpotential of 95 mV in alkaline medium.⁹³ The Ni-doped HER electrocatalysts are summarised in Table 4. View Article Online DOI: 10.1039/D5NR04327A

4.1.4 Mo-Doped Electrocatalysts for HER

Molybdenum doping influences morphology, conductivity, and interaction with other transition metals to maximize HER activity and stability, molybdenum doping in the HER has shown promise as a means of improving catalytic efficiency. As with other non-noble metal doping metals, the quantity of Mo doping influences catalytic performance as well. Therefore, the precise amount of doping needs to be carefully considered when designing catalysts. Mo doping also has a major effect on the catalyst's shape, promoting the formation of structures with large specific surface areas. On the other hand, too much Mo content may cause phase dissociation and reduce the activity of the catalytic process. As a result, it is difficult to precisely control Mo doping levels for a uniform distribution and ideal concentration. Moderate metal-H bonding might promote positive HER under such conditions. Furthermore, Mo improves the catalytic activity of carbides and provides pH-universal

S. No	Catalyst	Electrolyte	Overpotential (η) At 10mA cm ⁻²	Tafel slope (mV dec ⁻¹)	C _{dl} (mF cm ⁻²)	Stability (hours & cycles)	Reference
1	Mo-doped Ni ₃ S ₂	1M KOH	212	98	4.02	1000 CV cycles	96
2	Mo-Ni ₂ P NWs/NF	1M KOH	78	109	-	24h	97
3	NiMoCu-3	1M KOH	90	41	5.1	5000 CV cycles	98
4	Co _{0.8} Mo _{0.2} Se	0.5 M H ₂ SO ₄	186 at (100 mA cm ⁻²)	58.7	-	10h	99
5	200-SMN/NF	1M KOH	278 at (100 mA cm ⁻²)	72.9	-	-	100
6	CoMo-LDH	1M KOH	118	69	-	24h	101
7	Mo-doped Ni ₂ P HNs	1M KOH	81	53.4	38	10h	102
8	Mo _{5.9} Ni _{94.1} S/NF	1M KOH	61	39.2	11.4	-	103
9	Mo-Ni-NSs-3	1M KOH	91	62	30	50h	104
10	10% Mo-W ₁₈ O ₄₉	0.5 M H ₂ SO ₄	45	54	5.9	5000 CV cycles	105

Table 5. Mo-Doped Electrocatalysts for HER



ARTICLE

Journal Name

electrolysis with remarkable stability and characteristics. The observed improvement in HER activity is probably due to the synergistic action of Mo dopants together with other 3D transition metals. Mo dopants also result in exceptional electrocatalytic activity with low overpotential due to their porous design, enhanced electric conductivity, and cooperative effects with other transition metals.^{96,97,106} 3D arranged Molybdenum (Mo)-doped Nickel sulphide (Ni_3S_2) particles have been synthesized by *Chengrong Wu and co-workers* as an efficient dual-electrocatalyst for the overall splitting of water. This work aims to successfully synthesize Mo-doped Nickel sulfide (Ni_3S_2) three-dimensional (3D) curved nanosheets on Ni-foam using a one-step hydrothermal technique. Furthermore, a greater contact surface for adsorption, as well as desorption of electrolytes, was provided by the 3D fornicator design. Mo-inclusion has a significant impact on the structure and shape of Ni_3S_2 nanosheets shown in (Figure 9a). Additionally, when the electrode's surface and roughness grow due to Mo element doping more electrons from the electrolyte solution are adsorbed. The catalysts have exceptional electrochemical performance concerning HER. At 10 mA cm^{-2} , it displays a low overpotential of 212 mV which is a significant drop of 127 mV compared to un-doped nickel sulphide.⁹⁶ By the use of a two-step approach, *Yiqiang Sun and co-workers* have successfully synthesized Mo-incorporated Ni_2P nanowires (NWs) on a Ni foam (NF) substrate present, demonstrating their utility as a steady and strong electrocatalyst for HER throughout the pH spectrum (0-14). Molybdenum adding considerably increased the catalytic activity of Ni_2P , according to electrochemical analyses. After 24h of HER operation at different pH settings, Mo- Ni_2P NWs/NF demonstrated outstanding durability with low activity destruction. They needed overpotentials of 67 mV in acidic, 78 mV in alkaline, and 84 mV in neutral environments, as well, to reach a current density of 10 mA cm^{-2} . The remarkable HER performance can probably be ascribed to the mutually beneficial interaction between the atoms of Ni (Nickel) and Mo (Molybdenum).⁹⁷ *Zhengnan Wang and co-workers* used a single-step electrodeposition approach to produce a Mo-incorporated Ni-Cu catalyst for the HER catalysis. The catalyst's optimum composition of NiCuMo , with (8 % of Mo-content in solution) showed better HER performance than Ni-Mo and Ni-Cu catalytic compounds that were binary owing to the three metals' synergistic connection. Using the strong Molybdenum-H and weak Nickel-H binding, the combination of Nickel and Molybdenum enhanced HER activity in alkaline environments. Additionally, in comparison to the Ni-Mo catalyst the addition of copper greatly assisted in the produce of a thick solid nanoparticle shape. In an alkaline electrolyte, this Mo-incorporated Ni-Cu electrode (8 that% Mo-content in solution) outperformed both bimetallic Ni-Mo and Ni-Cu catalysts showing excellent electrochemical resistance and a minimal overpotential of 95 mV at a current density of 10 mA cm^{-2} . Bimetallic Ni-Mo and Ni-Cu catalysts show excellent electrochemical stability and a minimal overpotential of 95 mV at a current density of 10 mA cm^{-2} shown in (Figure 9d).⁹⁸ *Yan Zhou and co-workers* reported that molybdenum loading induced metallic characteristics in Co-Se by enhancing

the electrocatalytic synthesis of hydrogen. The existence of a mixed phase of $\text{Co}_0.8\text{Se}_{0.2}$ and $\text{Co}_0.8\text{Se}_{0.2}$ was required for the effective integration of Molybdenum. Molybdenum doping successfully tuned the crystalline and electronic configuration of Co-Se, causing lattice contracting and metallic properties that enhanced its electrocatalytic performance for the HER. This was confirmed by computational models, which showed that Molybdenum doping causes lattice contraction in Co-Se and causes the electron density of states to change in the direction of the Fermi level. The reduced cell volume and lower Co oxidation state are compatible with XPS and XANES studies, demonstrating that a small Mo substitution may compress the lattice despite Mo having a higher atomic radius than Co. Despite a small slope of Tafel of 58.7 mV dec^{-1} and the greatest HER activity of every substance examined, $\text{Co}_0.8\text{Mo}_{0.2}\text{Se}$ required only an 186.1 mV overpotential to reach a current density of 100 mA cm^{-2} .⁹⁹ An efficient and long-lasting electrocatalyst for water splitting can be synthesized by *Zheng Cui and co-workers* in their work, Optimized Synthesis of Mo-loaded Ni_3S_2 Nano-rods. As an instance of the way the atomic stoichiometric proportions of molybdenum and nickel may be controlled by varying the temperature of the reactions, they show that Mo-doped Ni_3S_2 can grow directly on nickel foams using sodium molybdate (Na_2MoO_4) as the Molybdenum source at different temperatures. DFT simulations and experimental investigations both demonstrate that the under-coordinated Mo-S sites on the outermost layer of MoS_2 have a high capacity for the hydrogen chemisorption process. XPS measurements were used to identify and characterize prominent constituent elements and their chemical valence states. A mild 278 mV overpotential at a 100 mA cm^{-2} hydrogen synthesis current density and a small 72.9 mV dec^{-1} Tafel slope is observed leading to increased reactions of hydrogen evolution performance.¹⁰⁰ *Liang Li and co-workers* developed an in situ phosphorization technique using CoMo-layered double hydroxide (CoMo-LDH) as the precursor for producing extremely uniform Mo-doped CoP materials (Mo-CoP). The well-organized cation configuration in the CoMo-Layer Double Hydroxide (LDH) promotes phosphorization, which produces molybdenum that is evenly distributed throughout the Co-P framework shown in (Figure 9c). This produces a remarkable bi-functional catalyst for the total splitting of water. Even molybdenum distribution inside the Co-P framework is facilitated by the ordered cation arrangement in the Layer Double Hydroxide nanosheet precursor, which occurs after in situ phosphorization. As a result, in acidic conditions, the molybdenum-doped cobalt phosphide shows increased HER activity and stability. The overpotential is just 116 mV when the current density in $0.5 \text{ M H}_2\text{SO}_4$ is 10 mA cm^{-2} .¹⁰¹ *Qin Wang and co-workers* report their results on creating Mo-doped Ni_2P hollow microspheres using a direct phosphorization approach in conjunction with a solvothermal process. The connected Gibbs free energy of H^* absorbance (ΔG_{H^*}) drops from 0.33 eV (P site) to 0.21 eV (bridge Mo-Ni site) after molybdenum doping, with the active centre transitioning to the molybdenum-



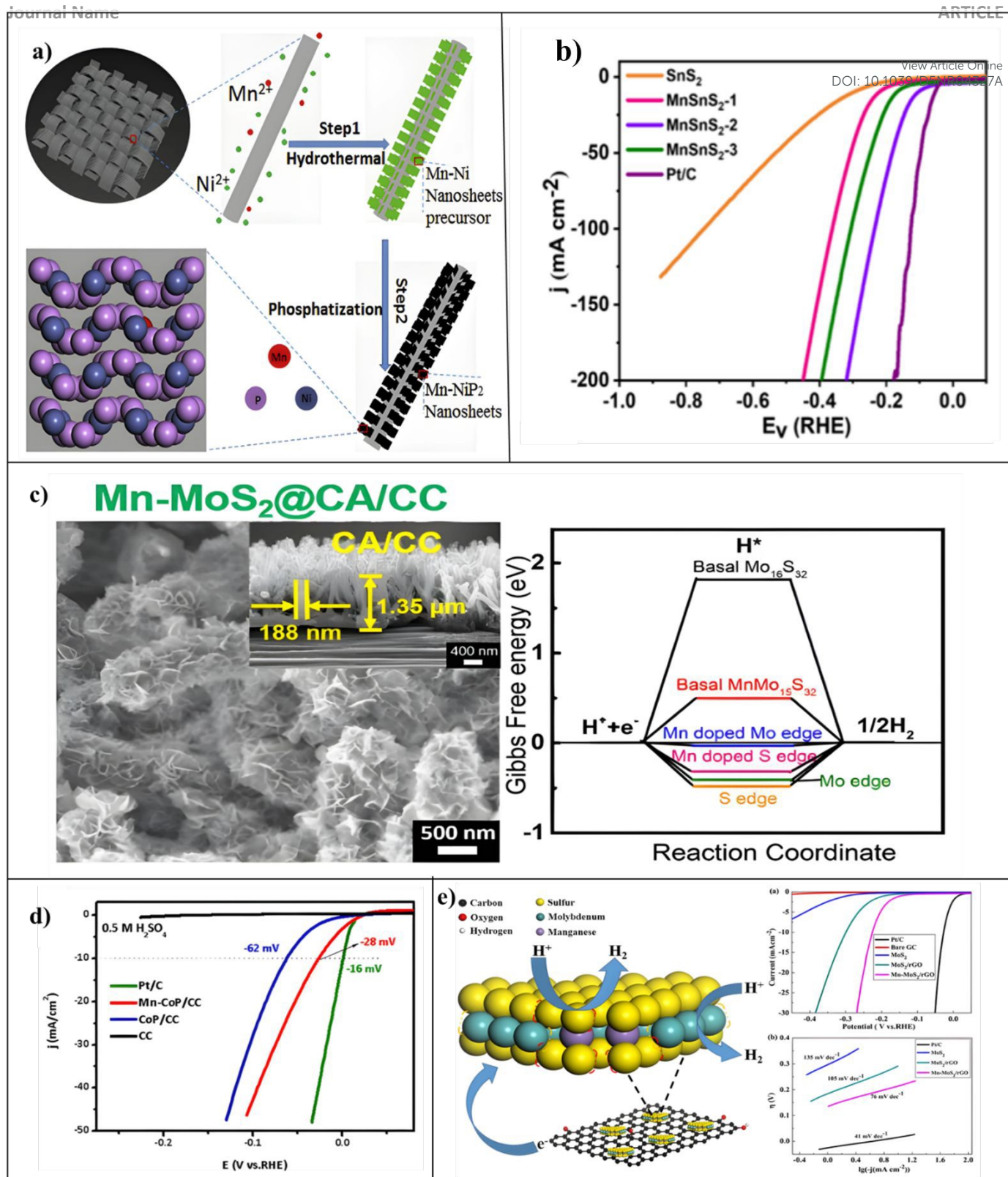


Figure 10. (a) Diagram showing the steps involved in creating manganese Mn-doped NiP₂ nanosheets over carbon cloth. reproduced from Ref.[¹¹⁰] with permission. Copyright 2018, Elsevier. (b) A demonstration of the process used to prepare the MnSnS₂-2. reproduced from Ref.[¹¹²] with permission. Copyright 2018, RSC. (c) TEM and HRTEM pictures of the 0.5 Mn-MoS₂ compound as well as a hydrogen ΔG_H^* diagram showing the dope and doped-free MoS₂. reproduced from Ref.[¹¹⁵] with permission. Copyright 2018, ACS. (d) The LSV curves for HER in 0.5 M H₂SO₄ for Mn-CoP/CC, CoP/CC, pure CC, and Pt/C catalysts at a scan rate of 1 mV/s. reproduced from Ref.[¹¹⁶] with permission. Copyright 2020, Elsevier. e) The Mn-MoS₂/rGO ball model. reproduced from Ref.[¹¹⁷] with permission. Copyright 2017, Elsevier.

nickel bridge site. The reduced ΔG_H^* of this ideal active site speeds up the charge exchange procedure for H* intermediates and results in the synthesis of H₂. With a modest Tafel slope of 53.4 mV dec⁻¹ and an inadequate overpotential of 81 mV (10 mA

cm⁻²) and the DFT results confirmed that the bridge Mo-Ni site was the active site in the alkaline HER process, with a ΔG_H^* of 0.21 eV. XPS confirmed that Mo-doped Ni₂P HNs have a greater intrinsic electrocatalytic property for electrochemical oxygen

ARTICLE

Journal Name

generation. The Mo-added Ni₂-P hollow microspheres demonstrate exceptional HER activity in the 1.0 M KOH approach.¹⁰² *Cheng Du and co-workers* synthesized a technique that uses a series of hydrothermal and sulfidation steps to produce 3D molybdenum-incorporated Ni₃-S₂ nanowire connections that are directly grown on nickel foam. The molybdenum-incorporated Ni₃-S₂/NF composite exhibits better catalytic activity due to its unique 3D hierarchical nanowire structures and effective molybdenum doping shown in (Figure 9b). The inherent features of Ni₃-S₂ are synergistically enhanced by the presence of molybdenum ions (Mo⁶⁺) in the solution containing the precursor which improves its catalytic activity towards the HER. In addition to changing the catalysts' morphology, molybdenum incorporation improves Ni₃-S₂'s electrical organization which affects the H₂/O₂ intermediates' binding energy during the water-splitting operation. To confirm the chemical states of Mo_{5.9}Ni_{94.1}S/NF, an XPS measurement was done. The resultant 3D network, Mo_{5.9}Ni_{94.1}S/NF exhibits impressive catalytic activity needing just 60.8 mV overpotentials to achieve 10 mA cm⁻² of current density for HER.¹⁰³ The development of ultrathin and hollow Molybdenum-Nickel nanosheet arrays as extremely effective electrocatalysts for the HER had been led by *Xiaoying Lu and co-workers*. Since molybdenum (Mo) may induce new active sites to boost electrochemical reactions and change the crystalline makeup of composites its distinctive physical and chemical features make Molybdenum-based materials especially appealing. Significantly, it has been shown that the bimetallic nickel-molybdenum catalysts because of their advantageous hydrogen binding power and greater corrosion resistance systematically show higher activity than pure nickel-based materials. The resultant Mo-Ni nano-sheets had a modest Tafel slope of 62 mV dec⁻¹ and an overpotential of 91 mV at 10 mA cm⁻² indicating improved HER effectiveness.¹⁰⁴ Molybdenum doping-induced improvements in the performance of urchin-like W₁₈O₄₉ nanostructures for the hydrogen evolution process have been developed by *Xing Zhong and co-workers*. Because the molybdenum dopant modifies associated chemical characteristics, more active sites develop, which accounts for Mo-W₁₈O₄₉'s improved water-splitting performance. Furthermore, the exposed large surface area of the urchin-like form decreases electronic transmission limits. These results are corroborated by density functional theory computations, which show that the Mo dopant's capacity to increase the number of active sites, optimizing the adsorption of hydrogen owing to electrical and geometric modification, is what allows for the notable performance improvement. Additionally, the 3-dimensional urchin-like shape with a lot of 1-dimensional nanowires facilitates electron transmission and ensures quick interfacial exchange of charges to improve electrocatalytic processes. The inherent enhancement in HER activity with Mo-W₁₈O₄₉ is demonstrated by both empirical and theoretical findings. With a modest starting potential of 23 mV and a Tafel slope of 54 mV dec⁻¹, the resulting 3D urchin-like Mo-W₁₈O₄₉ shows outstanding electrocatalytic activity for HER.¹⁰⁵ The Mo-doped HER electrocatalysts are summarised in Table 5.

4.1.5 Mn-Doped Electrocatalysts for HER

View Article Online

From the optimum use of its unique electrical and structural properties, manganese doping in the HER offers the potential for enhancing its catalytic effectiveness and stabilization, hence promoting the emergence of sustainable and effective techniques for producing hydrogen. The catalytic potential of transition metal-based catalysts is effectively activated by manganese doping, which results in lower |ΔG_{H*}| values. More active sites are generated by the addition of Mn doping, which causes mild atomic deformations and activates the HER.^{107,108} During catalysis, Mn-doped non-noble metal phosphides also show much lower |ΔG_{H*}| levels and overpotential over the pH range. Nevertheless, difficulties like phase dispersion and the ambiguity of the linkages between catalyst structures, doping concentrations, and electrocatalytic capabilities still exist.¹⁰⁹ Manganese-doped Ni-P₂ particles on carbon cloth (Mn-Ni-P₂ NSs/CC), which function better than pure Ni-P₂ in three dimensions and are more stable at all stages of pH, have been successfully synthesized by *Xiaodeng Wang and co-workers* shown in (Figure 10a). The addition of Mn increases the catalytic activity of NiP₂ from electrochemical analyses. With a high phosphorous material, the Mn-Ni-P₂ NSs/CC acts as a polyphosphide and provides many active sites that are favorable to catalytic activity. Increased specific surface exposure to catalytically active sites is provided by the 3D nano-sheet structure of Mn-Ni-P₂ NSs/CC which further facilitates electron transport. According to calculations using DFT the presence of Mn elevates the electrocatalytic performance by lowering the kinetic energy limit for H atom adsorption on the surface of Ni-P₂ NSs. XPS studies indicate that Mn doping leads to a reduced transfer of electron density from Ni to P, potentially improving HER performance. It takes overpotentials of 97 mV in 1.0 M KOH to get the same current density.¹¹⁰ Mn incorporation into pyrite CoSe₂, resulting in minor atomic rearrangements to provide more active edge sites for the HER, has been reported by *Youwen Liu and co-workers*. Using DFT simulations, it was discovered that Mn inside the CoSe₂ lattice lowers the kinetic energy barrier and promotes the formation of H-H bonds between neighbouring adsorbed hydrogen atoms, thereby improving H₂ generation. CoSe₂ ultrathin nanosheets doped with Mn provide a way to modify the electronic structure for HER dynamics that are optimal. Considering an exchange current density of 68.3 μA cm⁻², a quite modest Tafel slope of 36 mV/dec, and a very low overpotential of 174 mV these Mn-doped CoSe₂ ultrathin nanosheets indicate an impressive feat in HER performance.¹¹¹ *Tingting Liu and co-workers* report the first development of Mn-loaded Co-P (Mn-Co-P) nanosheets arranged on titanium mesh (Mn-Co-P/Ti) as an effective three-dimensional electrodes for the hydrogen evolution process with strong stability at all different pH values. Density functional theory simulations indicate that Mn-Co-P has a higher thermo-neutral hydrogen energy than Co-P which accounts for its increased HER activity. As the ΔG_{H*} gets closer to thermo neutrality, the catalytic activity of HER is enhanced. Further investigation of the electrical structures shows that neighbouring cobalt and phosphorous atoms get electron donations from doped Manganese atoms. The XPS spectrum of



S. No	Catalyst	Electrolyte	Overpotential (η) At 10mA cm ⁻²	Tafel slope (mV dec ⁻¹)	C_{dl} (mF cm ⁻²)	Stability (hours & cycles)	Reference DOI: 10.1039/D3NR04327A
1	Mn-NiP ₂ NSs/CC	1.0 M KOH	97	45	64.3	20h	110
2	Mn-incorporated CoSe ₂	0.5 M H ₂ SO ₄	174	36	-	2000 CV cycles	111
3	Mn-Co-P/Ti	1.0 M KOH	76	55	50.32	10h	108
4	MnSnS ₂ -2	1.0 M KOH	108	41	2.56	50h	112
5	Mn-FeP	1.0 M KOH	173	59	4.90	10h	109
6	Mn-Ni ₂ P/NF	1.0 M KOH	103 at (20 mA cm ⁻²)	135	3.98	25h	113
7	Mn-CoP	0.5 M H ₂ SO ₄	127	53	49.5	18h	114
8	0.5 Mn-MoS ₂ @CA/CC	0.5 M H ₂ SO ₄	130	44	40.4	2000 CV cycles	115
9	Mn-CoP PMFs/CC	1.0 M KOH	90	47.3	10.8	24h	116
10	Mn-MoS ₂ /rGO	0.5 M H ₂ SO ₄	110	76	17.37	2000 CV cycles	117

Table 6. Mn-Doped Electrocatalysts for HER

Mn-Co-P indicates the presence of Mn, Co, and P elements. Signals of C and O elements may be due to product contamination or surface oxidation. According to a Bader charge analysis, nearby cobalt atoms get up to 0.38 electrons from nearby Manganese atoms. The Mn-Co-P nano-array integrated on titanium mesh requires overpotentials of 49 mV and 86 mV in 0.5 M H₂SO₄ and 1.0 M KOH respectively to get a current density of 10 mA cm⁻².¹⁰⁸ Athibala Mariappan and co-workers studied Mn@SnS₂-2 to improve the hydrogen generation process. A simple doping approach for developing a S vacancy-rich Mn@SnS₂ electrocatalyst in alkaline medium (1MKOH). The as-synthesized Mn@SnS₂-2 catalyst exhibits outstanding bifunctional electrochemical performance, with overpotentials of 260mV (OER) and 108mV (HER) at 10mAcm⁻². The preparation process for the MnSnS₂ heterostructure material is given in (Figure 10b). The improved catalytic efficiency of the Mn@SnS₂-2 catalyst is due to the development of numerous Mn dopants generate sulfur defects. Doping Mn into SnS₂ crystal structure increases active sites, facilitates charge transfer, and improves intermediate adsorption and desorption.¹¹² Min Wang and co-workers developed a simple and regulated synthesis method for a mesoporous Manganese doped Fe-P (Mn-FeP) catalyst for the hydrogen evolution process that is both highly effective and persistent. Mesoporous Fe-P undergoes a broad pH range electroactivity boost due to

Manganese doping. Topology engineering and heteroatom implantation techniques work together to maximize the reaction kinetics for HER by increasing the specific surface area of Fe-P and altering its electronic makeup. Based on physical/electrochemical analysis and DFT calculations, it was determined that adjacent doped Mn atoms with weaker electron negativity provided partial electrons to the Fe atoms in Mn-FeP. This resulted in free energy for thermoneutral hydrogen adsorption on active sites, improving intrinsic activity. By utilizing a template-free technique to increase the specific surface area, this approach avoids the problems associated with traditional template approaches such as synthesis that is unpredictable and tedious and ensures the effective doping of Manganese into the phosphide. With overpotentials of 69 mV and 173 mV in H₂SO₄ and KOH electrolytes respectively, at 10 mA cm⁻² the mesoporous Mn-FeP catalyst demonstrates outstanding activity and stability for HER over an extended pH range.¹⁰⁹ The synthesis of Mn-doped Ni₂-P nanosheet arrangements on nickel foam (NF) (Mn-Ni₂-P/NF) as reported by Ya Zhang and co-workers and this catalyst serves as extremely effective electrodes for the hydrogen evolution process in alkaline environments. The electrical driving capacity of Mn-Ni₂-P/NF in 1.0 M KOH is 20 mA cm⁻² at an overpotential of 103 V which is 82 mV less than that required to operate Ni₂-P/NF. It also shows outstanding long-term electrochemical endurance

ARTICLE

Journal Name

for a minimum of 25h. When comparing Mn-Ni₂-P/NF to Ni₂-P/NF, electrochemical impedance spectroscopy (EIS) shows a lower radius of semicircle for Mn-Ni₂-P/NF suggesting higher electron mobility rates and quicker catalytic responses. A potential catalyst material for water-splitting devices aiming at producing hydrogen fuels on an extensive basis is provided by this study.¹¹³ *Xiumin Li and co-workers* have reported a technique that combines the procedures of thermal phosphorization and uni-polar pulse electro-deposition to generate Mn-incorporated cobalt phosphide (Co-P) electrocatalyst-coated electrode from Co-Mn LDH precursors as well. The inclusion of Mn significantly improves the catalytic function and conductance of the Co-P catalysts as shown by the results of electrochemical impedance spectroscopy (EIS) and linear scan voltammetry (LSV). The nano-sheet microstructure arranges into a porous nanoparticle cluster shape during phosphorization converting the Co-Mn LDH precursor into Mn-CoP catalysts. Mn-CoP-coated electrodes require a significantly lower overpotential of 108 mV to keep a current density of 10 mA cm⁻² in 0.5 M H₂SO₄ solution as compared to CoP-coated electrodes.¹¹⁴ *Liyang Zhang and co-workers* report the synthesis of manganese-doped Mo-S₂ ultrathin particles that are vertically oriented and fixed on a hierarchical carbon skeleton resembling fin tubes to optimize both intrinsic performance and electrode design synergistically. For enriched Mo-S₂ all the hydrogen adsorption liberated energies of the basal surfaces, sulfur edges, and molybdenum edges decrease according to computational models. Moreover, the Mn-doped Mo-S₂ monolayer's electrical composition shows a zero-band gap a sign of enhanced intrinsic conductance. The formation of Mo-S₂ ultrathin particles surrounding carbon nanowires in a vertical orientation improves the exposure of active edge areas which lowers the charge transport resistance and improves the durability of the 3-dimensional self-supported electrode as well shown in (Figure 10c). Having a Tafel slope as low as 44 mV dec⁻¹, this carefully constructed, self-supported, binder-free electrode with integrated architecture shows exceptional endurance even at an elevated cathodic current density of 200 mA cm⁻² in 0.5 M H₂SO₄. It also has a modest overpotential of 130 mV at -10 mA cm⁻².¹¹⁵ An outstanding electrocatalytic activity for the HER in both alkaline and acidic conditions has been demonstrated by *Siran Xu and co-workers* through the development and manual production of an extremely efficient electrocatalyst with a unique 3-dimensional (3D) permeable peony-like micro-flower Mn-CoP tiny structure on adaptable carbon cloth (Mn-CoP PMFs/CC). Doping with magnesium increases electron transport and reduces the thermo-neutral adsorption of hydrogen-free energy (ΔG_{H^*}), according to DFT calculations. When manganese is added to Co-P the electrical structure is altered, the number of places that are active rises, and basic nanowire arrays become permeable nanorod-like nanostructures. All these changes improve Co-P's inherent performance in HER. For 0.5 M H₂SO₄ and 1.0 M KOH approaches the catalyst exhibits an ultra-low excessive potential of 28 mV and 90 mV as well to achieve a current density of 10 mA cm⁻² shown in (Figure 10d). These results are attributed to the catalyst's unique 3D porous structure with

enormous surface areas and exceptional electron conductivity for rapid mobility of electrons and fast gas release routes.¹¹⁶⁻¹¹⁷ The synthesis of a hybrid catalyst used, Mn-doped MoS₂/reduced graphene oxide (Mn-MoS₂/rGO), was accomplished by *Liqian Wu and co-workers* using the hydrothermal approach. This catalyst's exceptional HER performance is mostly due to reduced graphene oxide's excellent electrical conductivity, but it also greatly benefits from the basic catalytic function boost that comes from adding magnesium Mo-S₂. XPS measurements were performed to study the chemical composition of the Mn-MoS₂/rGO hybrid. With a minimum Tafel slope of 76 mV dec⁻¹ significant cathodic currents, and a tiny overpotential of 110 mV the Mn-MoS₂/rGO hybrid catalyst demonstrates remarkable HER activity shown in (Figure 10e).¹¹⁷ The Mn-doped HER electrocatalysts are summarised in Table 6.

4.1.6 Cu-Doped Electrocatalysts for HER

Using Copper (cu) as a dopant or a composite material component can accelerate the HER process. Moreover, Cu may modify the electrical structure of the doped material (such as carbon-based materials or transition metal oxides). Improved catalytic activity in the direction of the HER could arise from this modification. To be more precise, Cu can improve the overall reaction by modifying the binding energies of reaction intermediates involved in the HER, such as adsorbed species and hydrogen atoms. Additionally, Cu incorporation can increase the number of active spots on the material's surface. At these sites, hydrogen atoms may more easily bond and react to generate hydrogen gas, acting as nucleation observes for hydrogen evolution. The HER process is now more efficient as an outcome. Alongside other metals or materials like Pt, Ni, or carbon-based compounds like graphene, Cu can produce heterostructures or alloys. These hybrid structures may demonstrate synergistic effects. In which the combined materials outperform the individual components in terms of catalysis. In conclusion, Cu can reduce the activation energy needed for the HER by improving the kinetics of the reaction and promoting electron transport pathways. This implies that it is possible to accelerate the rate at which hydrogen gas develops off the catalyst surface resulting in higher total HER rates of reaction.¹¹⁸⁻¹²⁰ Cu-doped Ni₃S₂ interconnected nano-sheet Arrays are very effective electrodes for improving alkaline hydrogen development, which was developed by *Yangyang Ding and co-workers*. However, because of the intense S-H bond connection on the outermost layer of Ni₃S₂, there is still room for improvement in the electrochemical reactions of the cathode-reducing process. The 2-step hydrothermal technique was used to produce an extensive range of non-precious metal Cu-Ni₃S₂/NF hybrids to solve this specific issue. Copper and Nickel provide a good basis for introducing copper into Ni₃S₂ since they are neighbouring elements in the same interval with comparable electronegativity and radius of atoms. Copper doping which generates morphological modifications, raises the



number of electrochemically active sites, and improves the intrinsic activity of the catalyst itself, is directly responsible for

the outstanding characteristics and improved efficiency of HER. Experimental results and DFT calculations¹⁰ reveal that Cu⁺

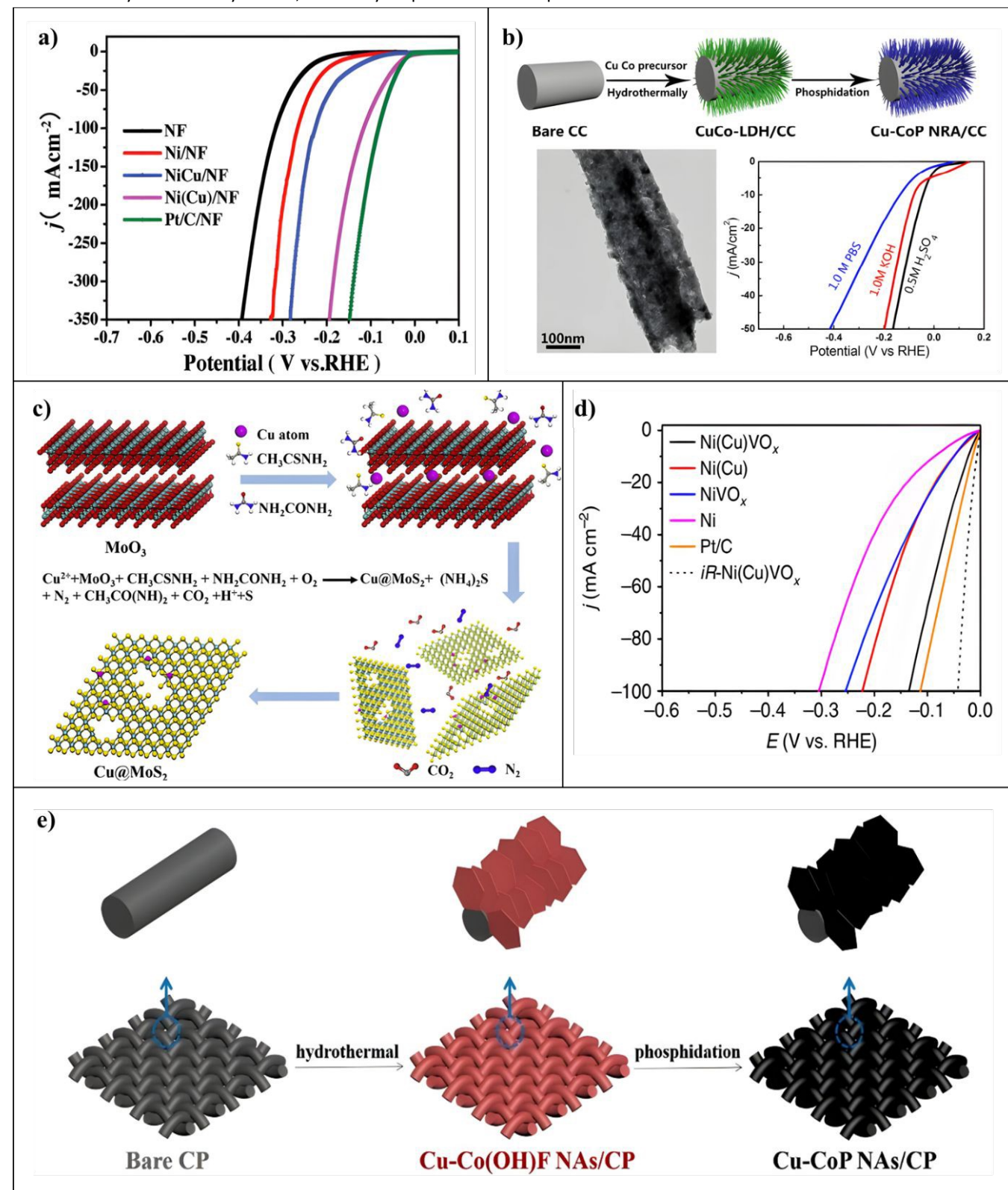


Figure 11. (a) HER polarization curves at 2 mV s⁻¹ with 95% iR-compensations for NF, Ni/NF, NiCu/NF, Ni (Cu)/NF, and Pt/C/NF. reproduced from Ref.^[118] with permission. Copyright 2018, Wiley. (b) The Cu-CoP NRAs/CC utilized as an electrocatalyst for HER are prepared. reproduced from Ref.^[122] with permission. Copyright 2018, ACS. (c) Diagrammatic representation of Cu@MoS₂ mechanism. reproduced from Ref.^[123] with permission. Copyright 2019, Elsevier. (d) LSV curves for iR-Ni (Cu)VO_x. reproduced from Ref.^[125] with permission. Copyright 2020, Nature. (e) Diagrammatic representation of Cu-CoP NAs/CP formation. reproduced from Ref.^[129] with permission. Copyright 2019, Elsevier.



ARTICLE

Journal Name

$\text{Ni}_3\text{S}_2/\text{NF}$ performs other samples consistently. XPS was used to assess the deterioration of a catalyst. Under a low overpotential of 92 mV, the copper-doped material enables current densities of 10 mA cm^{-2} during the HER process.¹²¹ For the HER, *Qiangqiang Sun and co-workers* have developed a new 3-dimensional hierarchically arranged nano-tubular copper-added nickel catalyst on nickel foam ($\text{Ni}(\text{Cu})/\text{NF}$). The catalyst was synthesised using a simple procedure that included electrodeposition and selective electrochemical dealloying processes. Density functional theory simulations show that a more favourable energy state for the adsorption of hydrogen is produced by copper replacement and the production of nickel oxide (Ni-O) on the outer layer. A considerably improved catalytic efficiency is the result of the distorted lattice of nickel caused by copper substitution, the enhanced interfacial activity brought about by oxidation at the surface of nanoporous nickel, and the abundance of sites of activity provided by the 3D hierarchical porous design. Furthermore, the interfacial function of $\text{Ni-O}/\text{Ni}$ is improved by developing a nickel oxide shell around a portion of the Ni nanoparticle cores. This promotes hydrogen adsorption at nearby open nickel sites and increases HER activities. The catalytic efficiency is further enhanced by the significant synergistic effects of copper doping, which replaces the nickel sites and optimizes ΔGH^* for

the adsorption of hydrogen while preserving a balance between desorption and absorption. The resulting $\text{Ni}(\text{Cu})/\text{NF}$ electrode¹²¹ has an enormous electrochemical active surface area and shows Pt-like electrocatalytic properties for HER, with only a 27 mV overpotential needed to achieve a 10 mA cm^{-2} current density and a 33.3 mV dec^{-1} Tafel slope shown in (Figure 11a).¹¹⁸ A straightforward technique utilizing a combination of hydrothermal and low-temperature phosphidation procedures for producing self-supported nanoporous copper-incorporated cobalt phosphide nanorod grids on carbon cloth (Cu-CoP NRAs/CC) with markedly increased catalytic activity has been reported by *Lulu Wen and co-workers*. The strong heteroatomic connections that cause many distorted lattices and defects and hence many reactive areas on the nano-rods are responsible for the remarkable HER performance that Cu-CoP NRAs/CC exhibited. The kinetic energy limit for hydrogen atom adsorption on the cobalt phosphide layer is subsequently significantly lowered because of the inclusion of copper inside the cobalt phosphide framework. The study presents a new approach to synthesizing a variety of eco-friendly HER catalysts that may be used for electrochemical water splitting at any pH level. For catalytic hydrogen generation across a wide pH range, the combined Cu-CoP NRAs/CC cathode exhibits outstanding

S. No	Catalyst	Electrolyte	Overpotential (η) At 10mA cm^{-2}	Tafel slope (mV dec^{-1})	C_{dl} (mF cm^{-2})	Stability (hours & cycles)	Reference
1	$\text{Cu-Ni}_3\text{S}_2/\text{NF}-1/4$	1.0 M KOH	92	45.26	79.22	12h	¹²¹
2	$\text{Ni}(\text{Cu})/\text{NF}$	1.0 M KOH	27	33.3	17.27	-	¹¹⁸
3	Cu-CoP NRAs/CC	1.0 M KOH	81	86	113.8	40h	¹²²
4	$\text{Cu}@\text{MoS}_2$	0.5 M H_2SO_4	131	51	-	-	¹²³
5	$\text{Cu-Ni}_3\text{S}_2/\text{Co}_3\text{S}_4$	1.0 M KOH	79	50.4	75.4	10h	¹²⁴
6	$\text{Ni}(\text{Cu})\text{VOx}$	1.0 M KOH	21	28	-	-	¹²⁵
7	$\text{Ni}(\text{Cu})/\text{NF}$	1.0 M KOH	203 at (100 mA cm^{-2})	-	-	-	¹²⁶
8	$\text{CuNiS}@\text{Ni}_2\text{P}/\text{NF}$	1.0 M KOH	144	103.2	27.91	24h	¹²⁷
9	$\text{Cu-Co}_3\text{O}_4 \text{ NAs}/\text{NF}$	1.0 M KOH	125	66	11.9	20h	¹²⁸
10	Cu-CoP NAs/CP	1.0 M PBS	81	83.5	17	3000 CV cycles	¹²⁹

Table 7. Cu-Doped Electrocatalysts for HER



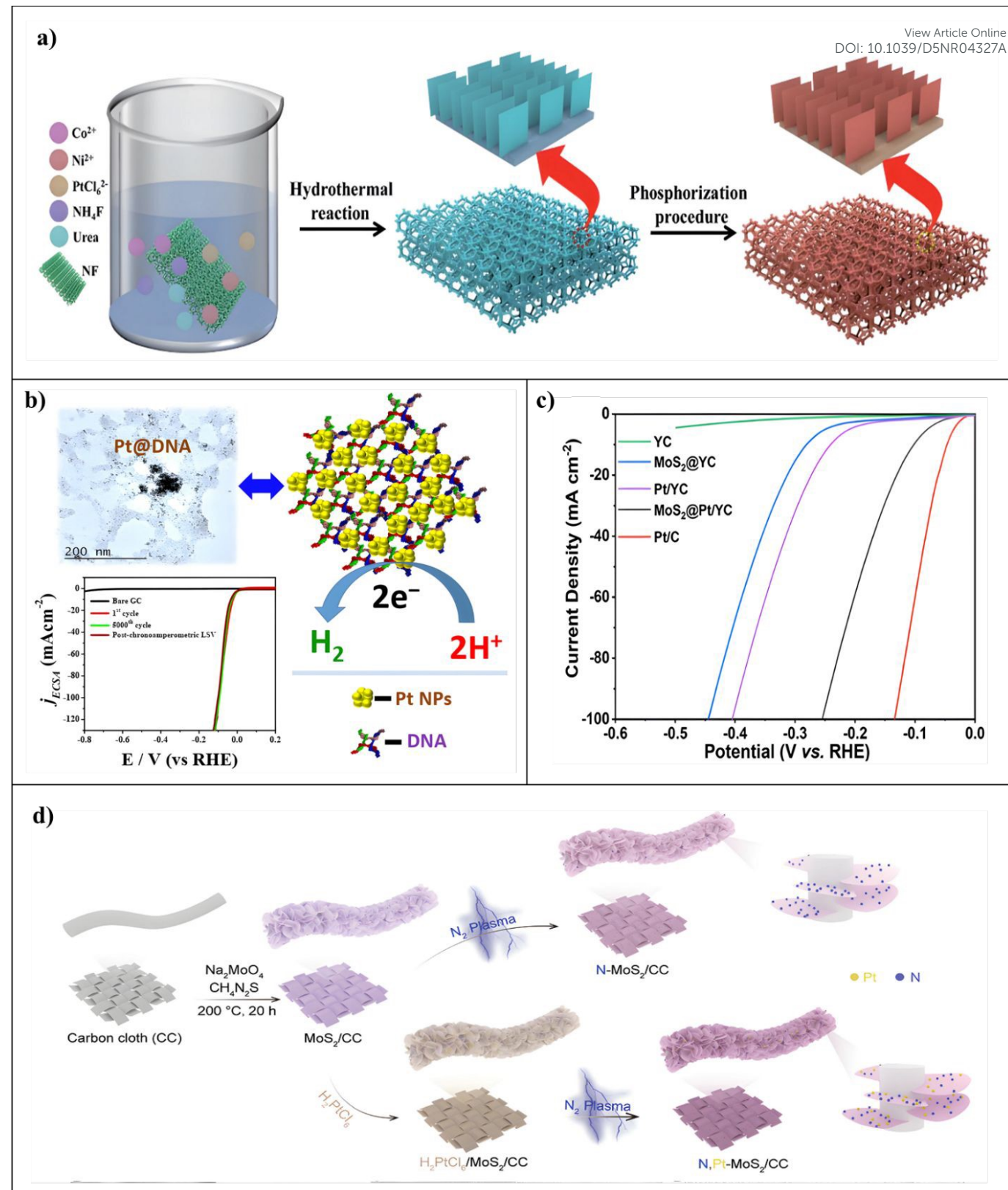


Figure 12. (a) An illustration of the Pt/Co₂P/Ni₂P/NF synthetic process. reproduced from Ref.[¹³²] with permission. Copyright 2020, RSC. (b) A representation of colloidal Pt@DNA molecular self-assembled general production for HER application. reproduced from Ref.[¹³³] with permission. Copyright 2016, ACS. (c) LSV curves in H_2SO_4 (0.5 M) for Pt/C, YC, MoS₂@YC, Pt/YC, and MoS₂@Pt/YC. reproduced from Ref.[¹³⁵] with permission. Copyright 2023, ACS. (d) Synthesis of nanosheets of N, Pt-MoS₂. Reproduced from Ref.[¹³⁶] with permission. Copyright 2022, RSC.

HER performance. Only 44 mV and 81 mV of overpotential are needed in 0.5 M H_2SO_4 and 1 M KOH respectively to reach a current density of 10 mA cm⁻² shown in (Figure 11b).¹²²

Molybdenum sulfide (MoS₂) is a promising non-precious-metal catalyst option that has been reported by *Liang Ji and co-workers* as a cheaper alternative to platinum (Pt) catalysts in the

ARTICLE

Journal Name

hydrogen evolution process. Nonetheless, the restricted amount of catalytic active sites and the inert basal layer of MoS_2 significantly limit its catalytic effectiveness. This was solved by using a simple one-pot solvothermal technique for producing porous 1T- MoS_2 combined with copper atom doping. While the doping of atoms of copper (Cu) promotes electron transport between copper and MoS_2 , the porous composition and 1T- MoS_2 in the resultant Cu@ MoS_2 material concurrently stimulate the base layer and supply additional active edge spots shown in (Figure 11c). Significantly, in comparison to the 2H- MoS_2 surface first principles based on first principles show the larger transfer of charge as well as greater stability when copper is adsorbed on the 1T- MoS_2 surface. These findings suggest that the metastable 1T- MoS_2 monolayer may be advantageous in improving HER efficiency by adsorbing single metal atoms. With a small overpotential of 131 mV at a current density of 10 mA cm^{-2} and a modest Tafel slope of 51 mV dec^{-1} , the Cu@ MoS_2 sample exhibits improved performance with HER.¹²³ Hui Su and co-workers have developed a simple method based on $\text{Ni}_3\text{S}_2/\text{Co}_3\text{S}_4$ to synthesize the bimetallic component sulfide hetero structuring electrocatalysts (M = Cu, Fe, Mo, Zn). Having just an overpotential of 79 mV required to attain current densities of 10 mA cm^{-2} for the HER analysis, the resulting Cu- $\text{Ni}_3\text{S}_2/\text{Co}_3\text{S}_4$ electrode demonstrates outstanding electrocatalytic activity for HER in a 1 M KOH electrolyte. XPS study validates that the addition of copper cations promotes the development of high-valent Nickel and cobalt (Ni/Co) sites. The density functional model calculations show that by regulating the d-band centre of cobalt and lowering the adsorption energy of hydrogen and oxygen-containing intermediary states (H^* , OH^* , OOH^*) on the surface of the catalyst, the addition of Cu boosts the formation of high-valent cobalt sites and boosts the charge transfer performance of the nickel and cobalt species, therefore improving the intrinsic catalytic capability. This work highlights the significance of transition metal ion doping for increasing the bimetallic component sulfide electrocatalytic efficiency.¹²⁴ Copper-added Nickel catalysts with Ni-O- VO_x domains integrated for the alkaline hydrogen evolution process have been reported by Yibing Li and co-workers. The development of Ni-O- VO_x sites in Ni (Cu) VO_x has been clarified using systematic X-ray absorption spectroscopy investigation. The nickel framework is considerably changed by VO_x , resulting in an increased surface area that is electrochemically conductive. The super activity of the Ni-O- VO_x sites is further supported by DFT calculations based on the first principle which facilitates charge transfer from nickel to VO_x and lowers the free energy related to H-adsorption and H_2 release over nickel. This contributes to the lasting reliability and excellent HER activity of the Ni (Cu) VO_x electrode. Having an initial overpotential of almost zero and an extremely small overpotential of 21 mV the optimized Ni(Cu) VO_x electrode achieves a current density of -10 mA cm^{-2} shown in (Figure 11d). which is similar to the benchmark Pt/C catalysts.¹²⁵ A solid nickel electrocatalyst doped with copper has been demonstrated by Qiangqiang Sun and co-workers for the HER. This nano-porous catalyst possesses an ultra-large ECSA and shows outstanding activity and durability in

HER. It was produced by a straightforward two-step electrodeposition-dealloying procedure over macro-porous Ni foam. Cu-added nano-tubular nickel catalyst has several benefits that contribute to its outstanding efficiency, notably a super-large ESCA, good hydrogen bubble dissolution as well as excellent electrical conductivity. By using the hydrogen evolution process rather than the oxygen evolution reaction, these characteristics allow for the energy-efficient electrolytic synthesis of hydrogen. Interestingly, the Ni(Cu)/NF combination only needs a cell voltage of 0.41V in a two-electrode alkali electrolyzer configuration to get a current density of 100 mA cm^{-2} for the evolution of hydrogen.¹²⁶ Hui Li and co-workers develop a simple and efficient method for synthesizing Cu-doped bimetallic phosphosulphide nanosheet arrangements (Cu-NiS@ $\text{Ni}_2\text{P}/\text{NF}$) on nickel foam. In the HER the CuNiS@ $\text{Ni}_2\text{P}/\text{NF}$ substance performs better, especially when the doping level of copper is optimum. Several variables contribute to the exceptional HER performance of CuNiS@ $\text{Ni}_2\text{P}/\text{NF}$ nanosheet arrays. The electrocatalyst's electronic composition and shape are effectively optimized by the moderate doping of copper. The typical configuration of nanosheet grids exposes more active places. The combined effect of various elements results in high intrinsic movement. Interestingly, Cu-NiS@ $\text{Ni}_2\text{P}/\text{NF}$ outperforms Cu-NiS@ $\text{Ni}_2\text{P}/\text{NF}$ -0.25 (206 mV) and Cu-NiS@ $\text{Ni}_2\text{P}/\text{NF}$ -0.125 (219 mV) with only a potential of 144 mV to obtain a current density of 10 mA cm^{-2} in 1.0 M KOH.¹²⁷ Yongshang Tian and co-workers produced copper-incorporated Co_3O_4 porous nanosheet arrangements on 3-dimensional Ni-foam (Cu- Co_3O_4 NAs/NF) by straightforwardly pyrolyzing bimetal-organic structure precursors. Research findings show that incorporating copper in Co_3O_4 materials affects the nano-sheet shape to obtain a large specific area and well-exposed places for activity. Additionally, open routes for continuous gas release and transfer of electrons are provided by the 3-dimensional electrode arrangement. Utilizing its distinct geometric and electrical structure, the Cu- Co_3O_4 NAs/NF electrode that has been developed demonstrates exceptional activity. Our Cu- Co_3O_4 NAs/NF electrodes' exceptional HER activity combined with its low voltage of 1.58 V allows for the output of a current density of 10 mA cm^{-2} for total water splitting.¹²⁸ A self-standing, non-noble metal, 3D connected ultrathin nanosheet arrangement (Cu-CoP NAs/CP) has been introduced by Liang Yan and co-workers. The resultant Cu-CoP NAs/CP exhibits outstanding efficiency for both the hydrogen evolution process because of its improved electronic composition and higher electrical conductivity, which facilitates both the desorption and adsorption of reaction products shown in (Figure 11e). The results of experiments and density functional theory calculations show that the incorporation of copper to Co-P greatly improves electrical conductivity and optimizes its electronic composition, which in turn facilitates the formation of O^* intermediaries (which lead to CoOOH active species) and H^* adsorption and desorption, which occurs This ultimately results in superior HER catalytic operations. The method of XPS was utilized to study the electronic structure and element states of Cu and CoP NAs. Excellent HER activity is attained using overpotentials of 81 mV to produce a current



density of 10 mA cm^{-2} in neutral media, owing to enhanced mass/charge transfer, optimized 3D $\text{Cu}_{0.08}\text{Co}_{0.92}\text{P}$ NAs/CP, and greater exposure of active areas.¹²⁹ The Cu-doped HER electrocatalysts are summarised in **Table 7**.

4.1.7 Pt-Doped Electrocatalysts for HER

Platinum (Pt) is often added to HER materials or used as a dopant to greatly increase the reaction for several important factors. Platinum is well known for having outstanding HER catalytic activity. Pt offers active areas where hydrogen atoms may bond and undergo the essential processes to develop into hydrogen gas when it is placed onto or doped into other materials. Pt's ideal electrical characteristics enable effective electron transport across the HER. This is significant because the reaction proceeds through several stages in which electrons are transferred to hydrogen ions, which form hydrogen gas in the final phase. Pt helps these electron transfer activities, which reduces the overpotential needed for the reaction to continue and raises the hydrogen evolution's general efficiency. When used for HER in electrochemical cells, Pt is quite durable and adaptable in acidic environments. Pt can be added to composite materials or used as a dopant to increase the catalyst's stability

against processes that cause degradation, such as active-site aggregation or dissolution. The long-term performance is assured by its stability, which prevents a noticeable decline in activity. Synergistic effects can happen when Pt is mixed with other materials, including transition metals. As Pt and the host material have complimentary electronic structures or optimal surface contacts, these pairings can result in improved catalytic activity as compared to Pt itself.^{140–142} Using sodium lauroyl sarcosinate ($\text{C}_{15}\text{H}_{28}\text{NNaO}_3$) as a structure-directing intermediary in hydrothermal conditions of use, *Piyali Bhanja and co-workers* have successfully synthesized mesoporous Sn-O (MTO-S). It is followed by calcination and subsequently adding Pt nanoparticles using straightforward wet-chemical techniques. The mesopore exterior of the Pt-loaded mesoporous tin oxide nanostructured materials exhibits a well-dispersed arrangement of metal and metal oxide micron-sized particles which facilitates easy electron leaping and increases the speed of the HER activity of Pt@MTO-S nanocomposites. These findings are supported by electrochemical water-splitting tests and its pore size distribution is calculated using DFT. Strong flow with H_2 bubbles over the Pt@MTO-S cathode is directly indicative of the

S. No	Catalyst	Electrolyte	Overpotential (η) At 10mA cm^{-2}	Tafel slope (mV dec $^{-1}$)	C_{dl} (mF cm $^{-2}$)	Stability (hours & cycles)	Reference
1	Pt@MTO-S	0.5M H_2SO_4	73	28	72.7uF	12h	130
2	Pt@MoS ₂	-	88	30.24	32.68	1000 CV cycles	131
3	Pt/Co ₂ P/Ni ₂ P/NF	1.0 M KOH	75	64	30.4	25h	132
4	Pt@DNA	0.5 M H_2SO_4	26	30	-	24h	133
5	Pt _{SA} –PtCo NCs/N–CNTs	1.0 M KOH	47	41	30	8000 CV cycles	134
6	MoS ₂ @Pt/YC	0.5 M H_2SO_4	118	74	19.07	24h	135
7	N-Pt-MoS ₂	1.0 M KOH	38	39	125	240h	136
8	PtNPs/PEDOT _{0.3} SG _{0.7}	0.5 M H_2SO_4	40	28.4	-	500 CV cycles	137
9	Pt-FeNi@C	0.5 M H_2SO_4	50	26.1	5.6	10h	138
10	Pt-(PtO _x)-NSs/C	0.5 M KOH	64	51	-	40h	139

Table 8. Pt-Doped Electrocatalysts for HER



ARTICLE

Journal Name

significant potential for real-world HER implementations that Pt design on the surface of mesoporous SnO_2 possesses. Furthermore, Pt@MTO-S has an ultralow overpotential of 73 mV at 10 mA cm^{-2} , demonstrating remarkable HER activity.¹³⁰ The Platinum-doped MoS_2 (Pt@ MoS_2) catalyst that *Yang Li and co-workers* have reported was synthesized using a potential cycling technique. This allowed for the effective introduction of platinum dopants into the MoS_2 structure and a partial transition of MoS_2 from the 2H to the 1T stage. XPS revealed the electrical structural evolution of MoS_2 following Pt doping. The role of platinum atoms in the electrical structural modification of MoS_2 has been clarified by a thorough investigation. The theoretical calculations further demonstrate that the sulfur atoms next to Platinum in MoS_2 are the most active sites for the hydrogen evolution process, with minimal adsorption of hydrogen-free energy (ΔG_{H^*}) of around 0.04 eV, like benchmark Pt catalysts. The findings of the experiments show that Platinum single-atom doping in 1T MoS_2 has good catalytic activity and is stable for HER. DFT studies also reveal the role of platinum atoms in the 1T MoS_2 arrangement, where the most active places are sulfur atoms next to Platinum atoms, with an optimum ΔG_{H^*} of about 0.04 eV. According to MoS_2 's excellent geometric and electrical framework, Pt@ MoS_2 exhibits a low overpotential of 88.43 mV at 10 mA cm^{-2} .¹³¹ *Xin Xiao and co-workers* have effectively produced very low quantities of Pt-incorporated $\text{Co}_2\text{P}/\text{Ni}_2\text{P}$ on nickel foam (Pt/ $\text{Co}_2\text{P}/\text{Ni}_2\text{P}/\text{NF}$) by an in situ controlled developmental technique, demonstrating its effectiveness as an electrode for the electrolytic splitting of water into H_2 shown in (Figure 12a). The accessible Pt/ $\text{Co}_2\text{P}/\text{Ni}_2\text{P}/\text{NF}$ substrate has higher activity areas because of the super-macroporous structure of the NF substrate which improves electron flow and provides open pathways for quick H_2 production. The enhanced pathways for actions of electrocatalytic efficiency are attributed to the complementary actions of Co_2P and Ni_2P , the number of active areas on Pt/ $\text{Co}_2\text{P}/\text{Ni}_2\text{P}/\text{NF}$, and the control of the electronic framework by platinum doping. Considering a low overpotential of 75 mV at a current density of 10 mA cm^{-2} Pt/ $\text{Co}_2\text{P}/\text{Ni}_2\text{P}/\text{NF}$ demonstrates outstanding HER activity. Furthermore, Pt/ $\text{Co}_2\text{P}/\text{Ni}_2\text{P}/\text{NF}$ runs for 25h with remarkable stability demonstrating exceptional durability.¹³² *Sengeni Anantharaj and co-workers* published a technique to produce small particles of platinum colloidal, with an average size of 3.5 ± 0.3 nm, and effectively secure them onto DNA molecules self-assemblies. A loading of 5 μL of the developed Pt@DNA homogeneous solution, or 15 $\mu\text{g cm}^{-2}$, was used to assess the solution straight for the electrochemical HER in 0.5 M H_2SO_4 . DNA's remarkable adherence to glassy carbon and FTO substrate electrodes, together with its electrical conductivity, stability during the potentiostatic process of electrolysis, and rapid decomposition have made the produced Pt@DNA colloidal solution an excellent HER electrocatalyst. Considering the preservation of electrocatalytic activities this technique makes it possible to manufacture ultra-small nanoparticles of titanium that have larger areas of surface without the requirement for an outside binder during the production step. beyond any binding agent, the Pt@DNA-GC interface displayed

overpotentials of -0.026 V and -0.045 V at current densities of 10 mA cm^{-2} and 20 mA cm^{-2} in that order shown in (Figure 12b).¹³³ The design has been shown by *Wenxia Chen and co-workers* that adjacent platinum atomic places contained within N-doped porous carbon nanotubes (PtSA-PtCo NCs/N-CNTs) control the local electronic configuration of cobalt-platinum small clusters. The combustion of zeolite imidazole MOF produced by melamine introduction with thimbleful platinum loading was used to accomplish it. Melamine is included to revive neighboring atomic carbons and start the directed development of nanotubes of carbon doped with nitrogen. A detailed investigation reveals the noteworthy influence of nearby low-coordinated Pt-N₂ sites in modifying the localized electronic configuration of Pt-Co tiny clusters. DFT calculations show that atomically isolated PtSA can affect the electronic states of PtCo NCs, lowering the energy barrier and enhancing kinetic processes and this leads to higher electrocatalytic activity. XPS was used to analyze the chemical compositions of PtSA-PtCo NCs and PtCo NCs/N-CNT-900 samples. The performance of the HER is further enhanced by optimum control of the electronic configuration by nearby platinum atoms, which lowers the reaction energy limit in the electrochemical step. In 1 M KOH, the optimized PtSA-PtCo NCs/N-CNTs-900 demonstrate remarkable HER catalytic activity attaining a current density of 10 mA cm^{-2} and a modest overpotential of 47 mV.¹³⁴ *Huiting Hu and co-workers* developed a simple hydrothermal approach for designing MoS_2 nanosheets that are deposited on Pt-incorporated yeast cell biomass (MoS₂@Pt/YC). The primary challenge is to reduce the noble metal loading without sacrificing efficiency. The nanosheets of MoS_2 are encouraged to develop on yeast cells' smooth surface, and metal Platinum may bind to its functional groups as well. As a result, nanosheets of MoS_2 are applied to the Pt/YC material improving the exposure of the hydrogen synthesis reaction's active sites (HER). Precious metal importing can be reduced without compromising qualities by adding transition metal sulfides with a considerable amount of specific surface area. This work provides a straightforward approach to the production of Pt-doped HER electrodes. Despite a tiny Tafel slope of 74 mV dec⁻¹ demonstrating its outstanding HER efficiency and an overpotential of 118 mV at the benchmark current density of 10 mA cm^{-2} the resultant MoS₂@Pt/YC material exhibits outstanding results shown in (Figure 12c).¹³⁵ *Yan Sun and coworkers* have presented a simple, adaptable N₂-plasma approach to facilitate the transformation of MoS_2 nanosheets from the 2H stage to the 1T stage with a remarkable conversion rate of almost 62%. XPS was employed to study the phase transition and composition of N- MoS_2 and N,Pt- MoS_2 nanosheets from 2H to 1T. In addition, the plasma processing promotes the decomposition of Platinum salts that have been deposited and the dispersion of platinum atoms into MoS_2 nanosheets which increases the 1T stage yield to around 87%. According to computational models and structural analysis, MoS_2 's electrical and coordination properties are successfully modulated by the deep doping of nitrogen and platinum atoms shown in (Figure 12d). This activation of the sulfur spots results in the generation of emptier 2p_z orbitals that are favourable for



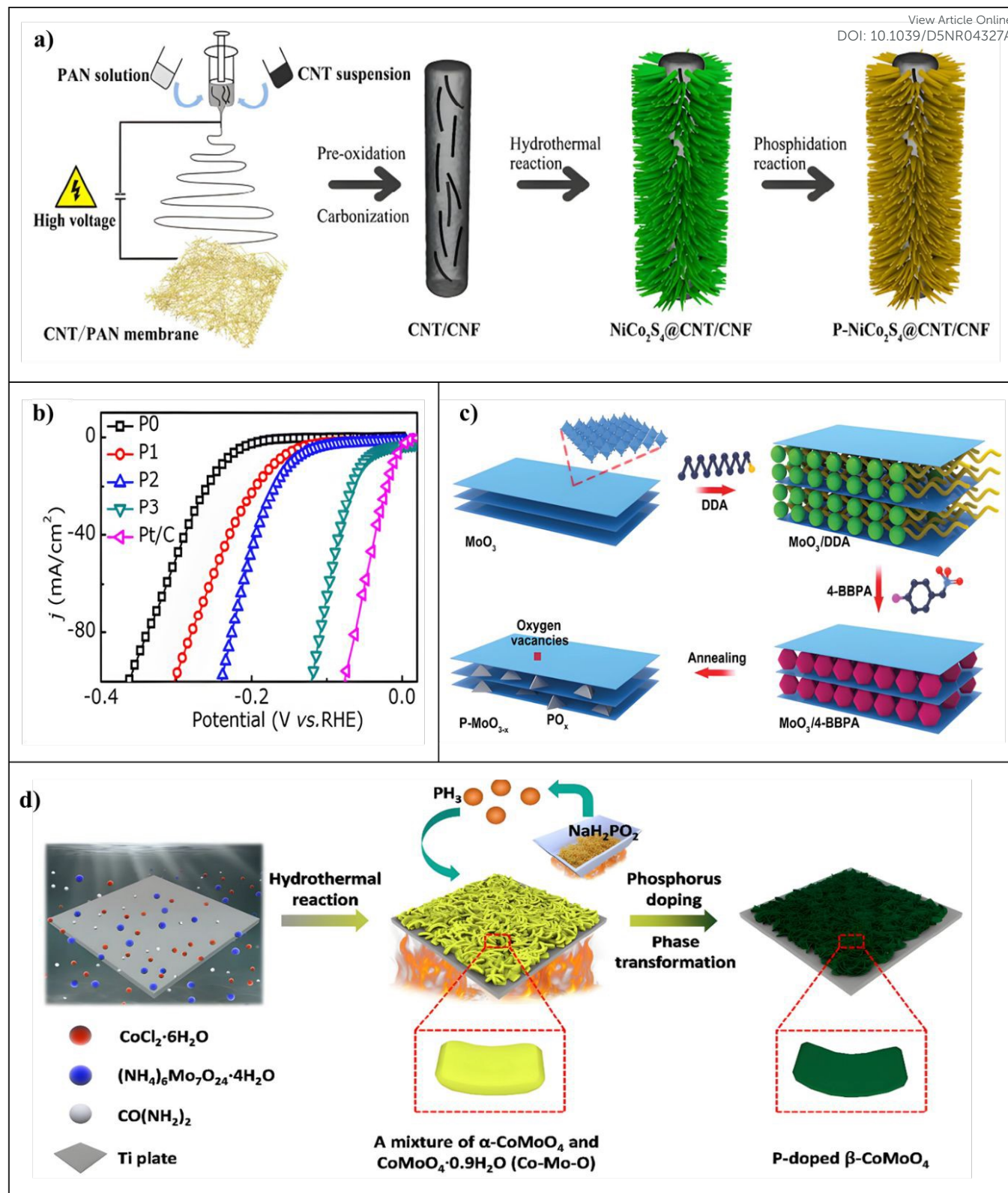


Figure 13. (a) Diagrammatic representation of the P-NiCo₂S₄@CNT/CNF hybrid preparation process. reproduced from Ref.[¹⁵¹] with permission. Copyright 2017, RSC. (b) P-doped CoS₂ and pure CoS₂ polarisation curves in 0.5 M H₂SO₄ at a scan rate of 2 mV/s⁻¹. reproduced from Ref.[¹⁵⁴] with permission. Copyright 2018, Elsevier. (c) Diagrammatic representation of the P-MoO_{3-x} nanosheet preparation procedure. reproduced from Ref.[¹⁵⁵] with permission. Copyright 2017, Wiley. (d) Diagrammatic representation of the P-doped β -CoMoO₄ synthesis process on a Ti plate. reproduced from Ref.[¹⁵⁶] with permission. Copyright 2018, ACS.

the adsorption of water and hydrolysis. Interestingly, the method for plasma production described in this study may be easily expanded to provide large-area N, Pt MoS₂ nanosheet-

coated carbon cloth that is 32 cm by 16 cm in size, with a homogeneous 1T-phase feature and a high capacity to generate hydrogen as well. The resultant Pt-MoS₂ nanosheet complexes

ARTICLE

Journal Name

mounted on carbon cloth show good alkaline HER activities, obtaining strong cycle endurance and a modest overpotential of 38 mV at 10 mA cm⁻².¹³⁶ A. Abdolmaleki and co-workers developed a tiny material made of sulfonated material graphene and poly(3,4-ethylene dioxythiophene) (PEDOT) conduct polymer adorned with platinum-based nanoparticles (PtNPs). PEDOT promotes proton diffusion on the surface of the electrode, which helps to facilitate the hydrogen synthesis process (HER) in addition to avoiding nanoparticle aggregation. Increased modification of graphene nanosheets with the addition of sulfonate moieties can further improve the efficiency of the electrodes. After 500 cycles, the resultant HER electrocatalyst shows negligible overpotential (around -0.040 V vs. RHE), modest charge transfer resistance (about 50 ohms), and steady efficiency. Tafel kinetics regulate the electrocatalytic process mainly; electrochemical adsorption-desorption is important because of kinetic factors (such as Tafel slope of 28.4 mV dec⁻¹).¹³⁷ Aixin Fan and coworkers have reported a simple method for synthesizing ultralow (0.66 wt%) Pt-doped FeNi metallic NPs that are embedded in a hollow graphene shell construction, or Pt-FeNi@C. Many core-shell Particles are arranged during the construction of Pt-FeNi@C to prevent the Pt-FeNi metallic core from aggregating and dissolving during electrocatalytic processes. The hollow carbon shell also speeds up electron transport, which greatly improves overall electrochemical efficacy. At an overpotential of 50 mV, Pt-FeNi@C notably shows a mass activity 63.0 times greater compared to that of the commercial Pt/C catalyst. The unique structural and electronic characteristics produced by adding tiny quantities of Platinum to a Fe-Ni composition encased in graphitic nano-carbon shells account for the remarkable catalytic behavior and stability.¹³⁸ Manas Kumar Kundu and coworkers reported hybrids of Pt nanostructures and N-doped carbon as effective catalysts for the synthesis of hydrogen. The Pt-(PtO_x)-NSs/C catalyst shows 4 to 6.5 times greater HER activity during basic and acidic environments than commercial Pt/C. It reaches 10 mA cm⁻² of current density in 0.5 M KOH at 51 mV of overpotential and 64 mV dec⁻¹ of Tafel slope. In acidic conditions, the HER activity of the Pt-(PtO_x)-NSs/C and PtO_x-free Pt Nanostructures/C (PtNSs/C) catalysts is equal. PtO_x increases the HER/HOR activity of Pt-(PtO_x)-NSs/C in an alkaline medium. In particular, the Pt-(PtO_x)-NSs/C catalyst has five times the activity of PtNSs/C under basic circumstances and equivalent activity under acidic conditions. As active sites for OH-adsorption in basic environments, PtO_x helps build OH_{ads}, which subsequently react with nearby Pt sites' hydrogen intermediaries (Hads) to produce H₂O and increase HER activity.¹³⁹ The Pt-doped HER electrocatalysts are summarised in **Table 8**.

5. Non-Metallic Heteroatom Doping

The incorporation of non-metallic dopants into catalyst matrices offers an effective strategy for modulating catalytic behavior without altering the metallic lattice structure. Non-metals such as nitrogen, phosphorus, sulfur, and boron

influence catalytic activity primarily by tuning the electronic properties of the active sites and inducing surface defects or heteroatom functional groups.¹⁴³ Unlike metallic dopants that often form solid solutions, non-metallic elements typically bond covalently with the host, leading to charge redistribution and local distortion in the coordination environment. These effects can significantly impact key parameters like the hydrogen ΔG_{H*}, which determines HER efficiency. Non-metallic doping can either donate or withdraw electrons, thereby shifting the electronic density at catalytic sites and influencing adsorption energetics. Although the volcano plot framework remains a useful tool to evaluate ΔG_{H*}, many non-metal-doped systems show enhanced HER activity even when ΔG_{H*} is suboptimal. This suggests that additional factors such as improved electrical conductivity, increased defect density, and enhanced hydrophilicity also contribute to catalytic performance. For instance, nitrogen doping introduces lone-pair electrons that facilitate electron transfer, while sulfur doping can create favorable active edge sites. Therefore, when evaluating the role of non-metallic dopants in HER catalysts, it is crucial to consider not just hydrogen binding energy but also the structural and electronic effects that alter the reaction pathway. These multifaceted enhancements will be further exemplified in the following sections.^{53,144,145}

5.1 P-Doped Electrocatalysts for HER

Phosphorous (P) provides more of an impact on the control of surface charge states because of its bigger atomic radius and enhanced electron-donating ability. Although introducing P from the same group to non-metallic elements found in pristine catalysts increases their catalytic efficiency, adding P from a different group to non-metallic atoms in hosting catalysts is expected to result in larger benefits. P enhances catalytic capabilities by influencing the electronic configurations of metal components. When P introduces itself, non-noble metal-based materials must be treated using phosphidation processes which reduce oxide impurities on the surface by reacting with active phosphorus compounds. To stabilize oxygen vacancies essential active sites for HER and improve electrocatalytic activity and P loading additionally changes the valence states of metal oxides. P doping boosts intrinsic activity against HER by increasing the electrical conductivity and optimizing hydrogen adsorption-free energy as demonstrated by theoretic calculations and experimental investigations.¹⁴⁶⁻¹⁴⁹ Suitable electrocatalysts for hydrogen production have been developed by Luozhen Bian and co-workers using Phosphorus (P)-doped MoS₂ nanosheets anchored on carbon cloths (CC). Molybdenum disulfide (MoS₂) nanosheets made on CC were directly loaded with P-using a simple low-temperature phosphatization method that they developed. This resulted in a combined electrode for an effective hydrogen evolution process. Higher current densities for useful applications may be generated more easily with this method, which makes it possible to fabricate phosphorus-doped MoS₂ on a flexible material. Increased internal basal plane active regions and improved material conductance are two ways that P stimulants in the MoS₂ matrix dramatically boost HER performance. To reach current densities of 20 mA



S. No	Catalyst	Electrolyte	Overpotential (η) At 10mA cm ⁻²	Tafel slope (mV dec ⁻¹)	C _{dl} (mF cm ⁻²)	Stability (hours & cycles)	View Article Online DOI: 10.1039/DENR04327A Reference
1	P-doped MoS ₂	0.5 M H ₂ SO ₄	133 at (20 mA cm ⁻²)	67	17.6	1h	150
2	P-NiCo ₂ S ₄ @CNT/CNF	0.5 M H ₂ SO ₄	74	65.9	33.8	10h	151
3	P-WN/rGO	0.5 M H ₂ SO ₄	46	54	32	20h	152
4	P-Mo ₂ C@C	0.5 M H ₂ SO ₄	89	42	15.6	3000 CV cycles	153
5	P-doped CoS ₂	0.5 M H ₂ SO ₄	53	57	49	10000 CV cycles	154
6	P-MoO _{3-x} -n	0.5 M H ₂ SO ₄	82	42	-	1000 CV cycles	155
7	P-β-CoMoO ₄ /Ti	1.0 M KOH	138	68.76	-	20h	156
8	MoP@PC	0.5 M H ₂ SO ₄	97	59.3	39.6	1000 CV cycles	157
9	P-MoS ₂ @CoP/CC	0.5 M H ₂ SO ₄	72	51.22	143	30h	158
10	NiCo-NiCoP@PCT	1.0 M KOH	135	77.79	5.07	10h	159

Table 9. P-Doped Electrocatalysts for HER

cm⁻² and 100 mA cm⁻² respectively, the optimized P-loaded MoS₂ nanosheets, which contain 3.3 at% phosphorus exhibits much reduced overpotentials of 133 mV and 189 mV. Additionally, they exhibit an outstanding tiny Tafel slope of 67.0 mV dec⁻¹.¹⁵⁰ Phosphorus-incorporated NiCo₂S₄ nanoparticles grown on carbon nanotubes that are embedded within a network of carbon nanofibers (P-NiCo₂S₄@CNT/CNF) are the basis of highly active electrocatalysts developed by *Huahao Gu and co-workers* shown in (Figure 13a). CNTs are added using an easy co-electrospinning technique to improve the electrical insulation of the 3-D CNF system and to facilitate electron transmission to the connected HER active substance. With the help of this nanofiber network the electroactive NiCo₂S₄ develops onto the CNT/CNF template parallel by hydrothermal reaction; however, revealing additional catalytically active regions. Through phosphidation responses phosphorus loading into the hybrid enhances the electrical composition of electroactive NiCo₂S₄, thereby lowering the energy resistance through the HER procedure. NiCo₂S₄'s electronic makeup is adjusted by loading phosphorous a non-chalcogen heteroatom to maximize the hybrid catalyst's hydrogen absorption energy. Lowering the kinetic energy barrier in the phosphidation process makes it easier to dope the hybrid with phosphorus. The P-NiCo₂S₄@CNT/CNF hybrid demonstrates exceptional HER

performance with an exceptionally low onset overpotential of 27 mV an amazing current density of 10 mA cm⁻² at η as low as 74 mV a staggering exchange current density of 0.79 mA cm⁻² and excellent long-term durability. This hybrid is made possible by the synergistic effects resulting from electrical improvement and nanostructured morphological and phosphorus doping-induced efficiency of the electronic framework.¹⁵¹ *Haijing Yan and co-workers* developed Phosphorus enhanced tungsten nitride (W₃N₂)/reduced graphene oxide (P-WN/r-GO) as an electrocatalyst for the HER process that is additionally highly efficient and affordable. When phosphorus is added to r-GO and WN, the work function increases significantly and approaches that of platinum metal. The peculiar characteristics of phosphorus which include lone-pair electrons in 3p orbitals and unoccupied 3d orbital spaces, allow it to modify the surface charging state to generate local densities of charge which is responsible for the amazing activity of phosphides. By modifying Phosphorus on tungsten nitride in a sensible way one may increase the activity of tungsten nitride catalysts in order. This is possible by making use of P's important function in the HER and its impact on the electrical state of metal components which in turn has a major effect on catalytic characteristics. In acidic conditions, the P-WN/rGO catalyst has a low onset overpotential of 46 mV, a Tafel slope of 54 mV dec⁻¹, and a

ARTICLE

Journal Name

significant exchange current density of 0.35 mA cm^{-2} . To attain a current density of 10 mA cm^{-2} the catalyst requires an overpotential of 85 mV .¹⁵² *Zhangping Shi and co-workers* offers a strategy for precisely adjusting the electrical composition of nanostructured Mo_2C using phosphorus testing, which results in a high efficiency that is on par with noble-metal-based electrodes in the HER process. Phosphorus provides a fascinating effect on Mo_2C by increasing the electron concentration close to the Fermi limit of Mo_2C which reduces the Mo-H interaction and accelerates HER rates. The phosphorus added to pristine Mo_2C causes a gradual rise in the negative hydrogen-binding energy balance (ΔGH^*) which is attributed to steric interference and electron migration by the phosphorus on the Mo_2C substrate. This effectively weakens the Mo-H connection. These findings are further supported by density functional theory computations. The presence of P-Mo bonds in $\text{P-Mo}_2\text{C@C}$ and the direct interaction between dopant and carbide, which is consistent with XPS findings. The ensuing $\text{P-Mo}_2\text{C@C}$ nanowires show outstanding behaviour with a small overpotential of 89 mV at a current density of 10 mA cm^{-2} and amazing kinetic metrics with a Tafel slope of 42 mV dec^{-1} .¹⁵³ *Jingyan Zhang and co-workers* offer a straightforward, one-step hydrothermal technique for producing Phosphorus (P)-doped cobalt disulfide materials. By lowering the intrinsic energy for hydrogen atomic adsorption ($\Delta\text{G}_{\text{H}^*}$) at the cobalt sites phosphorus substances may be able to increase the electrocatalytic function of hydrogen evolution.

Additionally, the metallic P-added CoS_2 improves HER function by speeding up HER rates and facilitating electron transport. It is conceivable for the P atom to move into the sulfide replacing the S atom vacancy to form new bonds with other substances and causing lattice deformation, given the near-atomic distance and electronegativity of P to S. Having an overpotential of just 46 mV and an current density of 10 mA cm^{-2} in a $0.5 \text{ M H}_2\text{SO}_4$ solution the optimized P-doped CoS_2 catalyst in this work exhibits outstanding behaviour shown in (Figure 13b).¹⁵⁴ P-doped MoO_{3-x} nanosheets were developed by *Ling Li and co-workers* as reliable and efficient electrodes for the evolution of hydrogen. It shows an overpotential of 166 mV in $0.5 \text{ M H}_2\text{SO}_4$ to get an average current density of 10 mA cm^{-2} . Additionally, it exhibits strong catalytic durability across a range of pH-varying electrolytes. The combined action of vacancies in oxygen and phosphorus element enrichment results in enhanced catalytic efficiency and durability. Phosphorus's weak electronegativity might make it easier for protons to adsorb and desorb, which would increase the catalyst's effectiveness for HER. Significant characteristics of P-added catalysts with plenty of oxygen vacancies include their fast HER kinetics, minimal HER overpotential, and superior stability in basic and acidic conditions shown in (Figure 13c). The P-loaded MoO_{3-x} nanosheets that are produced exhibit notable hydrogen evolution resistance (HER) qualities, such as minimal overpotential and rapid transport of electrons.¹⁵⁵ *Shu Li and co-workers* exhibited that phosphorus enrichment of $\beta\text{-CoMoO}_4$ nanoplates transforms them into active HER electrodes. P incorporated $\beta\text{-CoMoO}_4$ is incorporated directly onto the titanium plate to generate the self-supported electrode which

increases the number of active regions and improves electrolyte mobility through them. The electronic¹⁵⁶ composition of $\beta\text{-CoMoO}_4$ is modulated by phosphorus doping which also lowers the energy limit for H atom binding and increases its electrical mobility shown in (Figure 13d). The enhanced electrical conductivity of $\beta\text{-CoMoO}_4$ following P doping is verified by both theoretical simulations and experimental findings. The hydrogen adsorption-free energy is shifted into an ideal area via phosphorus loading. The compositional alterations of P doped $\beta\text{-CoMoO}_4$ were studied using XPS. DFT simulations were used to investigate the impact of P doping on the HER performance of $\beta\text{-CoMoO}_4$. As such P-doped $\beta\text{-CoMoO}_4$ exhibits considerably improved HER catalytic activity when compared to pristine $\beta\text{-CoMoO}_4$ with only an overpotential of 138 mV needed to drive the formation of hydrogen at a current density of 10 mA cm^{-2} .¹⁵⁶ *Ji-Sen Li and co-workers* reported synthesizing MoP nanostructures with a metal-organic lattice assist technique and confining them within P-doped porous carbon (Mo-P@PC). The pore constriction effect of MOFs is responsible for the small size of Mo-P particles as its pore size distribution is calculated using DFT. XPS was used to figure out the surface valence and material composition of Mo-P@PC . Additionally, Mo-P nanomaterials are contained inside the carbon framework by the naturally occurring ligands of MOFs which offer many exposed places for activity while preventing the particles from separating or accumulating. The carbon substrate also improves conductivity and decreases interfacial resistance. Phosphorous enrichment is essential for controlling the electrical structure of carbon atoms, which increases pores carbon's conductivity considerably. With a Tafel slope of 59.3 mV dec^{-1} , an initial overpotential of 97 mV and exceptional long-term durability the resultant Mo-P@PC composite demonstrates outstanding HER catalytic activity.¹⁵⁷ An approach for the rational development and easy construction of a MoS_2 -based dual-purpose electrocatalyst on carbon cloth (CC) is presented by *Yan Hu and co-workers*. Minimal overpotentials for hydrogen evolution are shown by the optimized P-doped $\text{MoS}_2@\text{CoP/CC}$ catalyst, with overpotentials of 64 mV in an alkaline solution and 72 mV in H_2SO_4 at a current density of 10 mA cm^{-2} . A thin layer of P-doped MoS_2 is formed on the Co-P nanoneedles' interface after P-doped MoS_2 arranging; when the amount of the molybdenum precursor rises, greater coverage of the surface is observed. It is intriguing that, in the absence of a Co(OH)F buffer layer the surface of P- MoS_2 modified CC shows significant clustering. XPS analysis of the charge transfer between Mo and Co spaces in the P- $\text{MoS}_2@\text{CoP}$ hybrid structure indicates synergy that enhances water dissociation which contributes to faster kinetics. XPS Nonetheless, an efficient charge transfer channel and open pathways for the quick release of gas bubbles after HER are provided by the nano-array framework formed in situ on the conducting CC.¹⁵⁸ A unique synthesis process for uniformly scattered NiCo-NiCoP nanoparticles implemented into P-doped CNTs (NiCo-NiCoP@PCT) is developed by *Ziqian Zhou and co-workers*. This method works by binding phytic acid (PA) on the outer layer of Ni-Co-precursor nanowires and then lowering the temperature. Because of its strong electrostatic attraction phosphorus atoms may draw electrons from metal



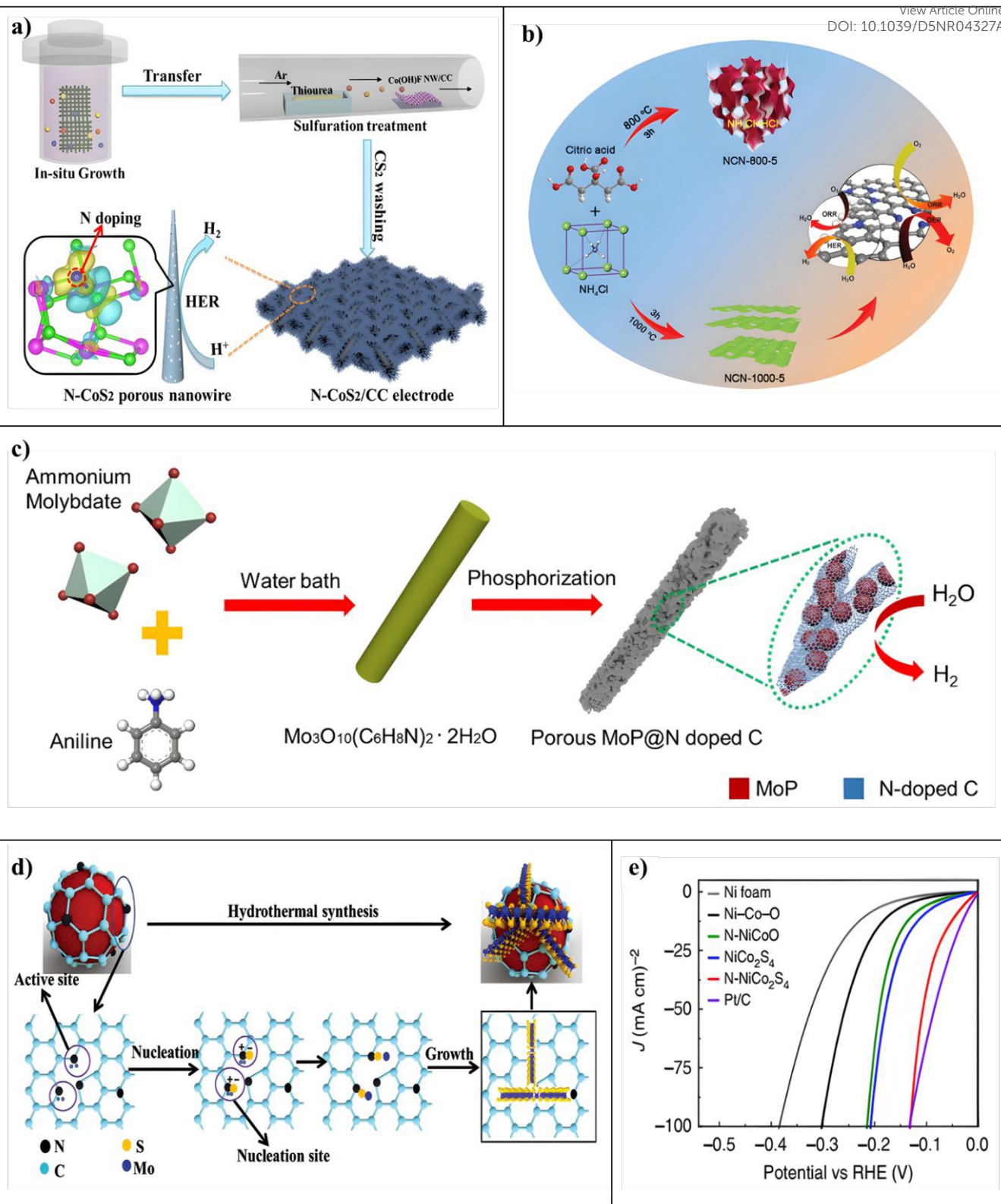


Figure 14. (a) Illustration of the NCoS_2 NWs/CC electrode material synthesis process. reproduced from Ref.^[160] with permission. Copyright 2017, ACS. **(b)** A schematic of the NCN synthesis process. reproduced from Ref.^[163] with permission. Copyright 2019, RSC. **(c)** The porous MoP @N hybrid NWs are shown schematically. reproduced from Ref.^[167] with permission. Copyright 2019, Elsevier. **(d)** Diagram showing the process by which the Ni @NC@ MoS_2 product forms. reproduced from Ref.^[168] with permission. Copyright 2019, Wiley. **(e)** LSV curves in a 1.0 M KOH solution with a scan rate of 5 mV s^{-1} . reproduced from Ref.^[161] with permission. Copyright 2018, Nature.

atoms to reveal extremely active locations and because of a negative charge, they can also function as proton catches which

gives rise to the amazing features of the ensuing TMPs. The remarkable electrocatalytic function of NiCo-NiCoP@PCT/CC

belongs to the combined actions of PCT which promotes effective electron flow, and the heterostructural NiCo-NiCoP that because of its distinct structure has a high intrinsic catalytic ability and many active regions. The NiCo-NiCoP@PCT being bi-functional electrodes has exceptional electrocatalytic performance for both hydrogen generation processes and achieves a minimal overpotential of 135 mV at 10 mA cm⁻².¹⁵⁹ The P-doped HER electrocatalysts are summarised in **Table 9**.

5.2 N-Doped Electrocatalysts for HER

The nitrogen (N) atom has three single electrons and one lone pair in its valence electron layer, providing N with a variety of bonding prospects. The N tiny atomic radius permits it to occupy intermediate locations in catalysts with ease while maintaining overall electrical conductivity.¹⁷⁰ Furthermore, N easily polarizes neighboring atoms due to its strong electronegativity which affects catalytic activity.¹⁷¹ Ammonization is one way to add N atoms to host catalysts; this can be done by solid reactions with nitrogenous reagents such as urea or thiourea or by treating NH₃ through elevated temperatures. N-doping enhances conductive properties and

helps charge transfer by maintaining the metallic nature of the host catalysts.¹⁷² In addition, N-doping can alter surface crystal arrangements, produce more active sites and reduce hydrogen adsorption pressures to enhance catalytic activity by improving HER reaction rates. In general, N atoms' empty orbitals provide advantageous conditions for Tafel and Volmer reactions which encourage effective hydrogen production. Therefore, N-doping is a very beneficial approach for raising HER efficiency in catalysts based on non-noble metals.¹⁷³ To promote the evolution of hydrogen, Pengzuo Chen and co-workers designed Nitrogen Altered Metallic Co-S₂ Porous Nanowire Arrays shown in **(Figure 14a)**. Their method utilized a simple nitrogen designing process that made it easier to alter catalytic active sites, electronic arrangement, and reaction kinetics in metallic Co-S₂ hollow nanowire arrays in a coordinated manner. As confirmed by XPS and XANES spectra, adding nitrogen to the Co-S₂ material changed its shape to add more active sites and enhanced its electrical ability, which sped up charge transfer during the hydrogen evolution process (HER). The density functional model simulations further verified that the N inclusion improved HER kinetics by optimizing the free energy of hydrogen adsorption for both sulphur and cobalt active sites.

S. No	Catalyst	Electrolyte	Overpotential (η) At 10mA cm ⁻²	Tafel slope (mV dec ⁻¹)	C_{dl} (mF cm ⁻²)	Stability (hours & cycles)	Reference
1	N-CoS ₂ NWs/CC	0.5 M H ₂ SO ₄	152 at (150 mA cm ⁻²)	58	-	3000 CV cycles	¹⁶⁰
2	N-NiCo ₂ S ₄	1.0 M KOH	41	37	18	1000 CV cycles	¹⁶¹
3	N-MoO ₂	0.5 M H ₂ SO ₄	96	33	3	1000 CV cycles	¹⁶²
4	NCN-1000-5	0.1 M KOH	51	43	-	500 CV cycles	¹⁶³
5	Fe ₃ C-Co/NC	1.0 M KOH	238	108.8	0.75	16.6h	¹⁶⁴
6	N-CoP/CC	1.0 M KOH	39	58	-	30h	¹⁶⁵
7	M-Co ₂ P/NCNTs	0.5 H ₂ SO ₄	104	68	15.4	1000 CV cycles	¹⁶⁶
8	MoP@NC NW	1.0 M KOH	149	61.7	14.15	5000 CV cycles	¹⁶⁷
9	Ni@NC@MoS ₂	0.5 H ₂ SO ₄	82	47.5	4.35	3000 Cv cycles	¹⁶⁸
10	CoP@NC-NG	0.5 H ₂ SO ₄	135	59.3	-	14h	¹⁶⁹

Table 10. N-Doped Electrocatalysts for HER



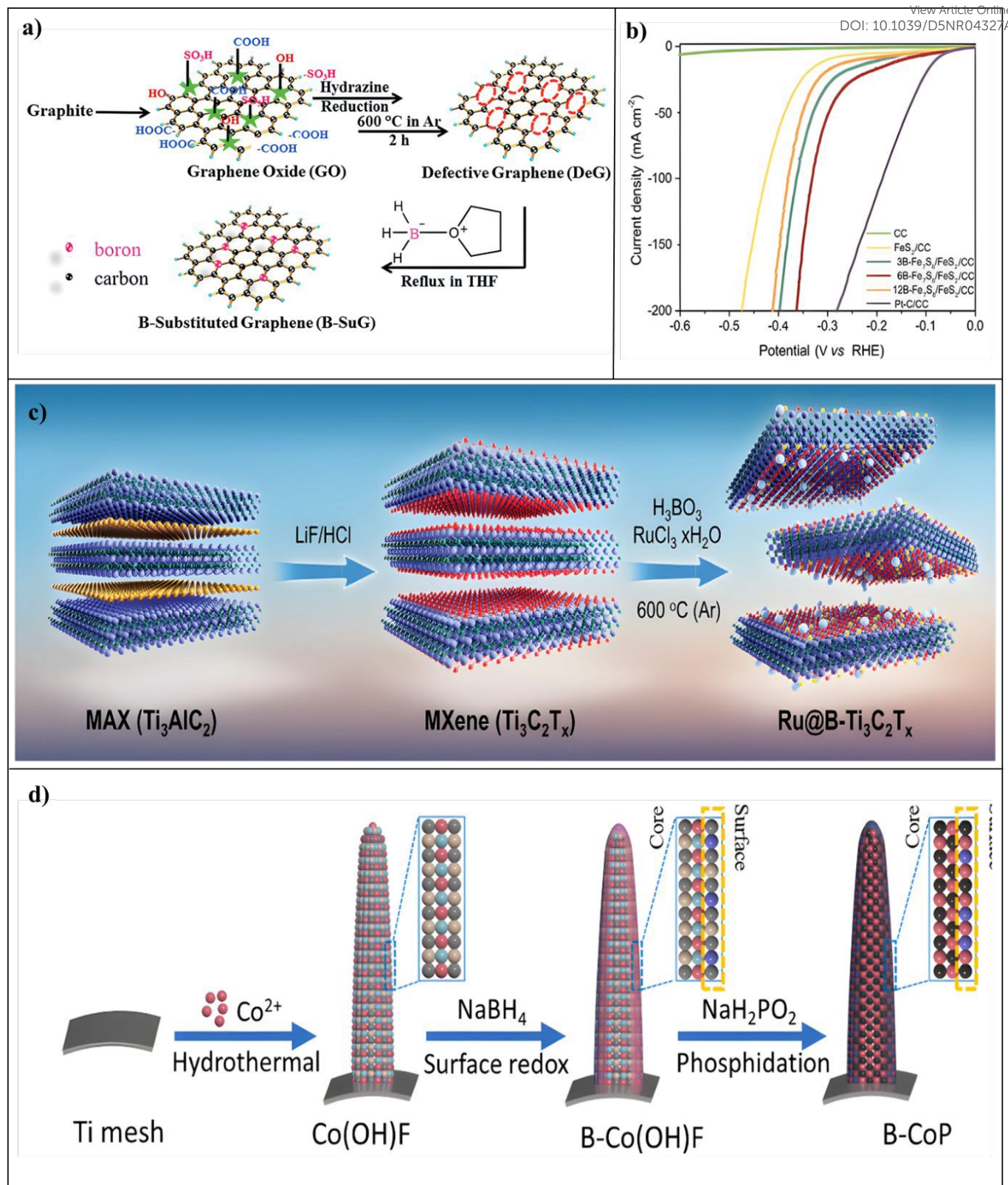


Figure 15. (a) Schematic representation of producing B-substituted graphene (B-SuG), reproduced from Ref.[¹⁷⁴] with permission. Copyright 2018, RSC. (b) The B-Fe_xS_y/FeS₂/CC electrocatalysts HER performance in a 1M KOH solution, reproduced from Ref.[⁴⁵] with permission. Copyright 2022, Wiley. (c) A schematic representation of the synthesis of Ru@B-Ti₃C₂T_x and Ti₃C₂T_x, reproduced from Ref.[¹⁷⁸] with permission. Copyright 2021, Wiley. (d) Synthesis procedure of B-CoP, reproduced from Ref.[¹⁸¹] with permission. Copyright 2023, Elsevier.

The resultant N-Co-S₂ NWs/CC electrode had a notably lower overpotential of 152 mV and a current density of 50 mA cm⁻², demonstrating a dramatically better HER performance.¹⁶⁰

To achieve extremely effective evolving hydrogen catalytic activity, *Yishang Wu and co-workers* developed NiCo₂-S₄ nanowires using N-inclusion. Because of the strong chemical

ARTICLE

Journal Name

bonds between adsorbed H and S, which is extremely electronegative, conventional metal sulphides employed for this purpose frequently have difficulties with hydrogen release. N-doping was repeatedly found to be an effective way to modify the exterior electron densities of NiCo_2S_4 by a combination of XPS, synchrotron-based X-ray absorption spectral analysis, and density functional analysis tests. The strategic development of extremely effective catalysts for hydrogen evolution appears to be promising given the capacity to control electron concentrations at catalytic locations. XPS and DFT simulations reveal that N dopants may influence the electrical characteristics of NiCo_2S_4 , enabling H^* desorption from sulfur sites and HO-H cleavage in water molecules. The NiCo_2S_4 nanowire networks that were nitrogen incorporated showed a Tafel slope of 37 mV dec^{-1} and an overpotential of 41 mV at 10 mA cm^{-2} shown in (Figure 14e).¹⁶¹ For the electrochemical hydrogen generation process, *Junqing Yan and co-workers* developed a single-step, consistent technique for producing Nitrogen incorporated molybdenum-dioxide nanosheets. This entailed producing N-added molybdenum oxide materials by calcining urea and layered molybdenum oxide at completely high temperatures. N increased the number of proton adsorption sites with lower binding energies and caused surface structure instability. XPS measurements revealed the production of N-NiO/Ni. In Fig. S21(c), the N-doped NiO/Ni sample demonstrated higher electrocatalytic water splitting activity than the unaltered NiO/Ni. DFT calculations were carried out to determine the internal reason of the N-MoO₂ sample's exceptional HER performance. Surface N doping, surface bending, and the inherent characteristics of molecular oxide worked together to produce a considerable and long-lasting hydrogen evolution action, with a Tafel slope of 33 mV dec^{-1} and an overpotential of 96 mV at 10 mA cm^{-2} .¹⁶² Ultrathin carbon nanosheets treated with N, initially developed by *Hao Jiang and co-workers*, provide a state-of-the-art metal-free electrocatalyst for the hydrogen-evolving process. They generated N-doped ultrathin carbon nanosheets (NCNs) via straightforward pyrolysis using a unique gas-foaming method shown in (Figure 14b). The carbon atoms at the armchair border and next to the graphitic N dopants were determined by the team to be inherent active sites for HER by DFT calculations. In acidic conditions, the catalyst also showed notable activity and durability for HER. The low Tafel slope of 43 mV dec^{-1} of NCN confirmed its exceptional kinetic characteristics.¹⁶³ A new electrocatalyst for the hydrogen evolution process was presented by *Chun Cheng Yang and co-workers*. It is made of Fe_3C -Co nanoparticles enclosed in an N-doped carbon stacked framework (Fe_3C -Co/NC). To further understand the electrocatalytic activity of Fe_3C -Co/NC, the surface electronic state and chemical composition were measured by XPS. DFT calculations were performed to determine the mechanism of the Fe_3C -Co/NC hybrid's ORR and HER electrocatalytic performance. This unique hybrid material which is manufactured for the first time by a simple template-removal technique, blends 2D carbon particles with 1D CNTs to produce many active sites that are produced from Fe_3C , Co, and NC species and the mesoporous carbon arrangement: Fe_3C , Co,

and NC are intimately linked. In both acidic solutions overpotential is 298 mV and alkaline overpotential is 238 mV conditions, the catalyst demonstrated strong HER activity.¹⁶⁴ For the hydrogen evolution process, *Yana Men and co-workers* designed N-Doped CoP as a long-lasting electrocatalyst. The development of N-doped CoP nanoflowers that exhibit exceptional HER efficacy and are produced on conductive carbon cloth (N- N-doped CoP/CC) is covered. According to experimental findings, N-doping effectively modifies the electrical properties of Co d-orbitals and maximizes the value of the free energy of hydrogen absorption, leading to improve HER performance. N-loading enhanced the free energy of adsorbed H for CoP to an ideal importance, according to DFT calculations, giving N-CoP/CC strong HER performance. With overpotentials of 39 mV and 25 mV respectively, to reach a current density of 10 mA cm^{-2} in 1.0 M KOH and $0.5 \text{ M H}_2\text{SO}_4$, the resultant N-doped CoP/CC nanoflowers showed impressive HER activity. The exceptional HER function and robustness of N-CoP/CC are attributed to its very open shape, greater exposure of the active regions, improved electrical properties, and simultaneous electronic effects induced by N doping. A broad pH range from 0 to 14 was demonstrated by N-doped CoP/CC's outstanding HER performance.¹⁶⁵ The impacts of doping transition metals (Fe, Ni, and Cu) on the electrocatalytic activity of M-Co₂P/N-doped-CNTs hybrid catalytic agents for the HER were studied by *Yuan Pan and co-workers*. The synthesis of these hybrid catalysts was carried out by a simple in situ thermal degradation method. It was discovered that doping with Fe atoms improved the crystal plane's development, increasing its specific surface area and exposing more catalytically active spots. Furthermore, upon doping, Fe^{2+} showed the largest positive charge of all the M-Co₂P/N-doped-CNT hybrid catalysts. Fe-Co₂P/N-doped CNTs, Ni-Co₂P/N-doped CNTs, and Cu-Co₂P/N-doped CNTs had onset overpotentials of 25 mV , 96 mV , and 140 mV according to comparison study.¹⁶⁶ N-doped carbon-plated highly porous Mo-P Nanowires have been developed by *Chaoran Pi and co-workers* as a very effective catalyst for the HER. They phosphorized organic-inorganic hybrid NWs to generate Heterogeneous Mo-P@NC NWs shown in (Figure 14c). The H⁺ utilization is facilitated by the in-situ development of NC, which is characterized by many tiny pores. Mo-P@NC exhibits synergistic advantages, many active sites, and quick ion/electron transport. DFT calculations reveal the strong electrocatalytic activity of the MoP@NC hybrid electrocatalyst. The XPS results indicate that the bonds in MoP@NC remain constant after cycling. However, without the carbon layer, the Mo-P bond decreases significantly, confirming the high oxidation resistance of the carbon covering. Excellent HER function and endurance are demonstrated by the electrocatalyst throughout a broad pH range. In acidic and alkaline solutions, correspondingly, modest overpotentials of 96 mV and 149 mV were notable, along with Tafel slopes of 49.2 mV dec^{-1} and 61.7 mV dec^{-1} . These results were supported by remarkable stability.¹⁶⁷ Ni@N treated Carbon@MoS₂ Nanosheets have been proposed by *Sayyar Ali Shah and co-workers* as a very effective electrocatalyst for hydrogen



evolution operation. Ni@NC@MoS₂ pyramidal microspheres were generated by vertically growing Mo-S₂ nanosheets with enlarged interfacial spacings on a Ni@N doped carbon (Ni@NC) material using a straightforward hydrothermal approach shown in (Figure 14d). The synergistic impact of compact catalytic regions on Mo-S₂ nanosheets with exposed margins and enlarged interlayer distances, together with fast electron transport from the Ni@NC surface to Mo-S₂ nanosheets, is responsible for the excellent HER efficiency of the Ni@NC@Mo-S₂ catalysis. A very small Tafel slope of 47.5 mV dec⁻¹ and a modest overpotential of 82 mV at 10 mA cm⁻² indicate that this exceptional electrocatalyst has great potential for use in practical hydrogen generation operations.¹⁶⁸ Polyaniline-induced N enriched Carbon-Coated Co-P particles embedded in N Infused Graphene is the effective electrocatalyst that *Jingwen Ma and co-workers* developed for the HER. N-added graphite nanosheets promoting N-doped carbon-coated CoP nanoparticles are generated in this production by pyrolysis and polyaniline-based phosphating methods. As the framework, N-doped graphene effectively inhibited the CoP nanoparticles from collecting, and the carbon shell made of polyaniline functioned as a shield, preventing the dissolution of the particles and improving their electrical mobility. In 0.5 M H₂SO₄, the electrocatalyst that was produced showed

remarkable electrochemical activity for HER, exhibiting a low Tafel slope of 59.3 mV dec⁻¹ and a modest overpotential of 135 mV at 10 mA cm⁻². Moreover, after 14 h of operation, the N-doped carbon shells enclosing the CoP nanoparticles demonstrated outstanding durability and resisting corrosion.¹⁶⁹ The N-doped HER electrocatalysts are summarised in Table 10.

5.3 B-Doped Electrocatalysts for HER

Boron has three valence electrons and an electron deficiency it is more likely to bond with oxygen single electron pairs from H₂O molecules which facilitates the release of protons during the HER catalysis process.¹⁸³ The redistributing of electrons made possible by B-doping strengthens the crystal structure of catalyst substances lowering the possibility of corrosion or structural degradation over extended HER operation.¹⁸⁴ Furthermore, the HER's reaction kinetics may be changed by boron dopants resulting in reduced overpotential and higher reaction rates. Thus, the catalyst's total energy efficiency is raised as a consequence of this kinetic increase which leads to more productive hydrogen synthesis at lower energy sources. Boron dopants are a useful tactic for accelerating the catalytic activity of catalysts based on non-noble metals. Nevertheless, there are currently few publications on B-doped non-noble metal-based catalysts which points to a unique possibility for

S. No	Catalyst	Electrolyte	Overpotential (η) At 10mA cm ⁻²	Tafel slope (mV dec ⁻¹)	C _{dl} (mF cm ⁻²)	Stability (hours & cycles)	Reference
1	B-SuG	0.5 M H ₂ SO ₄	130	99	-	18h	174
2	B-Fe ₇ S ₈ /FeS ₂	1.0 M KOH	113	57	12.4	1000 CV cycles	45
3	B-CoSe ₂ /CC	1.0 M KOH	153	85	58	24h	175
4	NiCo@BC	1.0 M KOH	209	60	08.63	200h	176
5	B-MoC	1.0 M KOH	285	128	17.28	1000 CV cycles	177
6	Ru@B-Ti ₃ C ₂ T _x	0.5 M H ₂ SO ₄	62	100	1.39	1000 CV cycles	178
7	Ni ₃ Fe@BC	1.0 M KOH	330	127	-	20h	179
8	A-NiCo LDH/NF	1.0 M KOH	151 at (100 mA cm ⁻²)	94	12	72h	180
9	B-CoP	1.0 M KOH	112 at (100 mA cm ⁻²)	61.9	-	20h	181
10	B-Rh@NC	1.0 M KOH	26	52	18.6	10h	182

Table 11. B-Doped Electrocatalysts for HER



ARTICLE

Journal Name

the synthesis of innovative catalysts using B-doping. By synthesizing metal liberated B loaded graphene, *Bhaskar R. Sathe and co-workers* demonstrated exceptional electrocatalytic ability in accelerating the hydrogen evolution process. Reduced conversion barriers are ascribed to the faster conversion of H^+ ions to H_2 which is made possible by the integration of B heteroatoms as well which is made possible by C–B relationships, within the graphene framework shown in (Figure 15a). The unique material was produced by carefully replacing the carbon atoms in graphene that were inadequate with B atoms using borane tetrahydrofuran, a borylating chemical that is widely accessible. When it comes to borylating substances, BH_3 -THF is the best option since it produces the most effective electrocatalyst. When B-SuG is applied in HER in a 0.5 M H_2SO_4 solution, there is a significant increase in current density at an overpotential as low as ~ 0.2 V vs. RHE.¹⁷⁴ To boost the alkaline HER, *Jing Wu and co-workers* developed B-Doped Fe_7S_8/FeS_2 catalysts. DFT simulations were carried out to assess the intrinsic activity of the electrocatalysts. The Iron and Sulfur atoms' electronic arrangements are successfully tuned by adding B atoms to the Fe_7S_8/FeS_2 electrodes. By reducing energy barriers for splitting water and increasing the efficiency of desorbing H_2 intermediate molecules, this optimization results in the production of ideal B- Fe_7S_8/FeS_2 catalysts. XPS was used to examine the electronic structures, composition, and chemical states of B- Fe_7S_8/FeS_2 electrocatalysts. This HER electrocatalyst has a 113 mV overpotential in alkaline conditions, enabling a current density of 10 mA cm^{-2} shown in (Figure 15b). Heteroatom adding shows promise in altering the electrical characteristics of transition metal sulfide electrocatalysts, hence speeding their kinetics in hydrogen evolution processes.⁴⁵ Boron-added Co- Se_2 nanowires are developed by *Zhiming Liu and co-workers* to serve as very effective catalysts for the hydrogen evolution process. The effective production of B-added Co- Se_2 nanoparticles on carbon cloth (Boron-Co Se_2 /CC) was shown by their study. XPS was employed to examine Co Se_2 /CC and B-Co Se_2 /CC to assess the impact of B doping on the electronic structure. Co- Se_2 has intrinsic catalytic properties, however its effectiveness is limited by the poor hydrogen adsorption on its active cobalt site. Anions are added to the catalyst to increase its electronic framework, which in turn improves HER efficiency. Simulations using DFT demonstrate that B loading improves Co- Se_2 's intrinsic conductance and maximizes the hydrogen ΔG^* at the selenium and cobalt sites. At 10 mA cm^{-2} , the Boron-Co Se_2 catalyst produces an overpotential of just 153 mV, while the Boron-Co Se_2 /CC sample's Tafel slope was determined at a modest 85 mV dec^{-1} .¹⁷⁵ Incredibly robust Ultrafine Boron treated NiCo@Carbon Nanocrystals were reported by *Bashir Adegbemiga Yusuf and co-workers* as a robust catalyst for the HER. They developed extremely stable ultrafine NiCo@boron treated carbon (NiCo@BC) hybrids using a simple reduction strategy. The remarkable catalytic activity results from the complementary interactions among the NiCo and B treated carbon stages in the hybrid substance, which has a crystalline structure, many catalytically active areas, and good electrical properties. The partial transfer of electrons from B to NiCo

metals is made easier by the abundance of active sites on the catalyst's surface which greatly increases ΔG^* . As such, this material exhibits great potential for use as an electrocatalyst for HER in alkaline environments. With a modest Tafel slope of $60\text{ mV}dec^{-1}$ and a low geometrical overpotential of 209 mV at a current density of 10 mA cm^{-2} the produced NiCo@BC nanoparticles catalyst demonstrates outstanding HER performance.¹⁷⁶ *Qin Lin and co-workers* developed boron-incorporated molybdenum carbide as an independent electrocatalyst for the hydrogen generation process. Boron doping was introduced, which decreased the free energy for H^* adsorption while increasing intrinsic reactivity. In the B-MoC framework, this alteration promoted charge movement and inhibited nanoparticle aggregation. Moreover, excess electron transfer to MoC nanoparticles caused by B-doping's induction of electron shortage resulted in the development of multiple proton adsorption sites and an increase in electrocatalytic activity. With outstanding stability and a low overpotential of 285 mV at a current density of 10 mA cm^{-2} and the B-MoC performed well over a wide pH range.¹⁷⁷ *Munkhjargal Bat-Erdene and co-workers* reported boron capped $Ti_3C_2T_x$ (MXene) nanosheets are an approach to improve electrocatalytic hydrogen production in an additive way. In applications involving electrocatalytic Ru nanoparticle encapsulation, these heteroatom-doped $Ti_3C_2T_x$ (MXene) nanosheets serve as effective solid substrates shown in (Figure 15c). XPS revealed the effective synthesis of $Ti_3C_2T_x$ and its oxidative states. Electrochemical experiments and quantum structural first-principles simulations have shown that B adding onto 2D MXene nanosheets significantly improves the rate of intermediate H^* adsorption and lowers the charge-transfer barrier during the HER mechanism. It increased active site responsiveness and advantageous electrode kinetics resulted from this improvement. Upon achieving current densities of 10 mA cm^{-2} and 100 mA cm^{-2} respectively, for the HER the Ru@B- $Ti_3C_2T_x$ nanosheets that exhibit excellent catalytic activity, and have tiny overpotentials of 62.9 mV and 276.9 mV.¹⁷⁸ A one-pot fabrication technique for boron-loaded C-enclosed Ni₃-Fe nanoparticles has been presented by *Yusuf Bashir Adegbemiga and co-workers* displaying excellent activity for hydrogen evolution processes. In alkaline environments, the Ni₃Fe@BC compound performs better electrochemically suggesting a synergistic interaction between the Iron and Nickel components. The catalytic activity of Ni₃-Fe@BC-500°C is attributed to the doping of B and the corresponding bonding of metal ions (Fe+Ni), which may augment the sites of catalysis. The one-pot production procedure of Ni₃-Fe@BC makes it extremely promising for HER electrocatalysis applications by utilizing low-cost component sources. Moreover, the high electrochemical surface area, boron-to-metal electron transfer, and tiny particle size are responsible for the remarkable electrochemical performance. Notably, Ni₃-Fe@BC exhibits tiny Tafel slopes, low overpotentials, and good stability for HER, it has a Tafel slope of $77\text{ mV}dec^{-1}$ and an overpotential of 280 mV.¹⁷⁹ The B-added amorphization of LDH was developed by *Hongyuan Yang and co-workers* to enable large current-density hydrogen evolution processes. As opposed to other



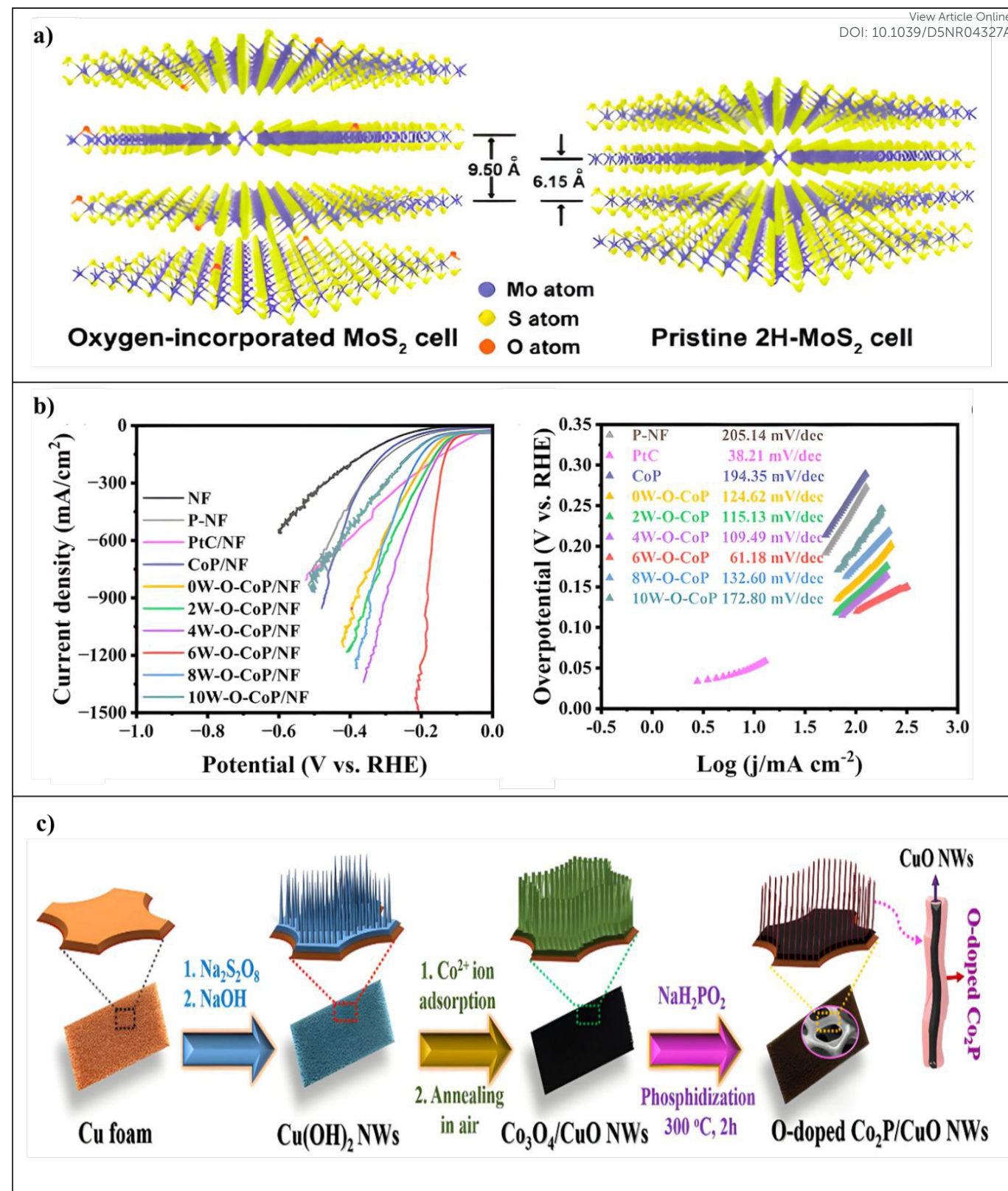


Figure 16. (a) TGA and DTA curves of ultrathin MoS₂ nanosheets with oxygen incorporation. reproduced from Ref.[¹⁸⁶] with permission. Copyright 2013, ACS. (b) HER polarisation curves for catalysts based on NF, P-NF, CoP/NF, commercial PtC/NF, and xW-O-CoP/NF ($x=0, 2, 4, 6, 8, 10$) together with the matching Tafel slopes. reproduced from Ref.[¹⁹⁰] with permission. Copyright 2023, Springer. (c) Diagram showing the steps involved in creating the O-doped Co₂P/CuO NWs/CF hybrid. reproduced from Ref.[¹⁹²] with permission. Copyright 2019, Elsevier.

materials where boride/phosphide manufacturing occurred from Boron/Phosphorous inclusion into LDHs for HER, this

amorphization caused by boron doping enhanced HER activity. Furthermore, it is easy to use this adjustable B doping-induced

ARTICLE

Journal Name

amorphization technique with other transition metal (TM) LDHs. The remarkable effectiveness of A-NiCo LDH/NF has been attributed to its distinct three-dimensional arrangement and the modulation of the crystalline-to-amorphous framework, consequently increasing the capacity for charge transfer and revealing active sites. The amorphous boron incorporated Ni-Co LDH supported on nickel foam (A-NiCo LDH/NF) exhibits remarkable robustness in alkaline conditions even after 72h and can achieve huge current densities at modest overpotentials of 1000 mA cm^{-2} at 381 mV, 500 mA cm^{-2} at 286 mV, and 100 mA cm^{-2} at 151 mV.¹⁸⁰ Using controlled surface redox processes, Yingying Gao and co-workers reported a technique for boron surface layer restricted doping on cobalt phosphide nanowire arrays shown in (Figure 15d). At 100 mA cm^{-2} , the resultant nanowire CoP with a B-doped surface layer composition is an outstanding electrocatalyst for the hydrogen evolution process, obtaining an overpotential of 112 mV. Cobalt is given electron-rich properties via Boron-doping which causes electron rearrangement inside the material according to theoretical understanding and XANES and XPS investigations. These low-valence cobalt centres have a significant affinity for H_2O molecules and maximize ΔG_{H}^* which speeds up reaction kinetics when coordinated with boron. Cobalt centres doped with boron on the surface layer showed increased HER activity in comparison to non-doped CoP. B-doping causes electron

redistribution and changes the d-band structure of cobalt which promotes the produce of low-valence cobalt centres and in the end leads to optimized ΔG_{H}^* and quicker reaction kinetics as both experimental results and DFT simulations showed.¹⁸¹ A boron doping method is developed by Qingping Yu and co-workers with starting intense metal-support connections of ultra-small Rh particles embedded in an N-doped carbon framework (B-Rh@NC). It is confirmed by both theoretical and experimental research that boron doping maximizes its electronic makeup and water adsorption power, hence triggering the metal-support connections between Rh and NC. As such, B-Rh@NC demonstrates excellent electrocatalytic activity for the HER over a wide pH range in addition to outstanding durability. To further increase HER activity boron loading efficiently controls the electrical framework and the absorption of water energy. Boron doping improves HER activity by regulating electrical structure and water adsorption energy, based on DFT analysis. On obtaining low overpotentials in 1.0 M KOH (26 mV) and 0.5 M H_2SO_4 (43 mV) the resulting B-Rh@NC nanospheres exhibit activity for HER. Additionally, a current density of 10 mA cm^{-2} in 1.0 M KOH could be generated by the built two-electrode system with just 1.53 V when B-Rh@NC is used as the cathode and Ru-O₂ is used as the anode.¹⁸² The B-doped HER electrocatalysts are summarised in Table 11.

S. No	Catalyst	Electrolyte	Overpotential (η) At 10 mA cm^{-2}	Tafel slope (mV dec ⁻¹)	C_{dl} (mF cm ⁻²)	Stability (hours & cycles)	Reference
1	O-NiCoP/Ni ₂ P	1.0 M KOH	58	68.8	55.3	24h	185
2	O-MoS ₂	0.5 M H_2SO_4	120	55	37.7	3000 CV cycles	186
3	O-WS ₂ -1T	0.5 M H_2SO_4	88	47	-	500 CV cycles	187
4	OMS/CC	0.5 M H_2SO_4	300	58	-	2000 CV cycles	188
5	CC@O-CoFeS	0.5 M H_2SO_4	105	62	9.13	24h	189
6	6W-O-CoP	1.0 M KOH	84	61.1	95.6	10000 CV cycles	190
7	VS ₄	0.5 M H_2SO_4	48	44	2.82	75h	191
8	O-Co ₂ P/CuO NWs/CF	1.0 M KOH	101	69.4	39.6	30h	192
9	H-NiCoP NWAs/NF	1.0 M KOH	44	38.6	71	30h	193
10	O-CoS _x	1.0 M KOH	-	72	-	24h	194

Table 12. O-Doped Electrocatalysts for HER



5.4 O-Doped Electrocatalysts for HER

Oxygen has a greater electronegativity (3.5) than boron, which means it has more of an impact on the movement of electrons after doping. Higher conductivity and an extensive number of active sites are balanced by the introduction of oxygen heteroatoms. Determining the relationship between catalytic effectiveness and oxygen doping levels is essential. To facilitate effective electron transport during the HER oxygen doping accelerates charge transfer kinetics at the catalyst-electrolyte interface. Increased performance optimization of the catalyst in the HER is possible by using oxygen doping to regulate surface morphology.¹⁹³ Reduction of band gap with oxygen incorporation which improves intrinsic conductivity and facilitates proton-catalyst contact with each other is responsible for the increased catalytic activity according to DFT simulations.^{195,196} Through an increasing phosphatization and dip-coating method, *Yan Wen and co-workers* developed O-doped hierarchical NiCoP/Ni₂P hybrid electrodes (O-NiCoP/Ni₂P) to reduce additional costs related to heteroatom doping. To achieve an effective alkaline HER, the resultant O-NiCoP/Ni₂P electrode shows an extremely low overpotential of 58 mV at 10 mA cm⁻² and retains long-term stability for 48h. The HER kinetics increase by O doping, which maximizes the free energy of hydrogen/water absorption, according to simulations using DFT simulations. Its catalytic efficacy is further enhanced by the strong coupling in O-NiCoP/Ni₂P that further improves electron transport. The transition-metal phosphide-based HER electrocatalysts reported by this work offer a viable method for their rational design.¹⁸⁵ The development of O-incorporated MoS₂ thin nanosheets for effective hydrogen evolution was developed by *Junfeng Xie and co-workers*. Several studies have been made to improve the conductivity or the number of active sites in MoS₂ catalyst to increase the HER performance. The unsaturated S-atoms are made available as HER targets by the formation of disorder, and the addition of oxygen efficiently modifies the electronic configuration to increase intrinsic conductance shown in (Figure 16a). An improved catalyst with a moderate amount of disorder was developed via controlled disorder design and oxygen incorporation, and it showed better electrocatalytic hydrogen evolution performance. HER activity is significantly increased when regulated disorder design and simultaneous oxygen inclusion in MoS₂ catalysts work together to regulate structural and electronic characteristics synergistically. DFT calculations show that oxygen inclusion can govern the electronic structure of MoS₂, resulting in improved properties. To analyze the chemical composition of the products, XPS and elemental mapping studies were performed. The catalyst that has been tuned has an initial overpotential as low as 120 mV overall.¹⁸⁶ For the hydrogen evolution reaction, O-included WS₂ particles with improved electrocatalytic activities have been presented by *Prasad V. Sarma and co-workers*. Using chemical exfoliation along ultrasonication

processes, as well, they provide a unique way for the controlled generation of very catalytically active O-incorporated 1T and 2H WS₂ tiny clusters from O-deficient WO₃ tiny rods. The generated 1T tiny clusters have an extremely low Tafel slope of 47 mV dec⁻¹, minimal onset overpotential of 88 mV, large exchange current density, and superior stability. They are further distinguished by customized edge sites and improved conductivity assigned to the metallic 1T phase and O-integration.¹⁸⁷ The synthesis of O-doped molybdenum disulfide nanosheets developed on carbon cloth, which produced a strong hydrogen generation process, was reported by *Junfeng Xie and co-workers*. On MoS₂, they together used elemental integration, disorder construction, and material bonding to enhance active sites and electrical conduction in a synergistic way that produced a very effective hydrogen-evolving efficiency. Frequently, the 2D electron coupling system can be harmed or degraded by the exposure of highly active edge regions of conducting MoS₂ which results in a decreased density of efficient active sites that are essential for activating the HER reaction. However, efficient synergistic improvement of both conductive properties and active sites is obtained by the combination of oxygen dopants with a distinct disordered shape. Consequently, the O-doped MoS₂/carbon fabric catalyst that is directed vertically exhibits an ultralow initial overpotential of 90 mV to start the HER activity.¹⁸⁸ O-doped Cobalt/Iron disulfides have been produced by *Chaonan Wang and co-workers* as highly successful catalysts for the generation of hydrogen process. While O-doped sulfur compounds were produced via a procedure encompassing calcination and sulfurization, Iron was added by exchange of ligands. Exceptional electrocatalytic HER performance was demonstrated by an optimized sample of CC@O-Co-Fe-S which showed remarkable endurance and an exceptionally low overpotential of 105 mV at a current density of 10 mA cm⁻². The shape of the O-Co-Fe-S nanosheet arrangement allowed for optimum exposure of the electrocatalytically active spots. O-adding greatly boosted the inherent catalytic activity and successfully modified the electronic framework causing the catalyst's charge to disperse. XPS was employed to examine the element compositions and electronic states of CC@O-CoFeS-0.025-500 and control samples. DFT studies show that pure CoS₂'s Co atoms are catalytically active, with a Gibbs free energy of 0.38 eV for hydrogen adsorption (ΔG_H^*).¹⁸⁹ [W-O] incorporated CoP was reported by *Ge Meng and co-workers* to improve hydrogen evolution at substantial current densities. A versatile catalyst for HER is produced when the [W-O] group, which is well-known for its powerful adsorption ability, is incorporated into CoP. In addition to acting as strong H₂O adsorption locations which accelerates the cathodic H₂O splitting, these [W-O] species also aid in the Heyrovsky step by changing the d-band center of cobalt sites due to the connected O in the [W-O] group which leads to in markedly improved catalytic results. Using this unique method, a hybrid catalyst with outstanding catalytic capabilities is produced by

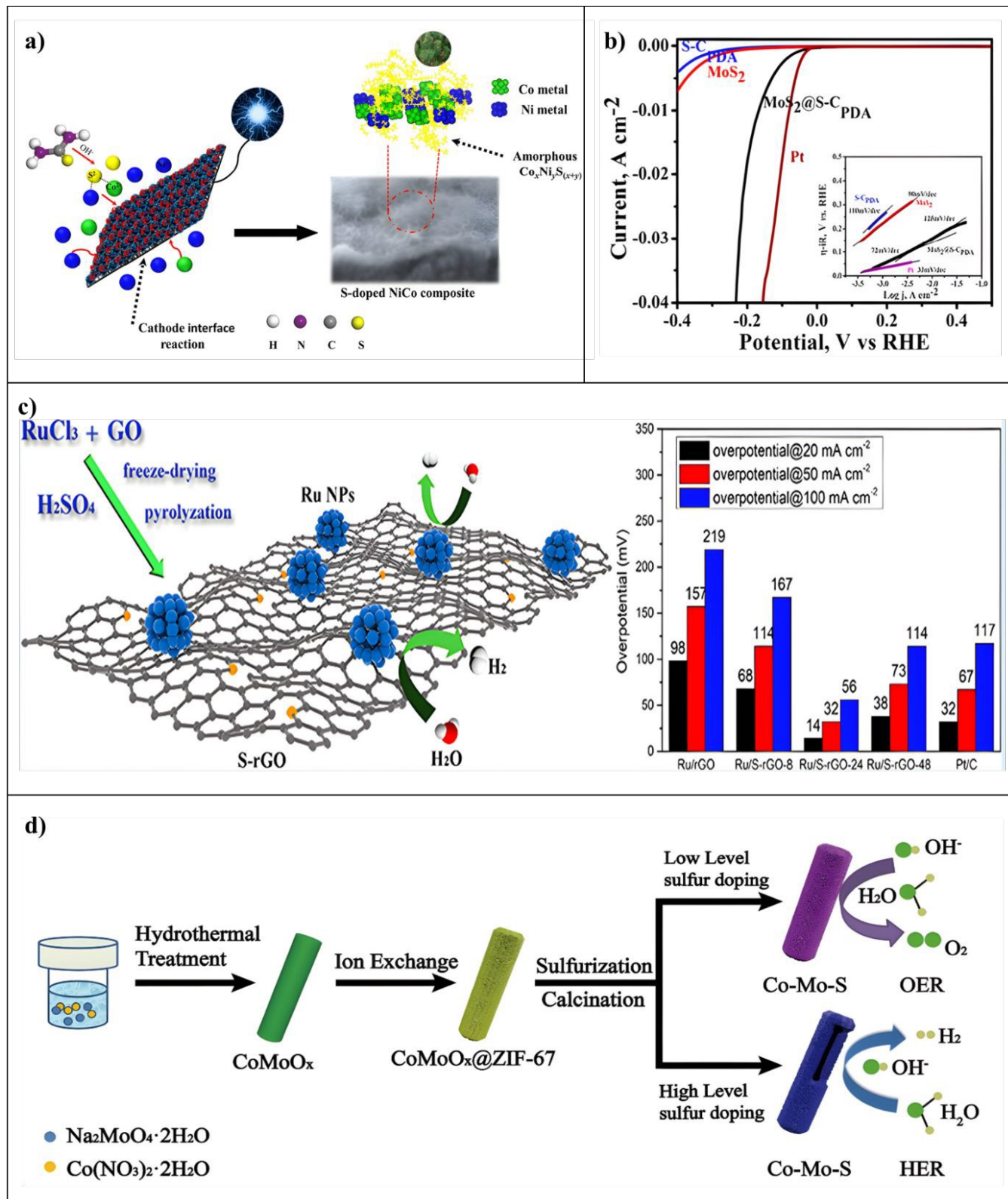
Figure 17. (a) The electron-induced mechanism for the synthesis of S-doped NiCo composite. reproduced from Ref.^[198] with permission. Copyright 2020, RSC. **(b)** MoS₂@S-CPDA, MoS₂, and SCPDA modified electrodes in 0.5M H₂SO₄ linear sweep voltammograms. reproduced from Ref.^[205] with permission. Copyright 2015, RSC. **(c)** Ru/S-rGO Synthesis Process. reproduced from Ref.^[201] with permission. Copyright 2020, ACS. **(d)** Illustration showing the steps involved in creating S-doped cobalt molybdate samples from Co-Mo precursor. reproduced from Ref.^[203] with permission. Copyright 2018, ACS.

introducing the [W-O] grouping which has a great adsorption capacity, into CoP nanoflakes. The theoretical computations



were carried out using the DFT approach. XPS measurements were carried out to analyze the surface composition and binding structure of the catalysts. The catalyst achieves a

workers in the form of O-Doped VS₄ Small particles with Abundant Sulfur Vacant positions. The VS₄spheres which were produced using a simple solution process have a significantly



minimal overpotential of 185.60 mV at 1000 mA cm⁻² shown in (Figure 16b).¹⁹⁰ A better electrocatalyst for the reaction of hydrogen evolution has been engineered by Jun Xu and co-

reduced band gap and enhanced intrinsic electrical conductivity due to their O-doping and abundance of S-vacancies. Fast charge transfer throughout the HER operation is made possible

by this improvement. Furthermore, many highly active areas with high catalytic activity are provided for the proton-to-hydrogen conversion by the abundant defects of O-heteroatoms and S-vacancies. XPS was used for assessing the chemical states of the VS_4 and VS_2 samples. DFT studies show that O-doping and S-vacancy significantly reduce the band gap of the VS_4 , increasing its inherent electrical conductivity. As a HER catalyst, VS_4 nanoparticles outperform 1T- VS_2 microflowers with an arrangement of layers owing to the combined benefits of defect design and electronics. With a modest Tafel slope of 44 mV dec⁻¹ and a low overpotential of 48 mV at 10 mA cm⁻² the VS_4 spheres catalyst exhibits impressive kinetic characteristics.¹⁹¹ For effective electrocatalytic water splitting, *Thi Luu Luyen Doan and co-workers* have developed a technique for producing oxygen-doped cobalt phosphide-layered shelled metal nanowires. Using a straightforward method they attached O-doped cobalt phosphide-layered shelled Cu nanowires vertically onto a 3D framework to build a hierarchical catalyst shown in (Figure 16c). Significant flaws are introduced by this special construction which also modifies the surface science. The product is an expanded surface area with plenty of pathways for the diffusion process, rich electroactive places, and regulated adsorption strength. Because of the small energy barrier for H

adsorption, Co-based catalysts stand out among other alternatives due to their relative availability, affordability, and high activity. For the HER process, the catalyst shows modest overpotentials of 101 mV resulting in a current response of 10 mA cm⁻².¹⁹² Oxygen doping to boost Atomic Hydrogen Binding Energy on Ni-Co-P for extremely efficient hydrogen synthesis was produced by *Chunlei Liu and co-workers*. They theoretically demonstrate how O-doping in Ni-Co-P may precisely modify the atomic hydrogen binding energy by DFT computations. To get an optimal atomic hydrogen binding energy, Ni-Co-P is strategically doped with oxygen. This is a powerful method that enhances intrinsic conductivity and augments exposed active areas to provide better HER activity. The exceptional HER activity results from the quick produce of the overpotential (30 mV) of NiCo-phosphate at the surface after mild oxygen doping, plenty of exposed active regions and fine-tuning the atomic H₂ binding energy on cobalt and Phosphorous places. H-NiCoP NWAs/NF exhibit remarkable HER performance in neutral and alkaline media with controlled O-doping outperforming most of the most advanced binaries and tertiary phosphide catalysts now. Thus, an O-doped Ni-Co-P (about 0.98% of O) nanowire array that has been tuned displays a tiny Tafel slope of 38.6 mV dec⁻¹ and an exceptionally low HER overpotential of 44 mV to drive 10 mA cm⁻².¹⁹³ To improve the evolving hydrogen

S. No	Catalyst	Electrolyte	Overpotential (η) At 10mA cm ⁻²	Tafel slope (mV dec ⁻¹)	C_{dl} (mF cm ⁻²)	Stability (hours & cycles)	Reference
1	S-RhNi	0.5 M H ₂ SO ₄	17 at (20 mA cm ⁻²)	24.61	-	10h	197
2	S-NiCo@50	1.0 M NaOH	28	82	-	24h	198
3	S-doped Ni-P	1.0 M KOH	55	70	16.5	25h	199
4	CSSe-0.10	0.5 M H ₂ SO ₄	157	28.2	2.79	3000 CV cycles	200
5	Ru/S-rGO-24	1.0 M KOH	14 at (20 mA cm ⁻²)	38	49.01	20h	201
6	SG-P	0.5 M H ₂ SO ₄	178 at (100 mA cm ⁻²)	86	16.5	3000 CV cycles	202
7	Co-Mo-S	1.0 M KOH	-	118	-	8h	203
8	S-AuPbPt-NWNs	0.5 M H ₂ SO ₄	12	60.67	-	5000 CV cycles	204
9	MoS ₂ @S-CPDA	0.5 M H ₂ SO ₄	150	63	-	1000 CV cycles	205
10	S-CoSe ₂	0.5 M H ₂ SO ₄	102	50	-	4000 CV cycles	206

Table 13. S-Doped Electrocatalysts for HER



ARTICLE

Journal Name

methods, *Ummul K. Sultana and co-workers* developed O-doped cobalt sulfide. They found that the most successful electrochemical method was to repeatedly cycle the potential instead of holding it constant. This produced an amorphous CoS_x layer that was injected with oxygen. Based on calculations using DFT, it was shown that amorphous materials with a lower S-Co coordination number ideally increase the binding energy needed for hydrogen adsorption, which in turn promotes effective electron transfer kinetics. Additionally, at alkaline circumstances, this material showed activity for the HER, converting to cobalt oxide as shown, and producing a small Tafel slope of 67 mV dec^{-1} .¹⁹⁴ The O-doped HER electrocatalysts are summarised in **Table 12**.

5.5 S-Doped Electrocatalysts for HER

Sulphur atoms assist the adsorption and dissociation of hydrogen ions and electrons by adding more active sites to the catalyst surface. The HER kinetics are accelerated by this increase in catalytic efficiency, leading to lower overpotential and higher responses with the sulphur. S-doping also makes the catalyst material more stable reducing corrosion or structural deterioration throughout prolonged electrochemical operations. Through sulfidation reactions sulfur a common chalcogen element can be added as a dopant to the host catalysts' lattice structure. Sulfur dopant electrolyte interaction is important because it influences charge movement kinetics at the catalyst electrolyte interface which helps to facilitate effective electron transport during the HER. Sulfur dopants can change the HER's rate of reaction resulting in lower overpotential and quicker reaction rates. The catalyst's total energy effectiveness improves as a result of this kinetics enhancement which facilitates more effective hydrogen production at lower energy inputs as well.^{198,207,208} S-loaded RhNi alloys were discovered as very effective electrocatalysts for the hydrogen evolution process by *Jiajia Lu and co-workers*. They used a method involving hydrothermal heating and high-temperature annealing to successfully produce the worm-shaped S-doped RhNi material. The HER is improved in these S-doped RhNi compositions (S-RhNi) by combining doped heteroatoms, alloying with nonprecious metals, and taking on distinctive morphologies and architectures. With a starting potential at 17 mV at 20 mA cm^{-2} and a Tafel slope of $24.61 \text{ mV dec}^{-1}$ experimental results show that S-RhNi shows Pt-like HER activity. The enhanced functionality is ascribed to the combined influence of the 3D arrangement of enriched S atoms and the worm-like RhNi material.¹⁹⁷ To generate the HER, *Qijun Che and coworkers* developed a unique approach called one-step electro-deposition of hierarchically organized S-doped NiCo films. This technique showed exceptional catalytic efficiency. Through the availability of many active sites detected through XPS spectrum analysis, their inquiry into the ideal concentration of doped sulfur demonstrated its critical significance in lowering the overpotential of hydrogen evolution. Furthermore, electron transport was made easier by the development of metallic nickel and cobalt. The amorphous $\text{Co}_x\text{Ni}_y\text{S}$ material and the crystalline nickel and cobalt metals seemed to work in concert to increase HER function shown in (**Figure 17a**). High-efficiency

water electrolysis may be achieved using S-doping and careful component management. DFT study shows that S-doped and component control are effective methods for high-efficiency water electrochemical reduction. With a hierarchical shape, the S-NiCo@50 electrode was notable for its very low overpotential of 28 mV at 10 mA cm^{-2} and 125 mV at 100 mA cm^{-2} .¹⁹⁸ A binder-free electrocatalyst consisting of S-added Ni-P nanospheres was developed by *Muhammad Aqeel Ashraf and co-workers* using a new pulse electrochemical deposition method to improve total water splitting. Through a highly electrochemically active surface, powerful synergistic effects between the sulphur and phosphorous, fast gas separation from the surface, decreased resistance by bubble pinning, and enhanced wettability due to using Nano-structuring, the resultant S-doped Ni-P small spheres demonstrated remarkable electrocatalytic capabilities for the HER. Among transition metal phosphides, Ni-Ps are the most notable because of their electrical conductivity, strength, and advantageous electrocatalytic capabilities. Ni-P phosphide-based samples are particularly significant because of their outstanding activity and stability. XPS analysis was used to analyze surface chemistry and element valence. DFT calculations show that doping resulted in a drop in ΔG_{H^*} , enhancing intrinsic electrocatalytic activity. With just a 55 mV overpotential needed to get a current density of 10 mA cm^{-2} for the evolution of hydrogen reaction, the electrode astoundingly showed exceptional performance.¹⁹⁹ *Xiaojiao Fang and co-workers* synthesized S-loaded Co- Se_2 rich with the 1T phase, which they used to generate an effective electrocatalyst for the reaction of hydrogen evolution. Co- Se_2 's intrinsic metallicity makes it a promising electrocatalyst for breaking down water, but its chemically inert base plane limits its use by creating a shortage of active places. By adjusting the sulfur doping level, they looked at how growth conditions affect hydrogen evolution and found that $\text{CoS}_{0.1}\text{Se}_{1.9}$ with an enriched 1T-phase showed strong HER action. It took only 157 mV (vs. RHE) to reach a current density of 10 mA cm^{-2} with a limited Tafel slope of 28.2 mV dec^{-1} .²⁰⁰ For the HER, *Xuzhuo Sun and co-workers* reported ruthenium nanoparticles widely distributed on sulfur-doped graphene. The results of their experiments demonstrated that the synthesis and improved distribution of ultrasmall Ru nanoparticles were enhanced by both sulphur treatment and a modest degree of oxidation of graphene oxide. This resulted in greater electrochemically active surface regions and increased exposure of active areas. XPS and electronic charge-difference investigations demonstrated that the metal-support relationship between S-doped graphene and Ru nanostructures led to a decrease in Ru's electron density, which in turn promoted electron release from H_2O and facilitated H-OH bond breakdown. Sulphur substances might accelerate water dissociation during the alkaline HER by lowering the energy barrier for breaking the H-OH bond, as shown by simulations using density functional theory. Interestingly, the catalyst had the lowest overpotential of 14 mV at a current density of 20 mA cm^{-2} shown in (**Figure 17c**).²⁰¹ *Ye Tian and co-workers* developed sulphur-incorporated, plasma-etched graphene as a unique means of enhancing the hydrogen-evolving process. They utilized a technique called plasma



engraving to produce more topological flaws in the S-doped graphene surface. At a current density of 10 mA cm^{-2} the S-doped graphene that resulted was plasma-etched and showed markedly enhanced HER operation exhibiting an overpotential of 178 mV. XPS is used to evaluate the impact of plasma etching on the degree as well as type of doping in SG. The enhanced performance was ascribed to the mutually beneficial interaction between sulphur doping and topological errors caused by plasma. Moreover, the investigation showed that HER activity could be maximized by adjusting the sulphur doping amount in conjunction with thiophene-S-rich molecules and a suitable number of topological imperfections. This effective pairing of heteroatom doping and plasma-assisted defect engineering presents a viable path toward the production of extremely *Xue Cui and co-workers* developed a new method to generate a tuneable water-splitting catalyst by gradually modifying the doping of sulphur (S) in cobalt molybdate (CoMoO_4) by employing thioacetamide (TAA) as the precursor for sulfur. Notably, the S-doped TAA demonstrated electrocatalytic performance comparable to state-of-the-art transition-metal (Co, Ni, and Fe)-based HER electrodes, with a high TAA/ CoMoO_4 mass ratio of 1.6 and outstanding selectivity for the HER shown in (Figure 17d). In particular, it exhibited outstanding HER results, with an onset potential of 87 mV and a Tafel slope of 63 mV dec^{-1} .²⁰³ *Xiang Zhang and co-workers* developed AuPbPt Alloy Nanowire-Networks doped with sulfur that acts as very efficient HER catalysts. These networks are reported by depositing Platinum onto S-doped Au-Pb NWNs, which are substrates that come from the directed self-assembly of Pb^{2+} ions and the reduction of 2nm gold nanoclusters by NaBH_4 . XPS and DFT studies show that the resultant S-doped Au-Pb-Pt alloy NWNs with an ideal PtS concentration have a considerably lower shift in the d-band center of platinum. By strengthening the active Pt sites' resistance to oxidation, this modification improves the overall stability of Pt surfaces as well as the catalytic activity towards HER. With an overpotential of 12 mV at 10 mA cm^{-2} in acidic conditions, the as-synthesized S-doped Au-Pb-Pt alloy NWNs exhibit outstanding electrocatalytic activity for HER. They also exhibit amazing durability.²⁰⁴ To improve the evolution of hydrogen reaction performance, *Thangavel Naresh Kumar and co-workers* developed the dimensional and electrical refinement of MoS_2 nanosheets using S-doped carbon. When Mo (VI)-polydopamine (PDA) is pyrolyzed in the presence of elemental sulfur, S-doped carbon is integrated between MoS_2 nano-sheets, resulting in an improvement of MoS_2 with extra edge planes (2H 1T), which increases the charge density and conductive properties. The greater concentration of unsaturated S at the edge regions as opposed to the basal planes is responsible for the enhanced activity observed, even though bulk MoS_2 's intrinsic conductive properties and crystallinity constraints need significant overpotentials for HER. Additionally, the metallic 1T polymorph of MoS_2 compounds and the existence of edge sites are related to the catalytic properties. Recent research has shown that the metallic 1T (octahedral) phase of semi-conducting 2H MoS_2 (trigonal prismatic) considerably improves HER catalytic efficiency. At a

current density of 10 mA cm^{-2} , the phase-transformed MoS_2 [@S-CPDA] exhibits better HER activity with overpotential of 160 mV shown in (Figure 17b).²⁰⁵ Highly porous CoSe_2 nanosheets that operated and treated with sulfur were developed by *Ning Xue and co-workers* as a powerful electrocatalyst for the hydrogen evolution process. An effective catalyst like CoSe_2 is made more active towards HER by adding foreign atoms like S to its structure. The solvothermal methods ion exchange method they employed to add sulfur to CoSe_2 nanosheets (NSs) was substantiated by theoretical and experimental studies, proving the efficacy of the resulting S-added CoSe_2 (S-CoSe₂) nanoporous NSs as a common and highly efficient catalyst for HER. High-resolution XPS spectra of S-CoSe₂-5 were acquired in the Se 3p region to illustrate the chemical bonding state of CoSe_2 before and after S doping. Based on DFT computations, it was revealed that S doping improves the efficiency of HER on S-CoSe₂ by reducing the kinetic barrier energy of the rate-determining step and decreasing the absolute value of ΔG_H which moves closer to 0. At a low overpotential of 88 mV, the improved S-CoSe₂ catalyst achieves a catalytic current density of 10 mA cm^{-2} for HER making it one of the most effective catalysts based on CoSe and CoS for HER.²⁰⁶ The S-doped HER electrocatalysts are summarised in Table 13.

6. Summary and outlook

Heteroatom doping has emerged as one of the most effective and versatile strategies for engineering electrocatalysts with enhanced performance toward the HER. Through the deliberate incorporation of both metallic and non-metallic dopants into host materials, researchers have successfully tuned electronic structures, introduced catalytic active sites, modulated hydrogen binding energies, and improved conductivity. The dual advantages of electronic modification and structural activation offered by dopants allow for a fine-tuning of intrinsic catalytic activity and reaction kinetics, even under demanding electrochemical conditions. Metal dopants such as Fe, Co, Ni, Mo, Mn, Pt and Cu contribute primarily by shifting the d-band center and enhancing conductivity, while non-metal dopants like N, P, S, and B introduce surface defects, facilitate charge redistribution, and influence hydrogen adsorption energetics. The increasing interest in co-doping strategies arises from their synergistic effects, where simultaneous metallic and non-metallic doping generates multi-functional active sites, thereby overcoming the limitations posed by single-element doping. These advances collectively contribute to higher catalytic efficiency, improved reaction dynamics, and enhanced durability of HER catalysts. Despite these achievements, challenges remain. The rational design of dopant combinations, atomic configurations, and optimal concentrations is still largely empirical. There is no universal framework to predict dopant performance due to the variability introduced by host substrates, synthesis conditions, and operating environments. Stability under industrially relevant conditions, particularly at high current densities and in harsh pH environments, remains a



ARTICLE

Journal Name

key hurdle. Moreover, bubble accumulation, dopant leaching, and structural degradation over extended periods continue to hinder practical deployment. Despite significant progress in doped electrocatalysts for the HER, certain challenges exist. Achieving precise control over dopant distribution and local coordination environments remains difficult, limiting reproducible and rational design, this can be addressed by new synthesis methodologies with improved atomic-level control. Furthermore, many doped catalysts undergo surface reconstruction or compositional changes when operated under HER conditions, requiring the use of operando and in situ characterisation approaches to determine the real active sites. Finally, establishing obvious structure-activity correlations remains difficult, necessitating further integration of experimental data with theoretical calculations in future research.

Looking forward, several research directions are poised to drive the next wave of innovation:

- **Design of model catalytic systems** that allow isolation of dopant effects and enable systematic investigations across various substrates.
- **Surface engineering strategies** to control wettability reduce bubble adhesion and enhance gas release during HER operation.
- **Advanced synthesis techniques** such as atomic layer deposition and molecular precursor-based doping for controlled dopant placement and uniform distribution.
- **Application of external stimulation** including electric and magnetic fields to boost mass transport, reduce overpotentials and facilitate gas detachment.
- **Integration of computational and experimental insights** particularly through machine learning, high-throughput DFT calculations, and in situ spectroscopies to accelerate rational catalyst discovery.
- **Scalability and sustainability considerations** ensuring that synthesis routes are compatible with industrial needs and environmentally benign.

In summary, while heteroatom doping has already unlocked significant advancements in HER catalysis, future efforts should focus on combining atomic-level understanding with scalable technologies to bridge the gap between laboratory discoveries and commercial realization of green hydrogen production.

Author contributions

Manova Santhosh Yesupatham and Rajini Murugesan contributed equally to this paper. **Manova Santhosh Yesupatham:** Conceptualization, Writing - original draft (equal), Methodology (equal), Validation (equal). **Rajini Murugesan:** Writing - original draft (equal), Methodology (equal), Validation (equal). **Donald Richard:** review & editing. **Akshaya Radhakrishnan:** review & editing. **Maruthapillai Arthanareeswari:** review & editing.

Conflicts of interest

[View Article Online](#)
DOI: 10.1039/D5NR04327A

There is no conflicts to declare.

Acknowledgement

The authors gratefully acknowledge the support of Danube Private University, Austria, and SRM Institute of Science and Technology, India. The authors sincerely thank Prof. Sabine Szunerits and Prof. Mandana Amiri for their constructive suggestions and insightful comments that helped improve the manuscript. The authors also sincerely thank to Dr. Karthikeyan Sekar for his suggestions to this review.

References

- 1 A. Kalair, N. Abas, M. S. Saleem, A. R. Kalair and N. Khan, *Energy Storage*, 2021, **3**, e135.



Journal Name

2 C. Gunathilake, I. Soliman, D. Panthi, P. Tandler, O. Fatani, N. A. Ghulamullah, D. Marasinghe, M. Farhath, T. Madhujith and K. Conrad, *Chemical Society Reviews*, 2024, **53**, 10900–10969.

3 X. Xu, Y. Pan, Y. Zhong, L. Ge, S. P. Jiang and Z. Shao, *Composites Part B: Engineering*, 2020, **198**, 108214.

4 M. S. Yesupatham, A. Augustin, N. Agamendran, B. Honnappa, M. Shanmugam, P. J. J. Sagayaraj, G. Thennarasu, N. C. S. Selvam and K. Sekar, *Sustainable Energy & Fuels*, 2023, **7**, 4727–4757.

5 K. M. Y. Baig, S. Marimuthu, G. Maduraiveeran and G. K. Kole, *Dalton Transactions*, 2025, **54**, 11025–11035.

6 F. Abdelghafar, X. Xu and Z. Shao, *Materials Reports: Energy*, 2022, **2**, 100144.

7 A. Mehtab, S. A. Ali, I. Sadiq, S. Shaheen, H. Khan, M. Fazil, N. A. Pandit, F. Naaz and T. Ahmad, *ACS Sustainable Resource Management*, 2024, **1**, 604–620.

8 E. A. Halpren, *University of Toronto (Canada)*, 2023.

9 R. Murugesan, N. C. S. Selvam and A. Maruthapillai, *Catalysis Science & Technology*.

10 H. Lu, J. Tournet, K. Dastafkan, Y. Liu, Y. H. Ng, S. K. Karuturi, C. Zhao and Z. Yin, *Chemical Reviews*, 2021, **121**, 10271–10366.

11 K. M. Y. Baig, S. Marimuthu, E. Zangrando, G. Maduraiveeran and G. K. Kole, *Materials Today Chemistry*, 2025, **43**, 102464.

12 J. Wang, Y. Gao, H. Kong, J. Kim, S. Choi, F. Ciucci, Y. Hao, S. Yang, Z. Shao and J. Lim, *Chemical Society Reviews*, 2020, **49**, 9154–9196.

13 Y. Liu, R. Duan, X. Li, L. Luo, J. Gong, G. Zhang, Y. Li and Z. Li, *Inorganic Chemistry*, 2022, **61**, 13210–13217.

14 J. Wang, T. Liao, Z. Wei, J. Sun, J. Guo and Z. Sun, *Small Methods*, 2021, **5**, 2000988.

15 A. Majumdar, K. D. Tran, D. Malhotra, D. T. Tran, N. H. Kim and J. H. Lee, *Heteroatom-Doped Carbon Allotropes: Progress in Synthesis, Characterization, and Applications*, 2024, 177–222.

16 A. Zhang, Y. Liang, H. Zhang, Z. Geng and J. Zeng, *Chemical Society Reviews*, 2021, **50**, 9817–9844.

17 R. Murugesan, M. S. Yesupatham, N. Agamendran, K. Sekar, C. S. S. Neethinathan and A. Maruthapillai, *Energy Technology*, 2400882.

18 Y. Zhao, W. Jiang, J. Zhang, E. C. Lovell, R. Amal, Z. Han and X. Lu, *Advanced Materials*, 2021, **33**, 2102801.

19 M. Du, F. Yu, S. Gong and F. Liu, *Advanced Functional Materials*, 2025, **35**, 2413826.

20 T. Guo, Y. Lin, X. Chen, J. Lu, X. Zhao, X. Yao, L. Meng, Y. Liu and X. Zhang, *International Journal of Hydrogen Energy*, 2023, **48**, 2990–2997.

21 Q. Cai, W. Hong, C. Jian, X. He and W. Liu, *Advanced Energy and Sustainability Research*, 2023, **4**, 2200178.

22 W. Chen, M.-K. Zhang, B.-Y. Liu, J. Cai and Y.-X. Chen, *Current Opinion in Electrochemistry*, 2022, **34**, 101003.

23 Y. Li, X. Wei, L. Chen and J. Shi, *Angewandte Chemie International Edition*, 2021, **60**, 19550–19571.

24 A. Kahyarian, B. Brown and S. Nesic, *Journal of The Electrochemical Society*, 2017, **164**, H365.

25 N. Mahmood, Y. Yao, J. Zhang, L. Pan, X. Zhang and J. Zou, *Advanced science*, 2018, **5**, 1700464.

26 F. Li, G.-F. Han, H.-J. Noh, J.-P. Jeon, I. Ahmad, S. Chen, C. Yang, Y. Bu, Z. Fu and Y. Lu, *Nature communications*, 2019, **10**, 4060.

27 P. F. Liu, H. Yin, H. Q. Fu, M. Y. Zu, H. G. Yang and H. Zhao, *Journal of materials chemistry A*, 2020, **8**, 10096–10129. [View Article Online](#)

28 M. Boshir Ahmed, J. Alom, M. S. Hasan, M. Asaduzzaman, M. S. Rahman, R. Hossen, M. Abu Hasan Johir, M. Taufiq Alam, J. L. Zhou and Y. Zhu, *ChemNanoMat*, 2023, **9**, e202200482.

29 Y. Pan, T. Jian, P. Gu, Y. Song, Q. Wang, B. Han, Y. Ran, Z. Pan, Y. Li and W. Xu, *Nature Communications*, 2024, **15**, 9631.

30 Y. Qin, G. Lu, F. Yang, C. Xu, S. Jiang, Y. Wang, Y. Tang and P. Wang, *Materials Advances*, 2023, **4**, 1226–1248.

31 S. Gbadamasi, M. Mohiuddin, V. Krishnamurthi, R. Verma, M. W. Khan, S. Pathak, K. Kalantar-Zadeh and N. Mahmood, *Chemical Society Reviews*, 2021, **50**, 4684–4729.

32 R. Paul, F. Du, L. Dai, Y. Ding, Z. L. Wang, F. Wei and A. Roy, *Advanced Materials*, 2019, **31**, 1805598.

33 S. Kumar, R. Sharma, S. J. Borah, A. Gupta, M. K. Gupta, R. Kumar, K. K. Dubey, Y. K. Mishra and V. Kumar, *Sustainable Energy & Fuels*, 2023, **7**, 4354–4395.

34 X. Feng, Y. Bai, M. Liu, Y. Li, H. Yang, X. Wang and C. Wu, *Energy & Environmental Science*, 2021, **14**, 2036–2089.

35 A. Zunger and O. I. Malyi, *Chemical reviews*, 2021, **121**, 3031–3060.

36 A. Ghosh, O. F. Mohammed and O. M. Bakr, *Accounts of Chemical Research*, 2018, **51**, 3094–3103.

37 N. R. Abdullah, M. T. Kareem, H. O. Rashid, A. Manolescu and V. Gudmundsson, *Physica E: Low-dimensional Systems and Nanostructures*, 2021, **129**, 114644.

38 R. Kronberg, H. Lappalainen and K. Laasonen, *The Journal of Physical Chemistry C*, 2021, **125**, 15918–15933.

39 C. Wei, S. Sun, D. Mandler, X. Wang, S. Z. Qiao and Z. J. Xu, *Chemical Society Reviews*, 2019, **48**, 2518–2534.

40 J.-F. Chen, Y. Mao, H.-F. Wang and P. Hu, *ACS Catalysis*, 2016, **6**, 6804–6813.

41 X. Du, J. Huang, J. Zhang, Y. Yan, C. Wu, Y. Hu, C. Yan, T. Lei, W. Chen and C. Fan, *Angewandte Chemie International Edition*, 2019, **58**, 4484–4502.

42 Z. Chen, H. Yang, Z. Kang, M. Driess and P. W. Menezes, *Advanced Materials*, 2022, **34**, 2108432.

43 G. Tian, Q. Zhang, B. Zhang, Y. Jin, J. Huang, D. S. Su and F. Wei, *Advanced Functional Materials*, 2014, **24**, 5956–5961.

44 Y. Wang, X. Duan, Y. Xie, H. Sun and S. Wang, *Acs Catalysis*, 2020, **10**, 13383–13414.

45 J. Wu, Q. Zhang, K. Shen, R. Zhao, W. Zhong, C. Yang, H. Xiang, X. Li and N. Yang, *Advanced Functional Materials*, 2022, **32**, 2107802.

46 Y. Ma, M. Chen, H. Geng, H. Dong, P. Wu, X. Li, G. Guan and T. Wang, *Advanced Functional Materials*, 2020, **30**, 2000561.

47 J. Xie, J. Qi, F. Lei and Y. Xie, *Chemical Communications*, 2020, **56**, 11910–11930.

48 W.-J. Jiang, T. Tang, Y. Zhang and J.-S. Hu, *Accounts of chemical research*, 2020, **53**, 1111–1123.

49 M. A. Bhat and K. Majid, *Energy & Fuels*, 2023, **37**, 18834–18842.

50 H. Bai, Y. Han, X. Rong, Y. Yu, J. Ma, T. Yang, H. Huang and J. Hu, *International Journal of Hydrogen Energy*, 2023, **48**, 20562–20576.

51 H. Jin, X. Liu, S. Chen, A. Vasileff, L. Li, Y. Jiao, L. Song, Y. Zheng and S.-Z. Qiao, *ACS Energy Letters*, 2019, **4**, 805–810.

52 B. Bayatsarmadi, Y. Zheng, A. Vasileff and S. Qiao, *Small*,



ARTICLE

Journal Name

2017, **13**, 1700191.

53 Z. Li, X. Lu, J. Teng, Y. Zhou and W. Zhuang, *Nanoscale*, 2021, **13**, 11314–11324.

54 J. Shan, C. Ye, C. Zhu, J. Dong, W. Xu, L. Chen, Y. Jiao, Y. Jiang, L. Song and Y. Zhang, *Journal of the American Chemical Society*, 2022, **144**, 23214–23222.

55 M. Zhou, C. Li and J. Fang, *Chemical Reviews*, 2020, **121**, 736–795.

56 J. Li, C. A. Triana, W. Wan, D. P. A. Saseendran, Y. Zhao, S. E. Balaghi, S. Heidari and G. R. Patzke, *Chemical Society Reviews*, 2021, **50**, 2444–2485.

57 F. Liu, C. Shi, X. Guo, Z. He, L. Pan, Z. Huang, X. Zhang and J. Zou, *Advanced Science*, 2022, **9**, 2200307.

58 T. Shi, B. Gao, H. Meng, Y. Fu, D. Kong, P. Ren, H. Fu and Z. Feng, *Green Chemistry*, 2024, **26**, 4209–4220.

59 Z. Li, X. Li, Y. Gu, X. Hu, L. Wang and P. Li, *Applied Surface Science*, 2024, **646**, 158959.

60 X. Liu, Q. Yu, X. Qu, X. Wang, J. Chi and L. Wang, *Advanced Materials*, 2024, **36**, 2307395.

61 X. Guo, X. Yu, Z. Feng, J. Liang, Q. Li, Z. Lv, B. Liu, C. Hao and G. Li, *ACS Sustainable Chemistry & Engineering*, 2018, **6**, 8150–8158.

62 M. Guo, S. Song, S. Zhang, Y. Yan, K. Zhan, J. Yang and B. Zhao, *ACS Sustainable Chemistry & Engineering*, 2020, **8**, 7436–7444.

63 C. Tang, R. Zhang, W. Lu, L. He, X. Jiang, A. M. Asiri and X. Sun, *Advanced materials*, 2017, **29**, 1602441.

64 T. H. Wondimu, G.-C. Chen, D. M. Kabtamu, H.-Y. Chen, A. W. Bayeh, H.-C. Huang and C. H. Wang, *international journal of hydrogen energy*, 2018, **43**, 6481–6490.

65 J. Yan, H. Wu, H. Chen, R. Jiang and S. F. Liu, *Journal of Materials Chemistry A*, 2017, **5**, 10173–10181.

66 C. Wan and B. M. Leonard, *Chemistry of Materials*, 2015, **27**, 4281–4288.

67 F. Li, Y. Bu, Z. Lv, J. Mahmood, G. Han, I. Ahmad, G. Kim, Q. Zhong and J. Baek, *Small*, 2017, **13**, 1701167.

68 P. Wang, Z. Pu, Y. Li, L. Wu, Z. Tu, M. Jiang, Z. Kou, I. S. Amiinu and S. Mu, *ACS applied materials & interfaces*, 2017, **9**, 26001–26007.

69 C. Lin, P. Wang, H. Jin, J. Zhao, D. Chen, S. Liu, C. Zhang and S. Mu, *Dalton Transactions*, 2019, **48**, 16555–16561.

70 H. Fan, H. Yu, Y. Zhang, Y. Zheng, Y. Luo, Z. Dai, B. Li, Y. Zong and Q. Yan, *Angewandte Chemie International Edition*, 2017, **56**, 12566–12570.

71 Y. Liu, Y. Yang, B. Chen, X. Li, M. Guo, Y. Yang, K. Xu and C. Yuan, *Inorganic Chemistry*, 2021, **60**, 18325–18336.

72 H. Xie, C. Lan, B. Chen, F. Wang and T. Liu, *Nano Research*, 2020, **13**, 3321–3329.

73 T. Liu, P. Li, N. Yao, G. Cheng, S. Chen, W. Luo and Y. Yin, *Angewandte Chemie*, 2019, **131**, 4727–4732.

74 D.-Y. Wang, M. Gong, H.-L. Chou, C.-J. Pan, H.-A. Chen, Y. Wu, M.-C. Lin, M. Guan, J. Yang and C.-W. Chen, *Journal of the American Chemical Society*, 2015, **137**, 1587–1592.

75 G. Zhang, X. Zheng, Q. Xu, J. Zhang, W. Liu and J. Chen, *Journal of Materials Chemistry A*, 2018, **6**, 4793–4800.

76 B. Seo, G. Y. Jung, Y. J. Sa, H. Y. Jeong, J. Y. Cheon, J. H. Lee, H. Y. Kim, J. C. Kim, H. S. Shin and S. K. Kwak, *ACS nano*, 2015, **9**, 3728–3739.

77 H. Lin, N. Liu, Z. Shi, Y. Guo, Y. Tang and Q. Gao, *Advanced Functional Materials*, 2016, **26**, 5590–5598.

78 I. Roger, R. Moca, H. N. Miras, K. G. Crawford, D. A. J. Moran, A. Y. Ganin and M. D. Symes, *Journal of Materials Chemistry A*, 2017, **5**, 1472–1480. [View Article Online](#)

79 F. Wang, Y. Zhu, W. Tian, X. Lv, H. Zhang, Z. Hu, Y. Zhang, J. Ji and W. Jiang, *Journal of Materials Chemistry A*, 2018, **6**, 10490–10496.

80 X. Dai, K. Du, Z. Li, M. Liu, Y. Ma, H. Sun, X. Zhang and Y. Yang, *ACS applied materials & interfaces*, 2015, **7**, 27242–27253.

81 W. Zhao, S. Wang, C. Feng, H. Wu, L. Zhang and J. Zhang, *ACS Applied Materials & Interfaces*, 2018, **10**, 40491–40499.

82 P. P. Patel, O. I. Velikokhatnyi, S. D. Ghadge, P. J. Hanumantha, M. K. Datta, R. Kuruba, B. Gattu, P. M. Shanthi and P. N. Kumta, *International Journal of Hydrogen Energy*, 2018, **43**, 7855–7871.

83 Y. Zheng, J. Rong, J. Xu, Y. Zhu, T. Zhang, D. Yang and F. Qiu, *Applied Surface Science*, 2021, **563**, 150385.

84 X.-Y. Yu, Y. Feng, Y. Jeon, B. Guan, X. W. Lou and U. Paik, *Advanced Materials (Deerfield Beach, Fla.)*, 2016, **28**, 9006–9011.

85 X. Peng, A. M. Qasim, W. Jin, L. Wang, L. Hu, Y. Miao, W. Li, Y. Li, Z. Liu and K. Huo, *Nano Energy*, 2018, **53**, 66–73.

86 K. Xiong, L. Li, L. Zhang, W. Ding, L. Peng, Y. Wang, S. Chen, S. Tan and Z. Wei, *Journal of Materials Chemistry A*, 2015, **3**, 1863–1867.

87 Z. Liu, H. Tan, J. Xin, J. Duan, X. Su, P. Hao, J. Xie, J. Zhan, J. Zhang and J.-J. Wang, *ACS Applied Materials & Interfaces*, 2018, **10**, 3699–3706.

88 W. Fang, D. Liu, Q. Lu, X. Sun and A. M. Asiri, *Electrochemistry Communications*, 2016, **63**, 60–64.

89 J. Ding, S. Ji, H. Wang, H. Gai, F. Liu, V. Linkov and R. Wang, *International Journal of Hydrogen Energy*, 2019, **44**, 2832–2840.

90 M. I. Abdullah, A. Hameed, N. Zhang and M. Ma, *International Journal of Hydrogen Energy*, 2019, **44**, 14869–14876.

91 Y. Yang, X. Zhao, H. Mao, R. Ning, X. Zheng, J. Sui and W. Cai, *International Journal of Hydrogen Energy*, 2020, **45**, 10724–10728.

92 T. Chen, B. Ye, H. Dai, S. Qin, Y. Zhang and Q. Yang, *Journal of Solid State Chemistry*, 2021, **301**, 122299.

93 X. F. Lu, L. Yu and X. W. Lou, *Science advances*, 2019, **5**, eaav6009.

94 A. Kumar, S. Kumar, S. Jana and R. Prakash, *Energy & Fuels*, 2023, **37**, 4552–4565.

95 Q. Luo, C. Wang, H. Xin, Y. Qi, Y. Zhao, J. Sun and F. Ma, *ACS Sustainable Chemistry & Engineering*, 2021, **9**, 732–742.

96 C. Wu, B. Liu, J. Wang, Y. Su, H. Yan, C. Ng, C. Li and J. Wei, *Applied Surface Science*, 2018, **441**, 1024–1033.

97 Y. Sun, L. Hang, Q. Shen, T. Zhang, H. Li, X. Zhang, X. Lyu and Y. Li, *Nanoscale*, 2017, **9**, 16674–16679.

98 Z. Wang, X. Ge, Z. Li, J. Wu, Z. Liang and S. Wang, *New Journal of Chemistry*, 2019, **43**, 9652–9657.

99 Y. Zhou, J. Zhang, H. Ren, Y. Pan, Y. Yan, F. Sun, X. Wang, S. Wang and J. Zhang, *Applied Catalysis B: Environmental*, 2020, **268**, 118467.

100 Z. Cui, Y. Ge, H. Chu, R. Baines, P. Dong, J. Tang, Y. Yang, P. M. Ajayan, M. Ye and J. Shen, *Journal of Materials Chemistry A*, 2017, **5**, 1595–1602.

101 L. Li, Y. Guo, X. Wang, X. Liu and Y. Lu, *Langmuir*, 2021, **37**, 5986–5992.

102 Q. Wang, H. Zhao, F. Li, W. She, X. Wang, L. Xu and H. Jiao,



Journal Name

103 *Journal of Materials Chemistry A*, 2019, **7**, 7636–7643.
C. Du, Y. Men, X. Hei, J. Yu, G. Cheng and W. Luo, *ChemElectroChem*, 2018, **5**, 2564–2570.

104 X. Lu, M. Cai, J. Huang and C. Xu, *Journal of Colloid and Interface Science*, 2020, **562**, 307–312.

105 X. Zhong, Y. Sun, X. Chen, G. Zhuang, X. Li and J. Wang, *Advanced Functional Materials*, 2016, **26**, 5778–5786.

106 I. S. Amiinu, Z. Pu, X. Liu, K. A. Owusu, H. G. R. Monestel, F. O. Boakye, H. Zhang and S. Mu, *Advanced Functional Materials*, 2017, **27**, 1702300.

107 T. Sun, J. Wang, X. Chi, Y. Lin, Z. Chen, X. Ling, C. Qiu, Y. Xu, L. Song and W. Chen, *ACS Catalysis*, 2018, **8**, 7585–7592.

108 T. Liu, X. Ma, D. Liu, S. Hao, G. Du, Y. Ma, A. M. Asiri, X. Sun and L. Chen, *ACS Catalysis*, 2017, **7**, 98–102.

109 M. Wang, Y. Tuo, X. Li, Q. Hua, F. Du and L. Jiang, *ACS Sustainable Chemistry & Engineering*, 2019, **7**, 12419–12427.

110 X. Wang, H. Zhou, D. Zhang, M. Pi, J. Feng and S. Chen, *Journal of Power Sources*, 2018, **387**, 1–8.

111 Y. Liu, X. Hua, C. Xiao, T. Zhou, P. Huang, Z. Guo, B. Pan and Y. Xie, *Journal of the American Chemical Society*, 2016, **138**, 5087–5092.

112 F. Yu, Y. Gao, Z. Lang, Y. Ma, L. Yin, J. Du, H. Tan, Y. Wang and Y. Li, *Nanoscale*, 2018, **10**, 6080–6087.

113 Y. Zhang, Y. Liu, M. Ma, X. Ren, Z. Liu, G. Du, A. M. Asiri and X. Sun, *Chemical communications*, 2017, **53**, 11048–11051.

114 X. Li, S. Li, A. Yoshida, S. Sirisomboonchai, K. Tang, Z. Zuo, X. Hao, A. Abudula and G. Guan, *Catalysis Science & Technology*, 2018, **8**, 4407–4412.

115 L. Zhang, M. Li, A. Zou, S. H. Yu, T. Xiong, L. Wang, J. He, Q. Fu, K. Sun and D. H. C. Chua, *ACS Applied Energy Materials*, 2018, **2**, 493–502.

116 S. Xu, X. Yu, X. Liu, C. Teng, Y. Du and Q. Wu, *Journal of Colloid and Interface Science*, 2020, **577**, 379–387.

117 L. Wu, X. Xu, Y. Zhao, K. Zhang, Y. Sun, T. Wang, Y. Wang, W. Zhong and Y. Du, *Applied Surface Science*, 2017, **425**, 470–477.

118 Q. Sun, Y. Dong, Z. Wang, S. Yin and C. Zhao, *Small*, 2018, **14**, 1704137.

119 J. Dai, D. Zhao, W. Sun, X. Zhu, L.-J. Ma, Z. Wu, C. Yang, Z. Cui, L. Li and S. Chen, *ACS Catalysis*, 2019, **9**, 10761–10772.

120 J. Zhang, B. Xiao, X. Liu, P. Liu, P. Xi, W. Xiao, J. Ding, D. Gao and D. Xue, *Journal of Materials Chemistry A*, 2017, **5**, 17601–17608.

121 Y. Ding, X. Du and X. Zhang, *ChemCatChem*, 2021, **13**, 1824–1833.

122 L. Wen, Y. Sun, C. Zhang, J. Yu, X. Li, X. Lyu, W. Cai and Y. Li, *ACS Applied Energy Materials*, 2018, **1**, 3835–3842.

123 L. Ji, P. Yan, C. Zhu, C. Ma, W. Wu, C. Wei, Y. Shen, S. Chu, J. Wang and Y. Du, *Applied Catalysis B: Environmental*, 2019, **251**, 87–93.

124 H. Su, S. Song, S. Li, Y. Gao, L. Ge, W. Song, T. Ma and J. Liu, *Applied Catalysis B: Environmental*, 2021, **293**, 120225.

125 Y. Li, X. Tan, R. K. Hocking, X. Bo, H. Ren, B. Johannessen, S. C. Smith and C. Zhao, *Nature communications*, 2020, **11**, 2720.

126 Q. Sun, L. Wang, Y. Shen, M. Zhou, Y. Ma, Z. Wang and C. Zhao, *ACS Sustainable Chemistry & Engineering*, 2018, **6**, 12746–12754.

127 H. Li, G. Gao, H. Zhao, W. Wang, Y. Yang, Y. Du, S. Li, Y. Liu and L. Wang, *International Journal of Hydrogen Energy*, 2021, **46**, 33078–33086.

128 Y. Tian, L. Cao and P. Qin, *ChemCatChem*, 2019, **11**, 4420–4426.
View Article Online
DOI: 10.1039/D5NR04327A

129 L. Yan, B. Zhang, J. Zhu, Y. Li, P. Tsiaikaras and P. K. Shen, *Applied Catalysis B: Environmental*, 2020, **265**, 118555.

130 P. Bhanja, B. Mohanty, A. K. Patra, S. Ghosh, B. K. Jena and A. Bhaumik, *ChemCatChem*, 2019, **11**, 583–592.

131 Y. Li, Q. Gu, B. Johannessen, Z. Zheng, C. Li, Y. Luo, Z. Zhang, Q. Zhang, H. Fan and W. Luo, *Nano Energy*, 2021, **84**, 105898.

132 X. Xiao, D. Sun, X. Liu, B. Qiu, X. Xu, D. Zhang and T. Yang, *Sustainable Energy & Fuels*, 2021, **5**, 1059–1066.

133 S. Anantharaj, P. E. Karthik, B. Subramanian and S. Kundu, *ACS Catalysis*, 2016, **6**, 4660–4672.

134 W. Chen, X. Zhu, W. Wei, H. Chen, T. Dong, R. Wang, M. Liu, K. Ostrikov, P. Peng and S. Zang, *Small*, 2023, **19**, 2304294.

135 H. Hu, Y. Zheng, Y. Zhu, J. Rong, Y. Dai, T. Zhang, D. Yang and F. Qiu, *Inorganic Chemistry*, 2022, **62**, 601–608.

136 Y. Sun, Y. Zang, W. Tian, X. Yu, J. Qi, L. Chen, X. Liu and H. Qiu, *Energy & Environmental Science*, 2022, **15**, 1201–1210.

137 A. Abdolmaleki, Z. Mohamadi, A. A. Ensafi, N. Z. Atashbar and B. Rezaei, *International Journal of Hydrogen Energy*, 2018, **43**, 8323–8332.

138 A. Fan, C. Qin, X. Zhang, J. Yang, J. Ge, S. Wang, X. Yuan, S. Wang and X. Dai, *Journal of Materials Chemistry A*, 2019, **7**, 24347–24355.

139 M. K. Kundu, T. Bhowmik, R. Mishra and S. Barman, *ChemSusChem*, 2018, **11**, 2388–2401.

140 J. Li, J. Zhang, J. Zhang, K. Pan, H. Xu, H. Chen, G. Liu, N. Wu, C. Yuan and X. Liu, *Journal of Materials Chemistry A*, 2023, **11**, 19812–19844.

141 S. A. Singh, K. Vishwanath and G. Madras, *ACS applied materials & interfaces*, 2017, **9**, 19380–19388.

142 X. Cheng, Y. Li, L. Zheng, Y. Yan, Y. Zhang, G. Chen, S. Sun and J. Zhang, *Energy & Environmental Science*, 2017, **10**, 2450–2458.

143 Y. P. Zhu, C. Guo, Y. Zheng and S.-Z. Qiao, *Accounts of chemical research*, 2017, **50**, 915–923.

144 Q. Hu, G. Li, Z. Han, Z. Wang, X. Huang, H. Yang, Q. Zhang, J. Liu and C. He, *Chemistry—A European Journal*, 2020, **26**, 3930–3942.

145 S. P. Kaur and T. J. D. Kumar, *Applied Surface Science*, 2021, **552**, 149146.

146 H. Hu, Z. Shi, K. Khan, R. Cao, W. Liang, A. K. Tareen, Y. Zhang, W. Huang, Z. Guo and X. Luo, *Journal of Materials Chemistry A*, 2020, **8**, 5421–5441.

147 C. Peng, L. Song, L. Wang, F. Yang, J. Ding, F. Huang and Y. Wang, *ACS Applied Energy Materials*, 2021, **4**, 4887–4896.

148 Y. Yoon, A. P. Tiwari, M. Choi, T. G. Novak, W. Song, H. Chang, T. Zyung, S. S. Lee, S. Jeon and K. An, *Advanced Functional Materials*, 2019, **29**, 1903443.

149 W. Fu, Y. Wang, W. Tian, H. Zhang, J. Li, S. Wang and Y. Wang, *Angewandte Chemie*, 2020, **132**, 23999–24007.

150 L. Bian, W. Gao, J. Sun, M. Han, F. Li, Z. Gao, L. Shu, N. Han, Z. Yang and A. Song, *ChemCatChem*, 2018, **10**, 1571–1577.

151 H. Gu, W. Fan and T. Liu, *Nanoscale Horizons*, 2017, **2**, 277–283.

152 H. Yan, C. Tian, L. Wang, A. Wu, M. Meng, L. Zhao and H. Fu, *Angewandte Chemie*, 2015, **127**, 6423–6427.

153 Z. Shi, K. Nie, Z.-J. Shao, B. Gao, H. Lin, H. Zhang, B. Liu, Y. Wang, Y. Zhang and X. Sun, *Energy & Environmental*



ARTICLE

Journal Name

Science, 2017, **10**, 1262–1271.

154 J. Zhang, Y. Liu, B. Xia, C. Sun, Y. Liu, P. Liu and D. Gao, *Electrochimica Acta*, 2018, **259**, 955–961.

155 L. Li, T. Zhang, J. Yan, X. Cai and S. Liu, *Small*, 2017, **13**, 1700441.

156 S. Li, N. Yang, L. Liao, Y. Luo, S. Wang, F. Cao, W. Zhou, D. Huang and H. Chen, *ACS applied materials & interfaces*, 2018, **10**, 37038–37045.

157 J.-S. Li, S. Zhang, J.-Q. Sha, H. Wang, M.-Z. Liu, L.-X. Kong and G.-D. Liu, *ACS applied materials & interfaces*, 2018, **10**, 17140–17146.

158 Y. Hu, H. Yu, L. Qi, J. Dong, P. Yan, T. Taylor Isimjan and X. Yang, *ChemSusChem*, 2021, **14**, 1565–1573.

159 Z. Zhou, L. Zeng, G. Xiong, L. Yang, H. Yuan, J. Yu, S. Xu, D. Wang, X. Zhang and H. Liu, *Chemical Engineering Journal*, 2021, **426**, 129214.

160 P. Chen, T. Zhou, M. Chen, Y. Tong, N. Zhang, X. Peng, W. Chu, X. Wu, C. Wu and Y. Xie, *ACS Catalysis*, 2017, **7**, 7405–7411.

161 Y. Wu, X. Liu, D. Han, X. Song, L. Shi, Y. Song, S. Niu, Y. Xie, J. Cai and S. Wu, *Nature communications*, 2018, **9**, 1425.

162 J. Yan, L. Li, Y. Ji, P. Li, L. Kong, X. Cai, Y. Li, T. Ma and S. F. Liu, *Journal of Materials Chemistry A*, 2018, **6**, 12532–12540.

163 H. Jiang, J. Gu, X. Zheng, M. Liu, X. Qiu, L. Wang, W. Li, Z. Chen, X. Ji and J. Li, *Energy & Environmental Science*, 2019, **12**, 322–333.

164 C. C. Yang, S. F. Zai, Y. T. Zhou, L. Du and Q. Jiang, *Advanced Functional Materials*, 2019, **29**, 1901949.

165 Y. Men, P. Li, F. Yang, G. Cheng, S. Chen and W. Luo, *Applied Catalysis B: Environmental*, 2019, **253**, 21–27.

166 Y. Pan, Y. Liu, Y. Lin and C. Liu, *ACS applied materials & interfaces*, 2016, **8**, 13890–13901.

167 C. Pi, C. Huang, Y. Yang, H. Song, X. Zhang, Y. Zheng, B. Gao, J. Fu, P. K. Chu and K. Huo, *Applied Catalysis B: Environmental*, 2020, **263**, 118358.

168 S. A. Shah, X. Shen, M. Xie, G. Zhu, Z. Ji, H. Zhou, K. Xu, X. Yue, A. Yuan and J. Zhu, *Small*, 2019, **15**, 1804545.

169 J. Ma, M. Wang, G. Lei, G. Zhang, F. Zhang, W. Peng, X. Fan and Y. Li, *Small*, 2018, **14**, 1702895.

170 C. Das, N. Sinha and P. Roy, *Small*, 2022, **18**, 2202033.

171 M. Li, L. Zhang, Q. Xu, J. Niu and Z. Xia, *Journal of catalysis*, 2014, **314**, 66–72.

172 S. Keshipour and F. Eyvavi-Ashnak, *ChemElectroChem*, 2023, **10**, e202201153.

173 T. Li, J. Liu, Y. Song and F. Wang, *ACS catalysis*, 2018, **8**, 8450–8458.

174 B. R. Sathe, X. Zou and T. Asefa, *Catalysis science & technology*, 2014, **4**, 2023–2030.

175 Z. Liu, D. Gao, L. Hu, H. Liu, Y. Li, Y. Xue, F. Liu, J. Zhang and C. Tang, *Colloids and Surfaces A: Physicochemical and Engineering Aspects*, 2022, **646**, 128903.

176 B. Adegbemiga Yusuf, M. Xie, W. Yaseen, C. Judith Oluigbo, W. Wei, Y. Xu and J. Xie, *ChemElectroChem*, 2021, **8**, 1337–1348.

177 Q. Lin, C. Shang, Z. Chen, X. Wang and G. Zhou, *International Journal of Hydrogen Energy*, 2020, **45**, 30659–30665.

178 M. Bat-Erdene, M. Batmunkh, B. Sainbileg, M. Hayashi, A. S. R. Bati, J. Qin, H. Zhao, Y. L. Zhong and J. G. Shapter, *Small*, 2021, **17**, 2102218.

179 Y. B. Adegbemiga, N. Ullah, M. Xie, S. Hussain, C. J. Oluigbo, W. Yaseen, A. J. Kumar, Y. Xu and J. Xie, *Journal of Alloys and Compounds*, 2020, **835**, 155267 DOI: 10.1039/D5NR04327A

180 H. Yang, Z. Chen, P. Guo, B. Fei and R. Wu, *Applied Catalysis B: Environmental*, 2020, **261**, 118240.

181 Y. Gao, S. Qian, H. Wang, W. Yuan, Y. Fan, N. Cheng, H. Xue, T. Jiang and J. Tian, *Applied Catalysis B: Environmental*, 2023, **320**, 122014.

182 Q. Yu, Y. Fu, J. Zhao, B. Li, X. Wang, X. Liu and L. Wang, *Applied Catalysis B: Environmental*, 2023, **324**, 122297.

183 Z. Huang, S. Wang, R. D. Dewhurst, N. V. Ignat'ev, M. Finze and H. Braunschweig, *Angewandte Chemie International Edition*, 2020, **59**, 8800–8816.

184 P. Joshi, H.-H. Huang, R. Yadav, M. Hara and M. Yoshimura, *Catalysis Science & Technology*, 2020, **10**, 6599–6610.

185 Y. Wen, J. Qi, D. Zhao, J. Liu, P. Wei, X. Kang and X. Li, *Applied Catalysis B: Environmental*, 2021, **293**, 120196.

186 J. Xie, J. Zhang, S. Li, F. Grote, X. Zhang, H. Zhang, R. Wang, Y. Lei, B. Pan and Y. Xie, *Journal of the American Chemical Society*, 2013, **135**, 17881–17888.

187 P. V. Sarma, C. S. Tiwary, S. Radhakrishnan, P. M. Ajayan and M. M. Shajumon, *Nanoscale*, 2018, **10**, 9516–9524.

188 J. Xie, J. Xin, G. Cui, X. Zhang, L. Zhou, Y. Wang, W. Liu, C. Wang, M. Ning and X. Xia, *Inorganic Chemistry Frontiers*, 2016, **3**, 1160–1166.

189 C. Wang, Z. Yu, H. Yao, R. Jin, K. Shi, Y. Li and S. Ma, *Journal of Alloys and Compounds*, 2023, **964**, 171257.

190 G. Meng, Z. Chang, L. Zhu, C. Chen, Y. Chen, H. Tian, W. Luo, W. Sun, X. Cui and J. Shi, *Nano-Micro Letters*, 2023, **15**, 212.

191 J. Xu, B. Yu, H. Zhao, S. Cao, L. Song, K. Xing, R. Zhou and X. Lu, *ACS Sustainable Chemistry & Engineering*, 2020, **8**, 15055–15064.

192 T. L. L. Doan, D. T. Tran, D. C. Nguyen, H. T. Le, N. H. Kim and J. H. Lee, *Applied Catalysis B: Environmental*, 2020, **261**, 118268.

193 C. Liu, G. Zhang, L. Yu, J. Qu and H. Liu, *Small*, 2018, **14**, 1800421.

194 U. K. Sultana, T. He, A. Du and A. P. O'Mullane, *RSC advances*, 2017, **7**, 54995–55004.

195 J. Cui, S. Liang, X. Wang and J. Zhang, *Materials Chemistry and Physics*, 2015, **161**, 194–200.

196 W. Shi and Z. Wang, *Journal of the Taiwan Institute of Chemical Engineers*, 2018, **82**, 163–168.

197 J. Lu, Z. Tang, L. Luo, S. Yin, P. K. Shen and P. Tsiakarlas, *Applied Catalysis B: Environmental*, 2019, **255**, 117737.

198 Q. Che, N. Bai, Q. Li, X. Chen, Y. Tan and X. Xu, *Nanoscale*, 2018, **10**, 15238–15248.

199 M. A. Ashraf, Y. Yang, D. Zhang and B. T. Pham, *Journal of Colloid and Interface Science*, 2020, **577**, 265–278.

200 X. Fang, Z. Wang, Z. Jiang, J. Wang and M. Dong, *Electrochimica Acta*, 2019, **322**, 134739.

201 X. Sun, X. Gao, J. Chen, X. Wang, H. Chang, B. Li, D. Song, J. Li, H. Li and N. Wang, *ACS Applied Materials & Interfaces*, 2020, **12**, 48591–48597.

202 Y. Tian, Z. Wei, X. Wang, S. Peng, X. Zhang and W. Liu, *International Journal of Hydrogen Energy*, 2017, **42**, 4184–4192.

203 X. Cui, Z. Chen, Z. Wang, M. Chen, X. Guo and Z. Zhao, *ACS Applied Energy Materials*, 2018, **1**, 5822–5829.

204 X. Zhang, S. Wang, C. Wu, H. Li, Y. Cao, S. Li and H. Xia, *Journal of Materials Chemistry A*, 2020, **8**, 23906–23918.

205 T. N. Kumar, N. Chandrasekaran and K. L. Phani, *Chemical*



Journal Name

ARTICLE

206 *Communications*, 2015, **51**, 5052–5055.
N. Xue, Z. Lin, P. Li, P. Diao and Q. Zhang, *ACS applied materials & interfaces*, 2020, **12**, 28288–28297.

207 F. Liu, W. He, Y. Li, F. Wang, J. Zhang, X. Xu, Y. Xue, C. Tang, H. Liu and J. Zhang, *Applied Surface Science*, 2021, **546**, 149101.

208 Y.-N. Zhou, W.-L. Yu, Y.-N. Cao, J. Zhao, B. Dong, Y. Ma, F.-L. Wang, R.-Y. Fan, Y.-L. Zhou and Y.-M. Chai, *Applied Catalysis B: Environmental*, 2021, **292**, 120150.

209 U. Sim, T.-Y. Yang, J. Moon, J. An, J. Hwang, J.-H. Seo, J. Lee, K. Y. Kim, J. Lee and S. Han, *Energy & Environmental Science*, 2013, **6**, 3658–3664.

210 C. Lv, Q. Yang, Q. Huang, Z. Huang, H. Xia and C. Zhang, *Journal of Materials Chemistry A*, 2016, **4**, 13336–13343.

211 X. Wang, H. Huang, J. Qian, Y. Li and K. Shen, *Applied Catalysis B: Environmental*, 2023, **325**, 122295.

212 X. Xu, K. Guo, J. Sun, X. Yu, X. Miao, W. Lu and L. Jiao, *Advanced Functional Materials*, 2024, **34**, 2400397.

[View Article Online](#)
DOI: 10.1039/D5NR04327A

Nanoscale Accepted Manuscript





Data availability statements

Dear Editor

Nanoscale

No primary research results, software or code have been included and no new data were generated or analyzed as part of this review.

Sincerely Yours (on behalf of all authors),

Dr. Arthanareeswari Maruthapillai

Professor & Chairperson

School of Basic Sciences

College of Engineering and Technology

SRM Institute of Science and Technology

Kattankulathur - 603 203 Tamil Nadu, India.

<https://www.srmist.edu.in/faculty/dr-m-arthanareeswari/>

